## 10.1 Introduction

When a metal melt or a molten alloy solidifies and cools its volume decreases in most cases. The shrinkage in castings and ingots, due to this volume decrease, is relatively big and may cause severe problems. The most important of them are:

- deformation of the casting by collapse of the surface shell at the beginning of the solidification process
- formation of cavities in the interior of the casting
- pipe formation
- appearance of casting strain, shrinkage cracks and faults in the castings.

The volume decrease can in some cases cause such severe difficulties that it is necessary to give up the use of an alloy even if it has excellent properties in other respects.

In this chapter we will discuss the causes and the effects of solidification and cooling shrinkage of metals and the available methods to eliminate or reduce their negative effects at casting.

## 10.2 Solidification and Cooling Shrinkage

### 10.2.1 Origin of Solidification and Cooling Shrinkage

All matter is in a state of incessant motion. The atoms/ions in a crystal or solid phase are exposed to forces from their neighbours and vibrate back and forth around their equilibrium posi-

tions. The higher the temperature is, the larger will the amplitudes of the oscillations be and the more space is required for each atom/ion. Thus a piece of metal extends when its temperature increases.

When the metal melts the strong bonds between the atoms/ions are broken. Even if strong forces still act between nearest neighbour atoms/ions and a certain short-distance order remains, they can move fairly freely relative to each other. The average distanses between the atoms/ions are larger in the melt than in the solid phase. In most cases melting of the metal thus causes an increase of its volume.

If the temperature of the melt is increased, the kinetic motion of the atoms/ions increases and causes further volume dilatation. At solidification and cooling the opposite processes occur to the ones described above.

### 10.2.2 Solidification and Cooling Shrinkage of Pure Metals and Alloys

The solidification and cooling of a metal melt after casting occurs in three stages:

- Cooling shrinkage of the melt from the casting temperature to the temperature when the solidification starts.
- Solidification shrinkage at the transition from melt to solid phase.
- Cooling shrinkage at the cooling of the solid phase down to room temperature.

The cooling shrinkage of the melt causes in most cases no major problems. Addition of more melt can compensate the shrinkage.

The figures 1 and 2 show how the specific volume, i. e. the volume of 1 kg of the metal, changes as a function of temperature during the cooling and solidification processes of a pure metal respectively an alloy.

A *pure* metal has a well-defined melting and solidification temperature, which is seen in figure 1 on next page. On the other hand, an *alloy* solidifies within a *temperature interval* defined

Figure 1. Left figure.
The solidification and cooling processes of a pure metal.

Figure 2. Right figure.
The solidification and cooling processes of an alloy.

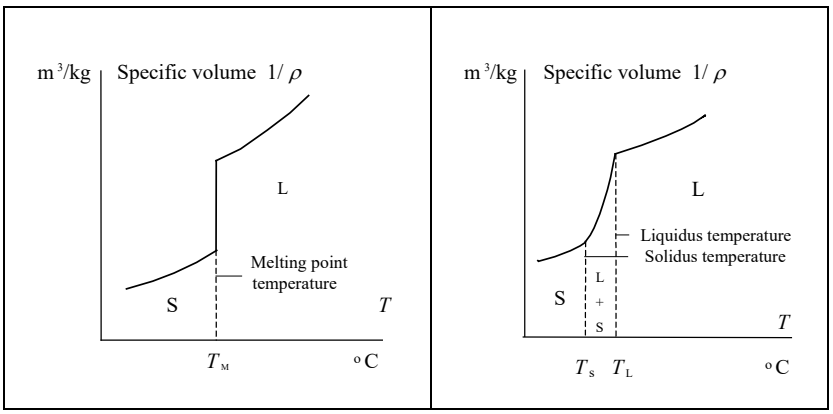


by the liquidus and solidus temperatures. This is illustrated in figure 2 above.

The difference between these two cases of *solidification shrinkage* is very important and results in completely different solidification processes. They will be discussed in sections 10.2.3 and 10.2.4 below.

*Cooling shrinkage* causes undesired volume- and shape changes of the casting and mechanical strain in the material. The shrinkage process will be discussed in section 10.6 and 10.7.

## 10.2.3 Solidification Shrinkage of a Pure Metal. Pipe Formation in an Ingot

A pure metal solidifies along a well-defined solidification front at a rate, which is controlled by the heat transport to the surroundings. When a melt is teemed into a mould it starts to solidify by heat transport away from the melt and out through the mould. The solid phase is nucleated on the cold mould surface and forms a layer which grows inwards to the melt, perpendicular to the surface.

The solidification shrinkage is in most cases inevitable at ingot casting. It is of great practical importance *where* the cavities, caused by solidification shrinkage, are situated in an ingot. There are in principle three different positions.

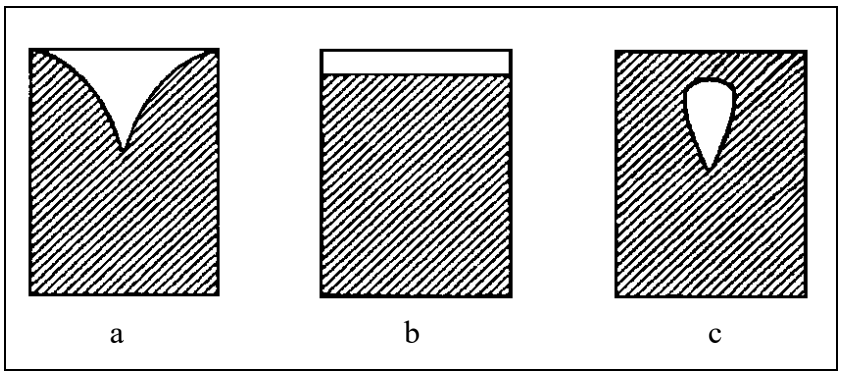


Figure 3.
Three alternative positions of shrinkage cavities in ingots.

In reality combinations between these distinguished cases occur. The positions and shapes of the shrinkage cavities depend on the composition of the melt and the mode of solidification, especially on the mechanism of heat conduction away from the ingot.

In *case a* the ingot has been cooled from the bottom and the sides or periphery. This case represents a typical ingot solidification.
*Case b* shows an example of ingot solidification from the bottom only.

In *case c* the upper surface has been cooled at the same time as the other sides and the bottom.

Final products must not contain any part of a pipe. At production of castings it is desirable to control the solidification process in such a way that the pipe ends up in an extra container with molten metal, conveniently situated outside the mould. Such a container is called a *feeder* or a *casting head*. It is important to let the melt in the feeder cool more slowly than the last melt in the mould. The method will be discussed in detail in section 10.5.1.

## 10.2.4 Solidification Shrinkage of an Alloy

An alloy solidifies within a temperature interval, defined by the composition of the alloy, i. e. its phase diagram.

Characteristic for the solidification process of alloys, which has been described in chapter 6, is that there is no well-defined solidification front. Instead solid phase precipitates anywhere in the melt. Dendrite crystals grow and form a network surrounded

by melt in the shape of more or less curved channels between the dendrites.

Initially the dendrites are thin and the channels broad enough to allow transport of melt. The solidification shrinkage can be compensated by melt, which is soaked through channels and fill the pores. The solidification process is generally the same as in a pure metal and may result in pipe formation. However, bridges of dendrites are formed across the pipe by crystal formation. Examples are seen on pages 37 and 58.

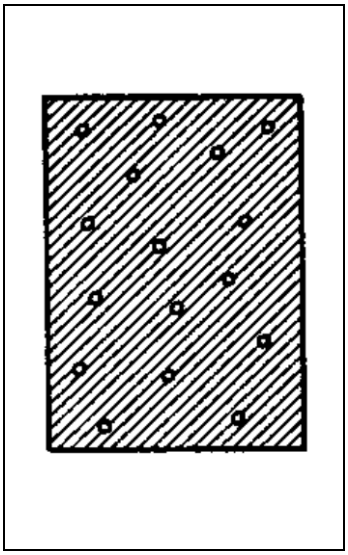

Figure 4.
Appearance of shrinkage pores in an alloy.

When the solidification process proceeds the dendrites become gradually thicker and the channels gradually thinner. It becomes more and more difficult to supply melt to the first solidified parts, close to the mould, through the channels. A lack of metal arises, which results in an *internal pore.* The shrinkage in the last solidified parts may result in *shrinkage cavities* in the shape of pores everywhere in the casting or the ingot. At the beginning of the solidification process, when the strength of the surface shell is not especially large, the shrinkage may result in a collapse of the whole casting shell, a so-called *external shrinkage cavity*. External and internal pores are called macropores with a common name. The volume decrease of the precipitated crystals may result in microscopic pores between the crystals, *micropores* or intercrystalline pores.

A shrinkage cavity is characterised by walls of a rough, crystalline appearance. In cast iron and steel the ”Norway spruce” structure, which is characteristic for these metals, can be seen. It is easy to distinguish these pores from gas pores, which have smooth surfaces.

Shrinkage cavities and micropores may reduce the mechanical strength of a casting and make it weak. The extension of the problem is hard to judge because the defect in the material can not be seen on the surface and is impossible to estimate with reference to the linear shrinkage of the metal. X-ray and gamma-radiation examinations are expensive examination methods, which are used only in the cases when a very high quality of the casting is required.

Efforts are made to prevent the formation of shrinkage cavities as much as possible, among other things by

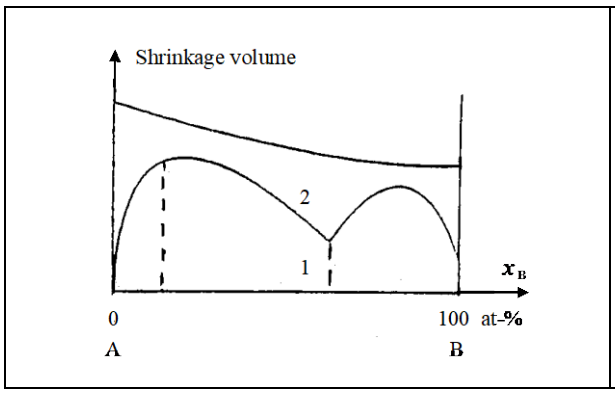


Figure 5.
The shrinkage volume as a function of the composition of the alloy.
Area 1: Shrinkage cavities.
Area 2: Pipe.

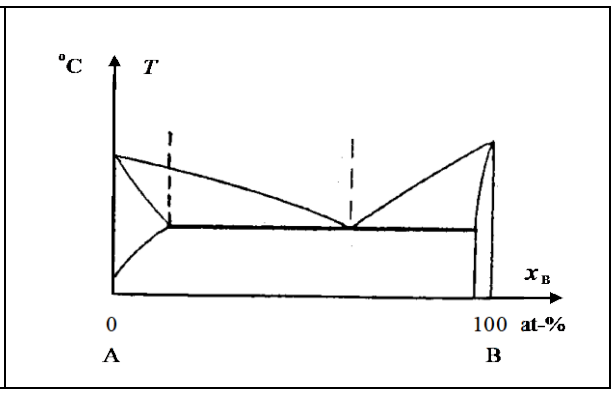


Figure 6.
Phase diagram of the binary system related to the alloy in figure 5.

- design with uniform thickness of the casting dimensions
- use of moulds and cooling bodies
- control of the casting temperature
- proper location and design of sprues and feeders
- optimal composition of the alloy
- optimal cooling conditions.

The last measures are the most important ones. The choice of alloy is of great importance. The problems can be mastered if the solidification interval of the alloy is comparably small, which is the case in brass and low carbon steel. Cast iron also works well because the solidification shrinkage is small, due to precipitation of graphite with a big relative specific volume. Corresponding circumstances are present in the case of ”red metal” (85%Cu5%Zn5%Sn5%Pb) by precipitation of lead at the end of the solidification.

The upper curve in figure 5 above shows the total volume of the shrinkage cavities respectively the pipe volume, which arises when a binary alloy solidifies. Inside area 1 , i. e. under the bent curve, the shrinkage appears in the shape of microcavities or pores distributed within the whole casting respectively the ingot. The remaining volume forms a pipe. Because the composition of the alloy changes during the solidification process, both a pipe and distributed shrinkage cavities are obtained.

## 10.3 Concepts and Laws. Methods of Measurement

### 10.3.1 Concepts and Laws

To be able to design a feeder or a hot top properly it is necessary to set up models for the solidification process and perform theoretical calculations of for example the volume of the feeder, the depth of the pipe and the height of the hot top. These calculations require the following concepts and laws.

- *Specific Volume* = the volume of a mass unit ($m^3/kg$)
- *Length Dilatation* $l = l_o\left[1 + \alpha_l \left(T - T_o\right)\right]$

  $\alpha_l$ = $\Delta l/\Delta T$ = the length dilatation coefficient
  $T$ = temperature
- *Volume Dilatation* $V = V_o\left[1 + \alpha_V \left(T - T_o\right)\right]$

  $\alpha_V$ = $\Delta V/\Delta T$ = the volume dilatation coefficient
  Approximately we have $\alpha_V = 3\alpha_l$

- *Solidification Shrinkage* is defined as

$$\beta = \frac{\rho_s - \rho_L}{\rho_s} = \frac{V_L - V_s}{V_L}$$

$\rho_s$ = density of the solid phase
$\rho_L$ = density of the melt
$V_s$ = volume of the solid phase
$V_L$ = volume of the melt

Chvorinov´s rule (chapter 4 on page 49):

$$t = C \cdot \left(\frac{V}{A}\right)^2$$

$A$ = contact area between mould and melt
$V$ = solidified volume at time $t$

The constant $C$ can be calculated from the relation

$$C = \frac{\pi}{4} \cdot \frac{\rho_{\text{metal}}^{2} \left(-\Delta H\right)^{2}}{\left(T_{\text{i}} - T_{\text{o}}\right)^{2} k_{\text{mould}} \rho_{\text{mould}} c_{p}^{\text{mould}}}$$

$\rho$ = density of the metal
$-\Delta H$ = heat of fusion of the metal
$T_{\text{i}}$ = temperature of the metal surface close to the sand mould ~ $T_{\text{L}}$
$T_{\text{o}}$ = room temperature
$k_{\text{mould}}$ = conductivity of the mould material
$\rho_{\text{mould}}$ = density of the mould material
$c_{\text{p}}^{\text{mould}}$ = heat capacitivity of the mould material.

## 10.3.2 Methods of Measurement

### Measurement of Small Volume Changes

Determination of densities, volume dilatation coefficients and solidification shrinkage of metals presumes careful measurements of small volume changes. It is also necessary to measure the temperature of the sample. The temperature measurement is normally performed by a thermocouple.

The volume determinations are often prevented by high melting points of the metals. Many direct and indirect methods are used, among others the ones below.

### Determination of Density and Volume Dilatation Coefficient of the Solid Phase

- Measurement of the lattice constant (distance between adjacent atoms in a crystal) of a metal sample at different temperatures by aid of X-ray diffraction. The mass and volume of the sample is also measured.

From the measured data the density of the metal at various temperatures and the volume expansion coefficient can be calculated.

- Direct measurement of length expansion of a metal sample as a function of temperature.

From the measured data the volume expansion coefficient can be calculated.

**Determination of Densities of Melts**

- Measurement of a given pressure difference by aid of a Hg manometer at room temperature and of a U-shaped tube of magnesium oxide, inserted in a furnace with the melt in question as manometer liquid. The height differences $h_{Hg}$ and $h_L$ are measured directly by aid of electrical contacts.

From the measurement data it is possible to calculate the density of the metal melt at the temperature in question, measured by a thermocouple. In addition, if the density of the melt is known as a function of temperature, its volume dilatation coefficient can be calculated.

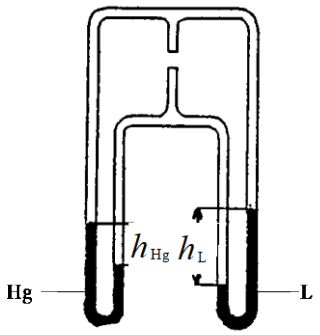


The density of the melt is determined from the relation

$$\rho_{Hg} g h_{Hg} = \rho_L g h_L$$

Figure 7.
Equipment for determination of the densities of metal melts.

- Weighing of a known volume of melt enclosed in an pycnometer of aluminium oxide. The pycnometer is submerged into the melt, is filled there, is removed and allowed to cool before weighing.
- Weighing of a plumb body, both in air and submerged in the melt.
- Measurement of the pressure required to release a gas bubble from a tube emerging at a certain depth under the free surface of the melt. From measurements at two or several different depths the density of the melt can be calculated.

**Determination of Solidification Shrinkage**

- Indirect calculation from the densities of the melt respective the solid phase at the melting point temperature.
- Measurement of the pressure in a gas with constant external volume in contact with a metal sample before and after solidification close to the melting point temperature. When the sample solidifies its volume decreases and the internal volume of the gas increases and the pressure decreases.

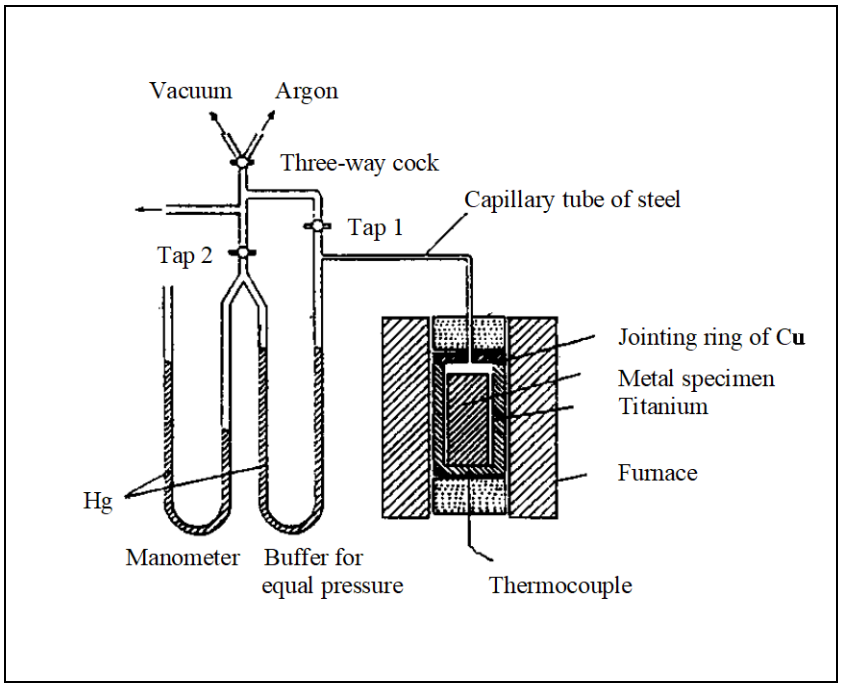


Figure 8.
Equipment for determination of solidification shrinkage.

The gas is enclosed in the sample container, which is connected to a manometer via a thin steel tube. Tap 2 is opened and can, as it is a three-way tap, either increase or decrease the pressure until the heights of the legs are equal in the right manometer. The pressure in the right leg in the left manometer is then equal to the pressure of the enclosed gas. It can easily be measured by reading the left manometer.

From the pressure measurements it is possible to calculate the internal volume increase of the gas, i. e. the volume decrease of the sample, and the solidification shrinkage of the metal. The ranges of application, sources of defects and accuracies of the various methods can not be discussed here for space reasons.

## Some Results of Measurements

The most examined and best known metals are iron and its alloys. Extensive data have been published in the scientific literature. Crystalline transformations in steel, for example from ferrite to austenite, also cause volume changes.

In table 1 below examples of data for some different metals are given.

Table 1.
Volume dilatation and solidification shrinkage of some different metals.

| Metal Alloy | Melting point/ melting interval °C | Density of the solid phase at 20 °C kg/m³ | Density of the solid phase at the melting point kg/m³ | Density of the melt at the melting point kg/m³ | Length dilatation coefficient in the solid phase at 20 °C $K^{-1}$ | Length dilatation coefficient in the solid phase at high temperature $K^{-1}$ | Solidification shrinkage close to the melting point $\beta = \frac{\rho_s - \rho_L}{\rho_s}$ % |
|---|---|---|---|---|---|---|---|
| Pure iron | 1535 | 7878 | 7276 | 7036 | $12.2 \cdot 10^{-6}$ | $14.6 \cdot 10^{-6}$ (800 °C) | 3.3 |
| Cast iron: grey iron | 1090-1310 | 7000-7500 | | | $10.6 \cdot 10^{-6}$ | $14.3 \cdot 10^{-6}$ (500 °C) | 1.9 |
| white iron | | 7700 | | | | | 4.0 – 5.5 |
| Low-C steel | 1430-1500 | 7878-7866 | | | $11.8 \cdot 10^{-6}$ | $14.2 \cdot 10^{-6}$ (600 °C) | 2.5 - 3.0 |

Table 1 continued.

| Metal Alloy | Melting point/ melting interval °C | Density of the solid phase at 20 °C kg/m³ | Density of the solid phase at the melting point kg/m³ | Density of the melt at the melting point kg/m³ | Length dilatation coefficient in the solid phase at 20 °C $K^{-1}$ | Length dilatation coefficient in the solid phase at high temperature $K^{-1}$ | Solidification shrinkage close to the melting point $\beta = \frac{\rho_s - \rho_L}{\rho_s}$ % |
|---|---|---|---|---|---|---|---|
| High-C steel | 1180-1460 | 7800-7860 | | | $12.5 \cdot 10^{-6}$ | $13.6 \cdot 10^{-6}$ (600 °C) | 4.0 |
| Stainless 18-8 steel | | 7500 | | | $15.9 \cdot 10^{-6}$ | $28.1 \cdot 10^{-6}$ (1000 °C) | 4 |
| Al | 660 | 2699 | | 2365 | $23.5 \cdot 10^{-6}$ | $26.5 \cdot 10^{-6}$ (400 °C) | 6.6 |
| Al-bronze 90%Cu+ +10%Al | 1070 | 7500 | | | $18.0 \cdot 10^{-6}$ (20-300 °C) | | ~ 5 |
| Cu | 1083 | 8940 | | 7930 | $17.0 \cdot 10^{-6}$ | $20.3 \cdot 10^{-6}$ (1000 °C) | 3.8 |
| Brass 63%Cu+ +37%Zn | 915 | 8400 | | | $20.5 \cdot 10^{-6}$ (20-300 °C) | | ~ 5 |

## 10.4 Solidification and Cooling Shrinkage at Casting

When a casting solidifies a central cavity is in most cases formed in the casting due to solidification and cooling shrinkage. It is not desirable that any part of the pipe is situated within the casting. To avoid this an extra container – *feeder* or *casting head* – filled with molten metal during the casting can be placed on top of the mould.

### 10.4.1 Feeder System

If the method with a feeder will work it is necessary to control the solidification process at casting in such a way that the shrinkage pores, formed at the solidification, in their whole extension end up in the feeder. Efforts are made to direct the solidification by suitable cooling in such a way that the melt in the feeder solidifies more slowly than the last parts of the casting.

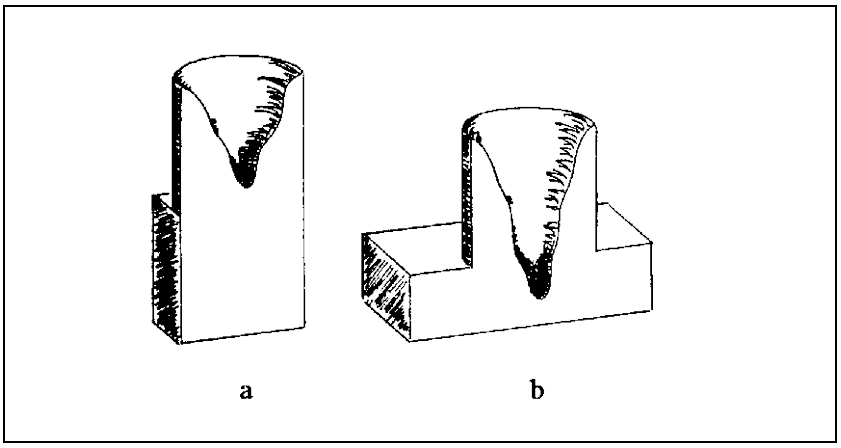


Figure 9.
Cylindrical feeder placed on two different castings, namely
a) a cube
b) a plate.
The plate has the same solidification time as the cube but a bigger volume.
The volume, shape and solidification time of the feeder is the same in both cases.

It is necessary to determine the volume of the feeder. It can possibly be easily found by applying Chvorinov´s rule (page 49 in chapter 4). By choosing the solidification time of the casting equal to the one of the feeder this equation may allow calculation of the feeder volume when the volume of the casting is known.

As can be concluded from figure 9 it is not sufficient with such a coarse calculation. In figures 9 a and 9 b the castings have different shapes and volumes but their solidification times are equal. Chvorinov´s rule thus gives the same value of the feeder in both cases.

Obviously the feeder volume is not big enough in case b to compensate the total solidification shrinkage of the casting. It is bigger in case b than in case a since the volume of the plate is bigger than that of the cube.

The volume of the feeder has to be adapted in such a way that two conditions will be fulfilled:

- The solidification time of the feeder must be equal to or longer than that of the casting. Then the melt in the feeder compensates the solidification shrinkage of the casting.
- The volume of the feeder must have a size. which at least is big enough to enclose the whole solidification shrinkage inside the feeder.

Thus we have a time condition and a volume condition. Both will be treated theoretically below.

**Time Condition of the Feeder**

At the beginning of the 1950$^{th}$ the American metallurgist Caine was the first one who pointed out that equal solidification time is not a sufficient condition for an efficient function of a feeder. He also pointed out that the pipe at equal solidification time often reaches the casting. He claimed that if the feeder solidifies at exactly the same time as the casting, the feeder volume has to be very much bigger than that of the casting. On the other hand, if the feeder solidifies essentially more slowly than the casting, the feeder volume can be chosen only slightly bigger than the volume decrease of the casting during the solidification process.

Adam and Taylor fulfilled Caine´s ideas theoretically. They derived a relation between the solidification shrinkage and the volumes of the feeder and the casting as a function of their corresponding contact areas with the melt.

Below we will use the following designations.

$A_c$ = contact area between the casting and the melt
$A_f$ = contact area between the feeder and the melt
$V_c$ = volume of the casting
$V_f$ = volume of the feeder
$V_{sm}$ = volume of solidified metal in the feeder
$\beta$ = solidification shrinkage = $\frac{\rho_s - \rho_L}{\rho_s}$.

The amount solidified metal in the feeder is equal to the feeder volume minus the *total* solidification shrinkage in feeder and casting:

$$V_{sm} = V_f - \beta\left(V_c + V_f\right) \tag{1}$$

Suppose that Chvorinov´s rule (pages 8-9) is valid for casting and feeder. The two solidification times are then

$$t_c = C_c\left(\frac{V_c}{A_c}\right)^2 \quad \text{and} \quad t_f = C_f\left(\frac{V_{sm}}{A_f}\right)^2 \tag{2) (3}$$

where $C_c$ and $C_f$ are proportionality constants. The minimum solidification time of the feeder equals the solidification time of the casting. This condition gives the relation

$$C_c\left(\frac{V_c}{A_c}\right)^2 = C_f\left(\frac{V_{sm}}{A_f}\right)^2 \tag{4}$$

$V_{sm}/V_c$ is solved from equation (4):

$$\frac{V_{sm}}{V_c} = \left(\frac{C_c}{C_f}\right)^{\frac{1}{2}} \cdot \frac{A_f}{A_c} \tag{5}$$

Equation (1) is divided by $V_c$, which gives

$$\frac{V_{sm}}{V_c} = \frac{V_f}{V_c} - \beta\left(1 + \frac{V_f}{V_c}\right) \tag{6}$$

After replacement of terms equation (6) can be written:

$$\left(1-\beta\right)\cdot\frac{V_f}{V_c} = \frac{V_{sm}}{V_c} + \beta \tag{7}$$

The value of $V_{sm}/V_c$ (equation (5)) is inserted into equation (7):

$$\left(1-\beta\right)\cdot\frac{V_f}{V_c} = \left(\frac{C_c}{C_f}\right)^{\frac{1}{2}} \cdot \frac{A_f}{A_c} + \beta \tag{8}$$

or

$$V_f = V_c \cdot \frac{\left(\frac{C_c}{C_f}\right)^{\frac{1}{2}} \cdot \frac{A_f}{A_c} + \beta}{\left(1-\beta\right)} \tag{9}$$

Equation (9) is the general time condition for the feeder volume. If feeder and casting both are made of sand, $C_c$ is equal to $C_f$ and $C_c / C_f = 1$ and we get a special case of equation (9):

$$V_f = V_c \cdot \frac{\frac{A_f}{A_c} + \beta}{(1-\beta)} \tag{10}$$

It is possible to calculate the volume of the feeder from equation (9) or (10) when all other quantities are known.

**Volume Condition of the Feeder**

The *efficiency of the feeder* is defined as the ratio ε of the volume of melt in the feeder, which has been added to the casting, and the volume of the feeder.

$$V_{add} = V_f - V_{sm} \tag{11}$$

and we get

$$\varepsilon = \frac{V_f - V_{sm}}{V_f} \tag{12}$$

The need of melt from the feeder is equal to the sum of the solidification shrinkage in the casting and the feeder.

$$V_f - V_{sm} = \beta \left(V_f + V_c\right) \tag{13}$$

From equations (12) and (13) we get the volume condition of the feeder:

$$V_f = \frac{\beta V_c}{\varepsilon - \beta} \tag{14}$$

A common cylindrical feeder with a height of 1.5 times its diameter has an efficiency of 14 %. If such a feeder is used at aluminium casting, which has a solidification shrinkage of approximately 7 %, equation (14) gives

$$V_f = V_c$$

which means that the volume of the feeder must be the same as that of the casting.

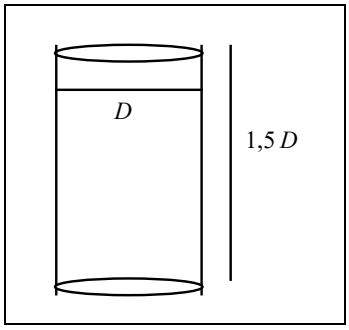

Figure 10.
Common type of feeder.

For steel with a solidification shrinkage of 3 % and the same shape of feeder and efficiency as above, the value of the feeder volume becomes far more favourable:

$$V_f = 0.27\ V_c$$

The efficiency of the feeder is obviously very important. It is desirable to have smallest possible feeder volume, especially at casting of big products. Equation (14) shows that the feeder volume decreases when the efficiency increases.

By insulation of the feeder it is possible to prolong its solidification time and increase its efficiency, which is apparent from figure 11.

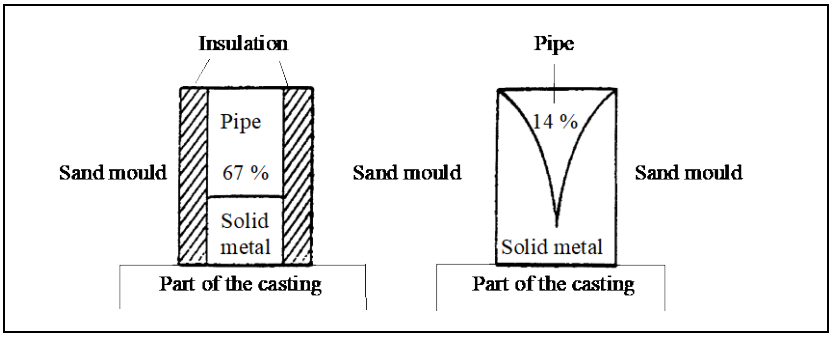


Figure 11.
Feeder with and without insulation of the envelope surface. The efficiencies ε are given in the figure.

A feeder will work in a satisfactory way only if both the time and volume conditions are fulfilled.

For compact castings the time condition gives a feeder volume, which is big enough for the pipe to be completely enclosed within the feeder.

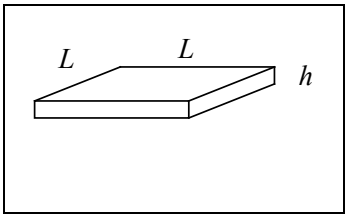


Figure 12.
If $L < 7h$ the feeder volume is determined by the volume condition. The feeder solidifies much more slowly than the plate.
If $L > 7h$ the feeder volume is determined by the time condition.

For thin flat castings (figure 12) the feeder volume is determined by the volume condition. They solidify rapidly and considerably much earlier than the melt in the feeder. The time condition is thus fulfilled simultaneously in this case. For thicker castings the time condition has to be considered.

---

**Example 1.**

A cube with the side 20 cm will be cast in carbon steel, which solidifies to austenite. To get a compact casting a cubic feeder is used. Due to heat losses the temperature of the melt in the casting is lowered 200 °C below the temperature of the feeder, when the casting starts to solidify. How large must the side of the feeder at least be in order to give a compact casting? The solidification shrinkage is 0.050.

**Solution:**

We assume that the side of the cubic feeder = $x$.

To solve the problem we will apply equation (8) on page 16. For this purpose we set up expressions for the constants $C_f$ and $C_c$ in Chvorinov´s rule for the feeder and the casting respectively by use of the formula given in the square on page 9.

Feeder constant:

$$C_f = \frac{\pi}{4} \cdot \left( \frac{\rho(-\Delta H) + c_p \rho (T_f - T_L)}{T_L - T_o} \right)^2 \cdot \frac{1}{k_{mould} \rho_{mould} c_p^{mould}} \quad (1')$$

Casting constant:

$$C_c = \frac{\pi}{4} \cdot \left( \frac{\rho(-\Delta H)}{T_L - T_o} \right)^2 \cdot \frac{1}{k_{mould} \rho_{mould} c_p^{mould}} \quad (2')$$

If we form the ratio $C_c / C_f$ the quantities $\rho$, $k_{mould}$, $\rho_{mould}$, $c_p^{mould}$ and $(T_L - T_o)$ disappear at the division and we get

$$\frac{C_c}{C_f} = \left( \frac{-\Delta H}{(-\Delta H) + c_p (T_f - T_L)} \right)^2 \quad (3')$$

This value is inserted into equation (8) on page 16 and we get

$$(1-\beta) \cdot \frac{V_f}{V_c} = \frac{A_f}{A_c} \cdot \left( \frac{C_c}{C_f} \right)^{\frac{1}{2}} + \beta = \frac{-\Delta H}{(-\Delta H) + c_p (T_f - T_L)} \cdot \frac{A_f}{A_c} + \beta \quad (4')$$

If we insert given values and table values into equation (8) we get:

$$0.95 \cdot \frac{x^3}{0.20^3} = \frac{5 \cdot x^2}{5 \cdot 0.20^2} \cdot \frac{276}{276 + 0.45 \cdot 200} + 0.050$$

One root of the equation is $x \approx 0.173$ m. The side of the cubic feeder ought to be chosen with a good margin.

**Answer:** The feeder shall be as big as the casting. i. e. the feeder cube shall have the side 20 cm.

---

---

$T_L$ = liquidus temperature and solidification temperature
$T_o$ = temperature of surroundings
$\rho$ = density of the steel melt
$-\Delta H$ = heat of fusion of steel
$c_p$ = heat capacitivity of steel
$T_f$ = temperature of the feeder
$k_{mould}$ = heat conductivity of the mould
$\rho_{mould}$ = density of the mould
$c_p^{mould}$ = heat capacitivity of the mould

---

---

**Example 2.**

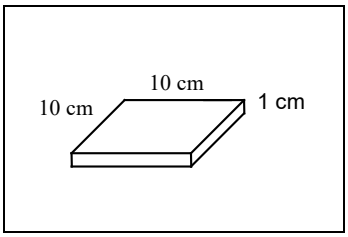


A square plate with the side 10 cm and the height 1.0 cm is to be cast. What volume shall the feeder at least have to make sure that the casting will be compact?

The efficiency of the feeder is 14 % and the solidification shrinkage of steel is 4 %.

**Solution:**

The height of the casting is small compared to its side. It is reasonable to use the volume condition for calculation of the feeder volume. Equation (14) will thus be used:

$$V_f = \frac{\beta V_c}{\varepsilon - \beta} = \frac{0.04 \cdot 0.01 \cdot 0.10^2}{0.14 - 0.04} = 40 \cdot 10^{-6}\ \mathrm{m}^3$$

**Answer:** The feeder volume must be at least 40 $\mathrm{cm}^3$, which corresponds to 40 % of the volume of the casting.

---

## 10.4.2 Influence of Alloying Elements and Mould Material on Pipe Formation

### Influence of Alloying Elements on Pipe Formation

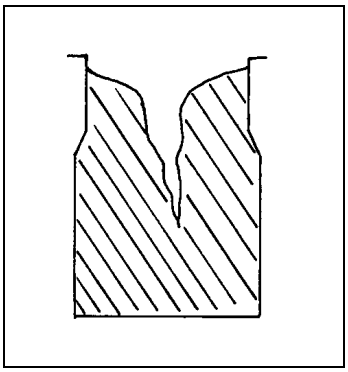

Figure 13.
Pipe in a pure metal.

The shape and extension of the pipe is strongly influenced by the concentration of alloying elements and by the mould material. There is a great difference in appearance of the pipe of a pure metal and the one of an alloy with a broad solidification interval.

- For a pure metal the pipe is concentrated to the upper, central parts of the casting.
- For an alloy the solidification shrinkage is distributed as pores over the whole volume.

The reason for this basic difference is, as has been mentioned before, that the pure metal solidifies along an even front while the alloy solidifies over a more or less broad solidification interval. In the latter case there is a dendrite network and melt simultaneously over the whole volume. As will be seen from examples 3 and 4 below, it is more difficult to supply melt as compensation for the solidification shrinkage to regions, which are solidifying through such a network of dendrites than in a homogenous melt without a solid phase.

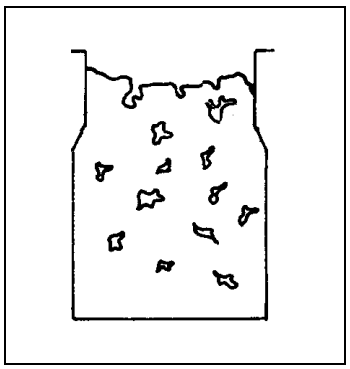

Figure 14.
Pipe in an alloy with a broad solidification interval.

**Fall of Pressure in Feeding Channels**

In each more or less viscous liquid a driving force must exist, which overcomes the internal friction in the liquid and forces the liquid through for example a tube or a channel. The driving force may be the gravitation force or caused by an applied external pressure difference between the two ends of the tube. The pressure in the streaming liquid – or in our case in the melt – decreases in the direction of its motion. The fall of pressure can be calculated by aid of the laws of hydromechanics.

---

**Example 3.**

Calculate the fall of pressure in the melt as a function of time $t$ during the solidification and distance $x$ along the casting in the figure below. The length $L$, the radius $r_o$ and the viscosity $\eta$ of the metal melt are known.

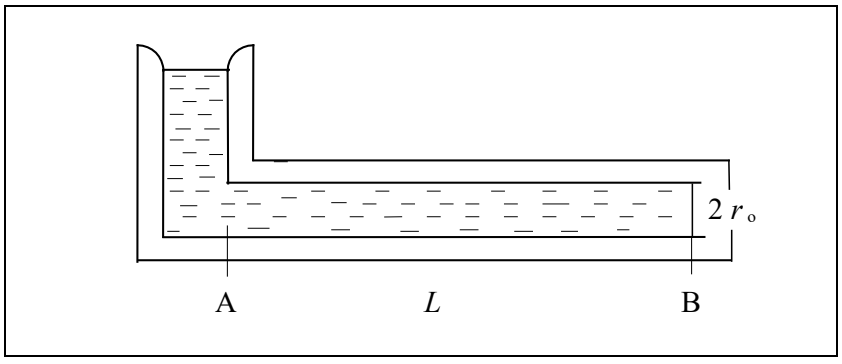

**Solution:**

When a pure metal melt solidifies in a mould of the shape given in the figure, solidification and cooling shrinkage occurs. The shrinkage cavities are filled with melt, which continuously flows through the open central channel available for the melt. Due to this flow a fall of pressure in the melt arises in the direction of the flow.

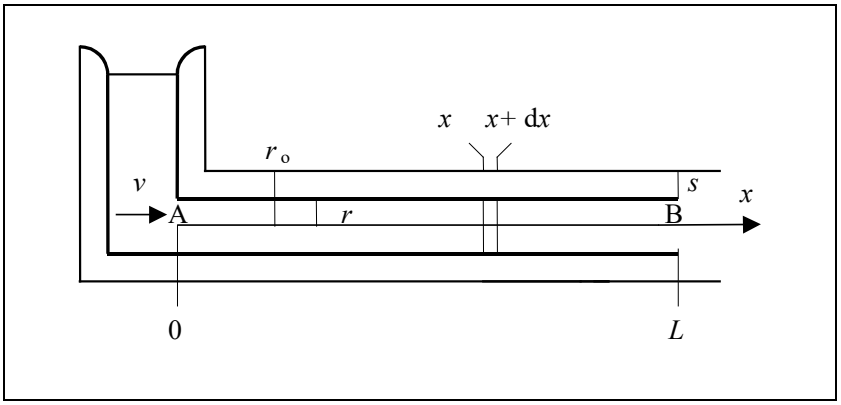


The pressure in point B is lower than that in point A because the melt flows in the channel to compensate the solidification and cooling shrinkage.

We introduce the following designations:

$\eta$ = viscosity of the metal melt
$r$ = radius of the channel
$v$ = rate of flow of the melt
$s$ = thickness of the solidifying shell = $r_o - r$.

Darcy′s law describes the fall of pressure $P$ in channels with streaming fluids:

$$\frac{dP}{dx} = -\frac{8\eta}{r^2} \cdot v \qquad (1')$$

During the time $\Delta t$ a layer with the volume

$$\Delta V_s = \Delta s \cdot 2\pi rx \qquad (2')$$

will solidify. Before this layer solidified it had the volume

$$\Delta V_{\mathrm{L}} = \frac{\Delta s \cdot 2\pi\, rx}{1-\beta} \qquad (3')$$

Both sides of equation (3′) are divided by $\Delta t$ and then $\Delta t \to 0$

$$\frac{\mathrm{d}V_{\mathrm{L}}}{\mathrm{d}t} = \frac{\mathrm{d}s}{\mathrm{d}t} \cdot \frac{2\pi\, rx}{1-\beta} \qquad (4')$$

In the same way we get from equation (2′):

$$\frac{\mathrm{d}V_{\mathrm{s}}}{\mathrm{d}t} = \frac{\mathrm{d}s}{\mathrm{d}t} \cdot 2\pi\, rx \qquad (5')$$

We introduce the solidification shrinkage $V = V_{\mathrm{L}} - V_{\mathrm{s}}$ and get by subtracting equation (5′) from equation (4′):

$$\frac{\mathrm{d}V}{\mathrm{d}t} = \frac{\mathrm{d}V_{\mathrm{L}}}{\mathrm{d}t} - \frac{\mathrm{d}V_{\mathrm{s}}}{\mathrm{d}t} = \frac{\mathrm{d}s}{\mathrm{d}t} \cdot 2\pi\, rx \cdot \left( \frac{1}{1-\beta} - 1 \right) = \frac{\mathrm{d}s}{\mathrm{d}t} \cdot 2\pi\, rx \cdot \frac{\beta}{1-\beta} \qquad (6')$$

The solidification shrinkage per unit time is replaced by new melt, which has the velocity *v*.

$$\frac{\mathrm{d}V}{\mathrm{d}t} = v \cdot \pi\ r^2 \qquad (7')$$

Equations (6′) and (7′), divided by $\pi\, r^2$, gives the equality:

$$v = \frac{\beta}{1-\beta} \cdot \frac{\mathrm{d}s}{\mathrm{d}t} \cdot \frac{2\pi\, rx}{\pi\, r^2} \qquad (8')$$

We apply Chvorinov′s rule (page 8):

$$t = C\left(\frac{V}{A}\right)^2 = C\left( \frac{\pi\, r_{\mathrm{o}}^2 x - \pi\, r^2 x}{2\pi \cdot \frac{r_{\mathrm{o}} + r}{2} \cdot x} \right)^2 = C\left(r_{\mathrm{o}} - r\right)^2 = C\,\mathrm{s}^2 \qquad (9')$$

where we have chosen an average value of the area *A* during the time interval 0 to *t*. *C* is the constant in Chvorinov′s rule.

$$s = \sqrt{\frac{t}{C}} \qquad (10')$$

We derive equation (10′) with respect to *t*

$$\frac{\mathrm{d}s}{\mathrm{d}t} = -\frac{\mathrm{d}r}{\mathrm{d}t} = \frac{1}{2\sqrt{C\,t}} \qquad (11')$$

We combine equations (1′), (8′) and (11′) and get

$$\mathrm{d}P = -\frac{8\eta}{r^2}\cdot\frac{\beta}{1-\beta}\cdot\frac{1}{2\sqrt{C\,t}}\cdot\frac{2\,\pi\,r}{\pi\,r^2}\cdot x\,\mathrm{d}x \qquad (12')$$

If we assume that $r$ is independent of $x$ we can integrate both sides of equation (12′) with respect to $x$.

$$\int_{P_o}^{P_x}\mathrm{d}P = P_x - P_o = -8\eta\cdot\frac{\beta}{1-\beta}\cdot\frac{1}{r^3\sqrt{C\,t}}\cdot\int_0^x x\,\mathrm{d}x \qquad (13')$$

Inserting $r = r_o - s = r_o - \sqrt{\frac{t}{C}}$ gives

$$P_x - P_o = -4\eta\cdot\frac{\beta}{1-\beta}\cdot\frac{x^2}{\left(r_o-\sqrt{\frac{t}{C}}\right)^3\sqrt{C\,t}}$$

**Answer:** $$P_o - P_x = 4\eta\cdot\frac{\beta}{1-\beta}\cdot\frac{x^2}{\left(r_o-\sqrt{\frac{t}{C}}\right)^3\sqrt{C\,t}}$$

---

The answer in example 3 above is valid for a pure metal. In example 4 below the conditions, which are present when an alloy with a broad solidification interval solidifies, will be illustrated.

---

**Example 4.**

Calculate the fall of pressure as a function of time $t$ during the solidification and the distance $x$ along the casting in the upper figure. The length $L$, radius $r_o$ and the viscosity of the melt are known. The figure in the margin illustrates the solidification process of the alloy.

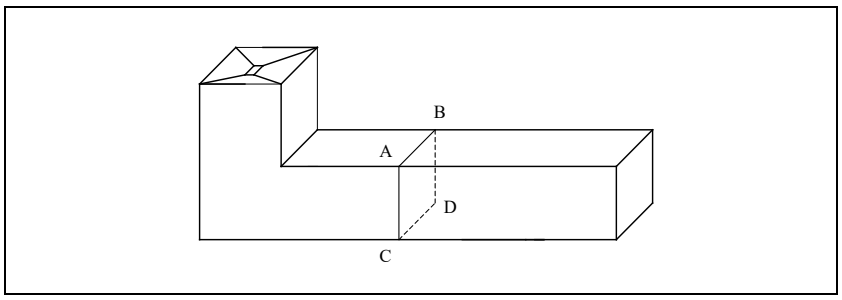


**Solution:**

In each single small and narrow channel a solidification shrinkage per unit time equal to

$$\frac{\mathrm{d}V}{\mathrm{d}t} = \frac{-\mathrm{d}r}{\mathrm{d}t} \cdot 2\pi rx \cdot \frac{\beta}{1-\beta} \qquad (1')$$

is obtained (compare equation (6′) in example 3 and use the relation d$s$ = – d$r$)) where $r$ is the radius of the channel. The solidification shrinkage will be compensated by new melt, which has the velocity $v$ and flows through the channel with radius $r$. In analogy with example 3 we get

$$\frac{\mathrm{d}V}{\mathrm{d}t} = v \cdot \pi \ r^2 \qquad (2')$$

If we equal the two expressions in equations (1′) and (2′) we get

$$v = \frac{\beta}{1-\beta} \cdot \frac{2x}{r} \cdot \left( \frac{-\mathrm{d}r}{\mathrm{d}t} \right). \qquad (3')$$

The further reasoning is identical with the corresponding one in example 3 above. The desired pressure difference will be the same as in example 3 if $r_\mathrm{o}$ is replaced by $\lambda/2$.

**Answer:** $$P_\mathrm{o} - P_x = 4\eta \cdot \frac{\beta}{1-\beta} \cdot \frac{x^2}{\left( \frac{\lambda}{2} - \sqrt{\frac{t}{C}} \right)^3 \sqrt{C\,t}}$$

where $\lambda$ is the distance between two dendrite arms and equal to the average distance between the channels in the alloy.

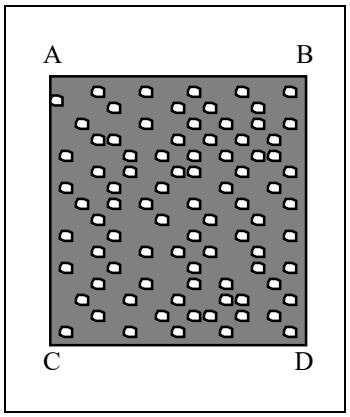


Dark areas are solidified metal. Bright areas represent a cross-sections of narrow channels containing melt.

---

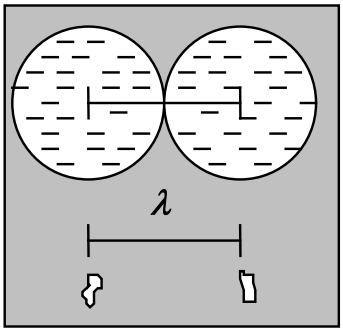


Figure 15.
Top: Appearance at the beginning of the solidification process.
Bottom: Appearance at the end of the solidification process.

The reason why $r_o$ equals $\lambda/2$ is as follows. In example 3 the radius of the channel is equal to $r_o$ before the solidification has started. The corresponding state in example 4 is when there is no solid phase and the many channels touch each other. Thus their initial radii equal half the average distance between the channels (upper part of figure 15).

When there are many narrow channels instead of a broad one the fall of pressure will be much larger and $\lambda/2 << r_o$. For this reason it is much more difficult to transport melt through materials with a broad solidification interval than through a pure metal.

**Effective Feeding Distance**

As can be concluded from examples 3 and 4 above the pressure in the channels, which supply melt to compensate the solidification shrinkage, decreases with the length of the channel.

The location of the feeder is thus very important. The feeder can only provide melt to a casting within a certain distance, the so-called *effective feeding distance*. If only one feeder is used and the casting has larger dimensions than the effective feeding distance a thin pipe appears at the centre line and the product will be wasted.

The shape of each casting can approximately be described as a composition of cubes, plates and rods. If the effective feeding distances are known for these basic units it is possible to estimate the effective feeding distance for the product in question.

Cubes offer minor feeding problems but rods must not be too long if the product is to be free from defects. The solidification processes of rods of different lengths and square cross-sections have been examined by careful and extensive experiments. Corresponding examinations have been performed for square plates of various thickness and cross-sections. The results of these examinations will be described on next page.

The general main rule for location of feeders is:

- It is necessary to control the solidification process in such a way that the melt solidifies last of all in the regions where the feeder is located.

As an example we choose the square rod in figure 16. The cooling is rapid at the corners of the end surface. The solidification is thus more rapid in these regions than in other parts of the casting. The cooling in these regions is slower than that at the end surface, because heat is conducted into the mould partly from the feeder and partly from the casting. The solidification occurs from the casting towards the feeder.

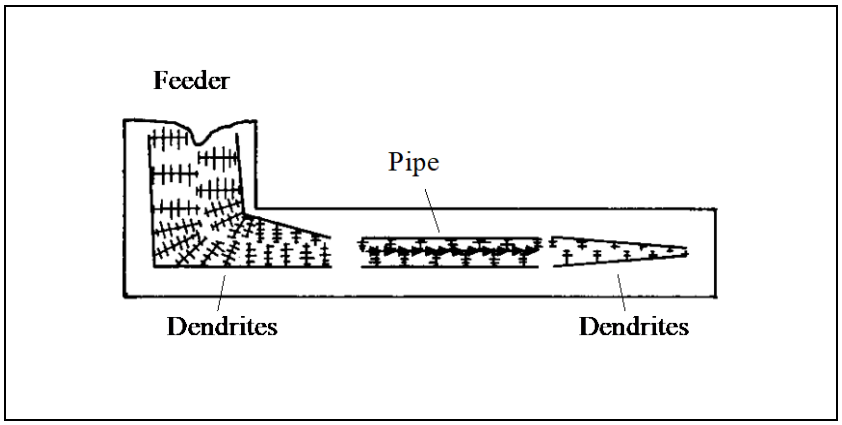


Figure 16.
Solidifying square rod with feeder.
The pipe and parts of the crystal structure have been drawn in the figure.

It is apparent from the example in figure 16 that it is not hard to get a compact casting close to the end surfaces and close to the feeder. To get a casting free from defects it is necessary to avoid pipe formation in the intermediate region. The *effective feeding distance* is defined as

Effective feeding distance = the longest total length, measured from the edge of the feeder, a pipe-free casting can have if pipe formation is to be avoided.

### *Effective Feeding Distance of a Square Rod*

If the rod is longer than the effective feeding distance a narrow central pipe is obtained. Due to boundary effects, caused by high temperature gradients at the feeder edge and the end surface of the rod, part of the central line becomes free from defects (figure 16).

For a square rod, cast in a low-carbon steel alloy, it has been found by experiments that the effective feeding distance $D_{max}$ is between two to four times the side $d$ of the cross-section square.

$$2d \leq D_{max} \leq 4d \qquad (15)$$

This condition is illustrated in figure 17.

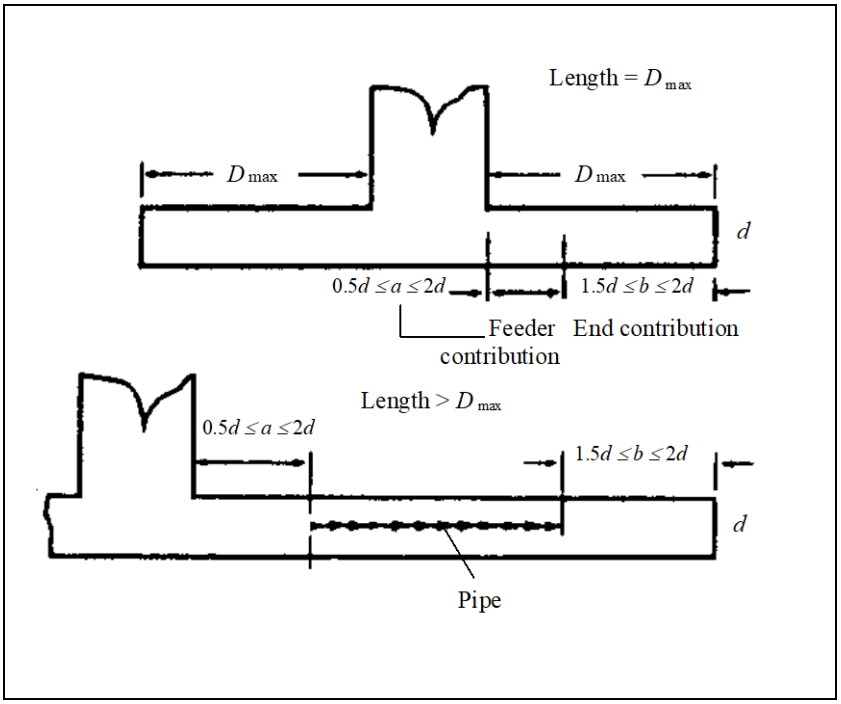


Figure 17.
Effective feeding distance of a rod with a square cross-section.
Simple feeder.

a) (upper figure)
Rod length = effective feeding distance.

b) (lower figure)
Rod length > effective feeding distance.

To avoid a result like the one in figure 17 b two feeders are used if one is not sufficient. Then there is no end surface and the cooling conditions will be different. Each feeder provides in this case maximum a distance of $2d$ with melt. The conditions are illustrated in figure 18.

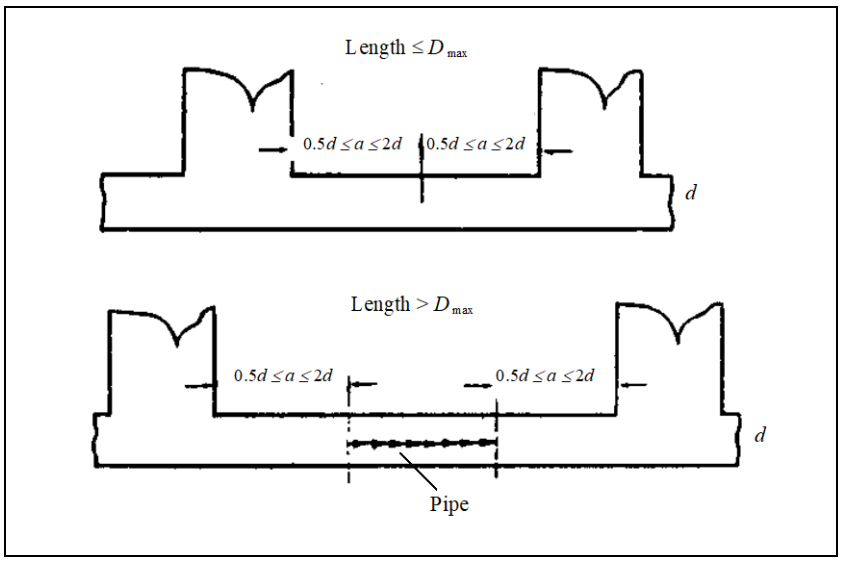


Figure 18.
Effective feeding distance of a rod with a square cross-section.
Double feeders.

a) (upper figure)
Rod length = effective feeding distance.

b) (lower figure)
Rod length > effective feeding distance.

### *Effective Feeding Distance of a Plate*

For a square plate of thickness *d*, cast in low-carbon steel, one has found that the temperature gradient at the feeder is responsible for 5*d* and the temperature gradient at the external edge of the plate for more than 6*d*. Thus one feeder is sufficient for a plate with a side equal to the width of the feeder plus (5*d*+6*d*)·2 = 22*d*. If the feeder is not sufficient a square-like pipe in centre of the plate is obtained. By aid of four feeders, conveniently located, plates with a diagonal equal to the widths of two feeders plus 5*d*·2 + (5*d*+6*d*)·2 = 32*d* can be cast without trouble (figure 19).

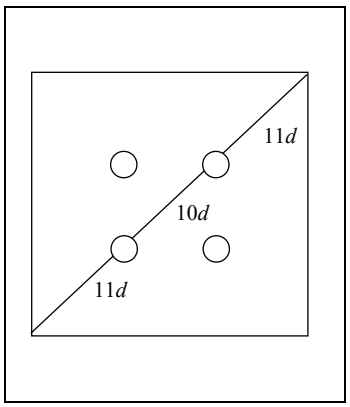


Figure 19.

Another way to increase the effective feeding distance is to use special cooling bodies in the way illustrated in figure 20.

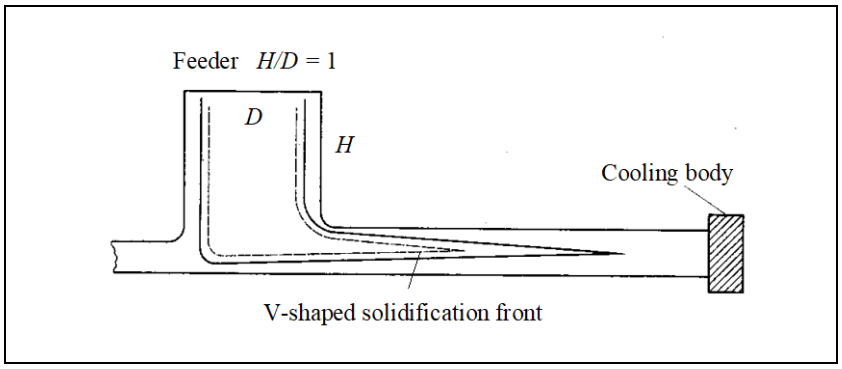


Figure 20.
Directed cooling is used to increase the effective feeding distances.

**Influence of Solidification Shrinkage on the Solubility Limit and Nuclei Formation at Gas Precipitation**

In examples 3 and 4 we have calculated the pressure fall, which arises in the melt during the solidification process due to solidification shrinkage. As a consequence of the reduced pressure in the interdendritic region the solubility limits of gases will decrease in these regions. The more material, which solidifies, the more will the pressure, and also the solubilities of the gases in the melt, decrease.

As an example to illustrate this effect we choose the segregation of hydrogen in iron base alloys. This has been treated earlier in the shape of solved example 5 on pages 52-53 in chapter 9 (figure 21 below).

The pressure fall in the melt can be calculated from the answer in example 4 on page 24. This equation is combined with Sievert´s law (chapter 9 page 9) for calculation of the hydrogen concentration in the melt as a function of the degree of solidification and the pressure in the melt. The degree of solidification is obtained by a heat balance equation. The result is described graphically in figure 22.

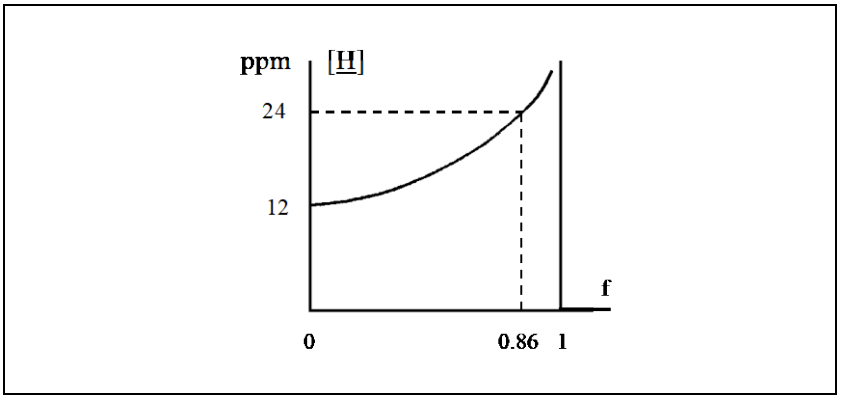


Figure 21.
Concentration distribution of hydrogen in a steel melt as a function of the degree of solidification with no attention to solidification shrinkage.

If the solidification shrinkage is disregarded (compare figure 22), the solubility limit at the pressure 1 atm is constant during the whole solidification process and equal to 24 ppm. As is seen in figure 22 the solubility limit of hydrogen decreases in reality strongly at the end of the solidification process and there is a great risk of pore formation and precipitation of hydrogen.

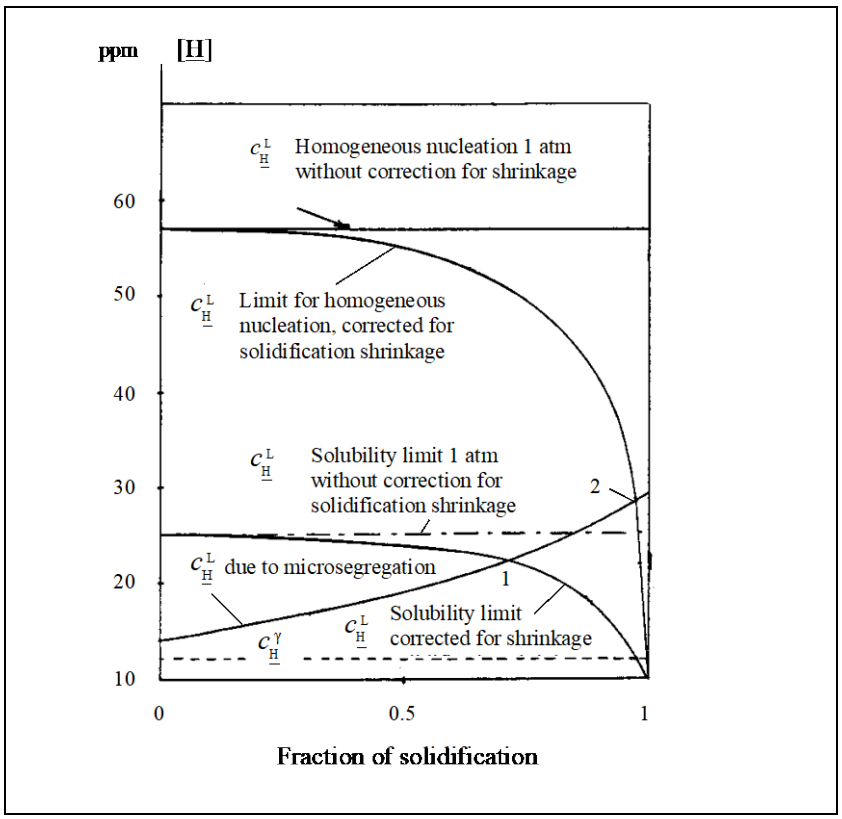


Figure 22.
The concentration distribution of hydrogen in the same steel melt as in figure 21 above, but with consideration to the influence of solidification shrinkage on the solubility limit of hydrogen precipitation.
The figure shows the influence of the pressure, due to the solidification shrinkage on the solubility limit of hydrogen.

The possibility to nucleate a pore increases drastically at the end of the solidification process.
The figure is valid for a given particular solidification rate.

Corresponding conditions are valid for nucleation of gas bubbles. The process is promoted by the solidification shrinkage, which can be seen in figure 22.

At point 1 the melt becomes supersaturated with $\underline{H}$ due to hydrogen segregation and pressure drop in the interdendritic regions. It will be difficult, though, to nucleate pores at this low supersaturation. Point 2 illustrates the possibility to nucleate a pore at the fraction of solidification $f = 0.96$.

## Influence of Mould Material on the Solidification Process

The *mould material* also influences the solidification process strongly. In a sand mould a mixture of solid and liquid phase exists in the centre of the casting during a very long time. In a cast iron chill-mould, which conducts heat more rapidly, this time is considerably shorter. These differences influence the appearance of the pipe in the same way as the differences in solidification interval of alloys do.

In a strongly cooled chill-mould the pipe get the appearance, which is illustrated in figure 13 on page 20, i. e. the same one as in a pure metal. In a sand mould the pipe has a similar appearance as the one in an alloy with a broad solidification interval ( figure 14 page 21).

Figure 23 a. Left figure. Appearance of the pipe at strong cooling during the solidification process.

Figure 23 b. Right figure. Appearance of a pipe at casting in a sand mould.

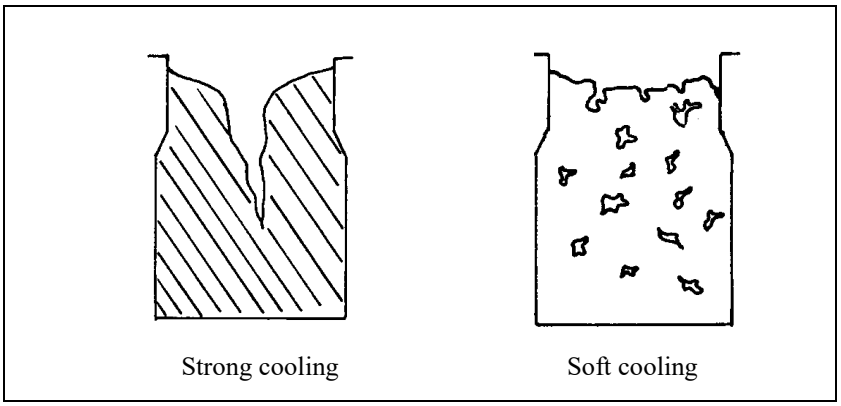


**Feeding of Alloys with Solidification Intervals**

Feeding of melt at casting of alloys with solidification intervals is more difficult than feeding castings of pure metals or eutectic alloys. A quantitative measure, which describes the type of feeding, is required. It is desirable that this measure is independent of the total solidification time. If so it can be used to compare different mould materials, different mould sizes and different alloys.

The longer there is a solid phase at the centre of the casting, the more difficult will the feeding be. As a quantitative measure of feeding the concept called Centreline Feeding Resistance (CFR) is often used. It is defined by aid of equation (16):

$$\mathrm{CFR} = \frac{t_{\mathrm{total}} - t_{\mathrm{initial}}}{t_{\mathrm{total}}} \cdot 100 \qquad (16)$$

where
CFR = measure of the feeding difficulty in %
$t_{total}$ = total solidification time
$t_{initial}$ = time when the solidification starts at the centreline.

It should be noticed that *the factor of solidification at the centreline* in reality is a *measure of the width of the solidification interval*. The essential fact is that CFR represents a *fraction* or a per cent part of the total solidification time and is *no* absolute time interval.

The centreline is most difficult to feed and thus is knowledge of the width of the solidification interval in this part of the casting especially important. However, we can not conclude that the presence of small amounts of solid phase at the centreline prevents feeding seriously. The start of the solidification process is just an experimentally suitable reference point on the time scale. It would be still better to use the time at which the melt cannot penetrate the crystal network, but this one is more difficult to determine experimentally and in addition dependent of the gas concentration of the metal.

If the solid phase of a pure metal is precipitated at the centreline for the first time at the end of the solidification time, the time of beginning solidification is approximately equal to the total solidification time, i. e. CFR ≈ 0. The broader the solidification interval of an alloy is the higher will its CFR be. An alloy has a CFR-value equal to 100 % if the solidification at the centre starts at $t = 0$. Table 2 gives examples of CFR-values for some alloys, solidified in a sand mould.

Table 2.
Central Feeding Resistance of some common alloys, solidified in a sand mould

| Alloy | CFR (%) |
|---|---|
| 18-8 steel (0.2 % C) | 35 |
| 12 % C Cr-steel | 38 |
| Cu | 0 |
| Brass | 26 |
| 0.6 % C-steel | 54 |
| Monel | 64 |
| Al- bronze | 95 |
| 92%Al+8%Mg | 91 |
| 95%Al+4.5%Cu | 96 |

**Feeder Volume as a Function of CFR**

It is possible to use CFR to calculate the size of a feeder. Instead of comparing the total solidification time $t_c$ of the casting and the total solidification time of the feeder $t_f$ we will compare $t_c$ with the time of beginning solidification at the centre of the feeder $t_{bscf}$.

We apply the definition of CFR on the feeder:

$$\mathrm{CFR} = \frac{t_\mathrm{f} - t_\mathrm{bscf}}{t_\mathrm{f}} \cdot 100 = \left(1 - \frac{t_\mathrm{bscf}}{t_\mathrm{f}}\right) \cdot 100 \tag{17}$$

or

$$t_\mathrm{bscf} = t_\mathrm{f} \cdot \left(1 - \frac{\mathrm{CFR}}{100}\right) \tag{18}$$

The value of $t_\mathrm{f}$ is taken from equation (3) on page 16 and inserted into equation (18).

$$t_\mathrm{bscf} = C_\mathrm{f} \cdot \left(\frac{V_\mathrm{sm}}{A_\mathrm{f}}\right)^2 \cdot \left(1 - \frac{\mathrm{CFR}}{100}\right) \tag{19}$$

If we introduce the condition that the solidification time of the casting is equal to the time of beginning solidification at the centre of the feeder

$$t_\mathrm{c} = t_\mathrm{bscf} \tag{20}$$

we get

$$C_\mathrm{c} \cdot \left(\frac{V_\mathrm{c}}{A_\mathrm{c}}\right)^2 = C_\mathrm{f} \cdot \left(\frac{V_\mathrm{sm}}{A_\mathrm{f}}\right)^2 \cdot \left(1 - \frac{\mathrm{CFR}}{100}\right) \tag{21}$$

If $C_\mathrm{f}$ is replaced by $C_\mathrm{f} \cdot \left(1 - \frac{\mathrm{CFR}}{100}\right)$ in equation (4) on page 16 it will be identical with equation (21). We can do the same in equation (8) on page 16 and get an expression, which can be used for calculation of the feeder size. If we assume that the condition $t_\mathrm{c} = t_\mathrm{bscf}$ is valid this relation will be

$$(1 - \beta) \cdot \frac{V_\mathrm{f}}{V_\mathrm{c}} = \left(\frac{C_\mathrm{c}}{C_\mathrm{f} \cdot \left(1 - \frac{\mathrm{CFR}}{100}\right)}\right)^{\frac{1}{2}} \cdot \frac{A_\mathrm{f}}{A_\mathrm{c}} + \beta \tag{22}$$

Apparently a different result is obtained when we use the condition $t_\mathrm{c} = t_\mathrm{bscf}$ than the one we get when the relation $t_\mathrm{c} = t_\mathrm{f}$ is applied. The higher CFR is the larger will the feeder volume be.

## 10.5 Solidification Shrinkage at Ingot Casting

### 10.5.1 Pipe Formation in Ingots

When a melt is teemed into a chill-mould it starts to solidify because heat is transported away from the melt and outwards through the chill-mould. The solid phase nucleates on the cold mould surface and form a layer, which grows inwards, perpendicular to the surface.

A thin film of solidified steel is formed at the bottom and walls of the cold chill-mould, which fixes the external shape of the ingot (figure 24 a). The cooling shrinkage results in a lowering of the free surface of the steel melt (figure 24 b).

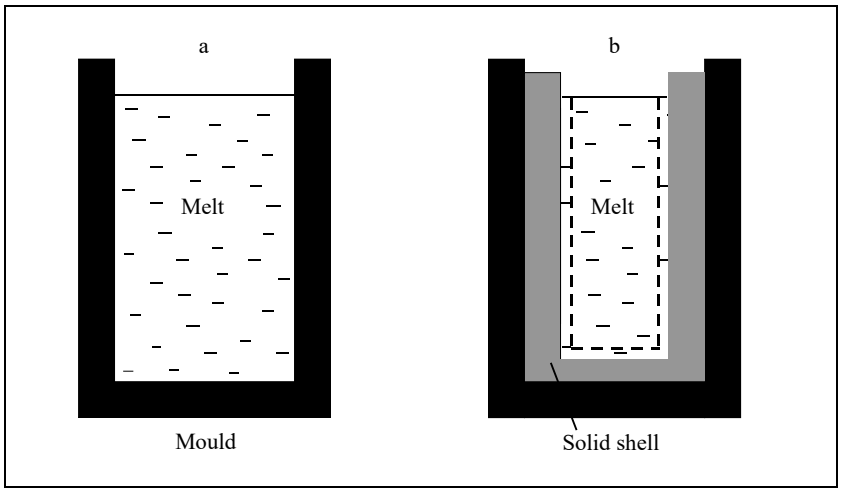


Figure 24.
Solidification process at solidification shrinkage.
a) no solidification
b) steel shell + melt.

The continued solidification is illustrated in figure 25. As a result of the proceeding solidification shrinkage the free surface of the remaining melt in the centre is gradually lowered. When the entire ingot has solidified a funnel-shaped cavity has been formed at the top of the ingot. Such a cavity is called a *pipe*.

The walls in a pipe oxidise and do *not* seal at rolling. The entire part of an ingot, which contains a pipe, is thus wasted.

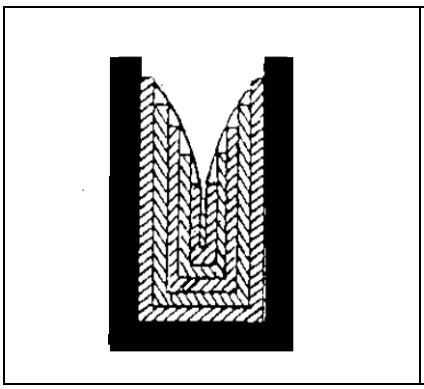

Figure 25.
Typical pipe of an unshielded ingot.

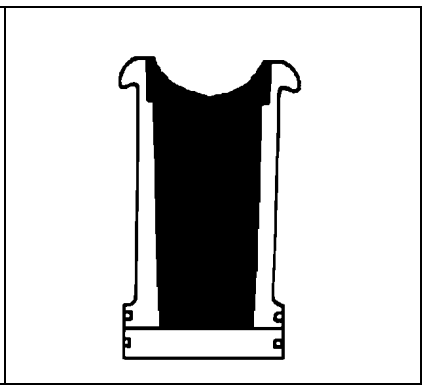

Figure 26.
Solidified ingot with a hot top.

In order to get a maximum yield it is desirable to make the pipe volume as small as possible. To reduce the height of the pipe, a so-called *hot top* is used to insulate the upper part of the ingot. Then this part cools more slowly than the rest of the ingot. This method is successful when properly applied, which can be seen in figure 26. The better the hot top is, the smaller will the pipe volume be.

The method will be treated in detail on page 44.

**Pipe Formation in Ingots**

At the beginning of the 20th century the English metallurgist Brearley used a stearine melt in his simulation experiments to study the formation of a pipe at solidification of an ingot.

Molten stearine was cast in an ordinary small chill-mould and was allowed to solidify under specified times of various length. Then the ingots were rapidly decanted (emptied of molten stearine). The stearine ingots were cut lengthways and a series of instant pictures of the formation and development of the pipe was obtained.

Figure 27 shows sketches from Brearley´s original experiments. The solidification process proceeds by growth of the stearine crystals perpendicularly from the sides towards the centre of the

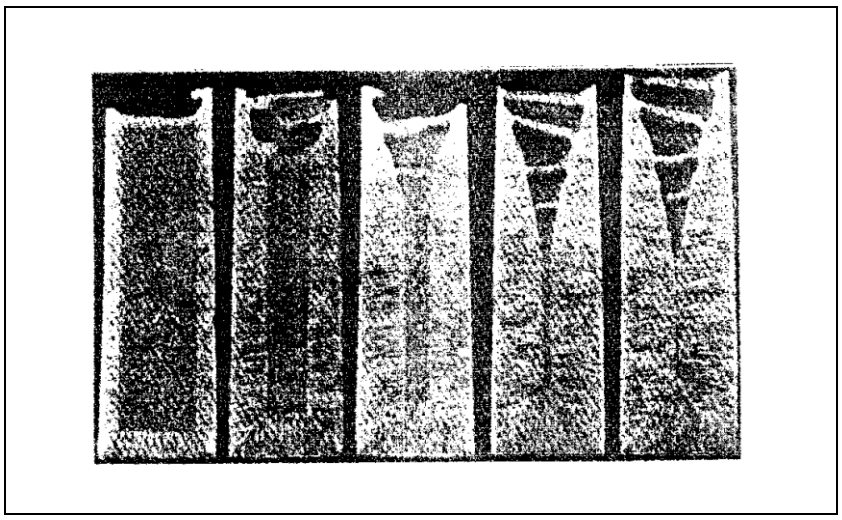

Figure 27.
Five different stages in the formation process of a pipe.

ingot. Simultaneously a shrinkage pore, shaped as an upside down cone, is formed at the top of the ingot.

Later experiments on metal ingots have shown good agreement with Brearley´s observations.

It is interesting to notice the bridges of solid metal across the pipe. When a closed pore is formed between the solid crust and the metal melt, the heat emission from the upper surface is drastically reduced. The upper surface is equivalent with an insulating cover. This model will be used at the theoretical treatment in sections 10.5.2 and 10.5.3.

Brearley also illustrated the difference in extension in ingot with only equiaxed crystals (figure 29) and ingots with columnar structure (figure 28) by aid of stearine ingots. A comparison between figures 28 and 29 shows that

*Ingots with equiaxed crystal structure have a smaller pipe than ingots with columnar crystal structure.*

The reason is probably that ingots with uniaxial crystals in addition to the pipe also contain a great number of micropores.

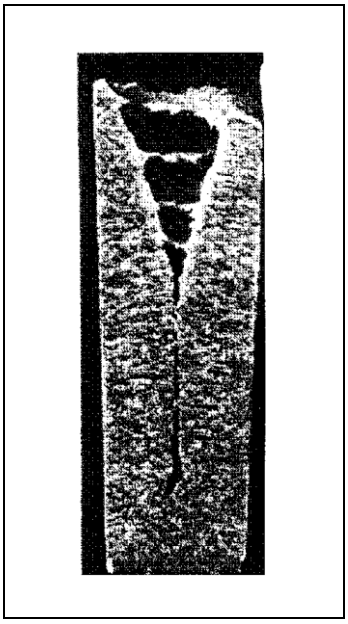

Figure 28.
The extension of the pipe in an ingot with columnar crystals.

In ingots with columnar crystal structure the transport of melt through the dendrite network occurs more and more slowly the thinner the free channels between the dendrite arms are.

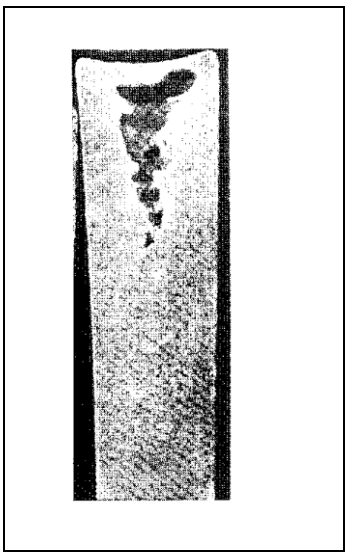

Figure 29.
The appearance of the pipe in an ingot with equiaxed crystal structure.

The pipe has a similar appearance in alloys with a broad solidification interval. In these cases the solidification front is very irregular. For this reason one might get a deep pipe, which partly consists of dendrites, from which the rest melt has been soaked away.

We have mentioned earlier that the volume of the pipe can be reduced by insulation of the upper surface of the ingot during the solidification process with a so-called hot top. In this way the yield of useful ingot can be increased.

In the following sections theoretical treatments of the pipe formation with and without a hot top are performed. The advantage of using a hot top is illustrated by comparison of two solved examples.

## 10.5.2 Theory of Pipe Formation in Ingots

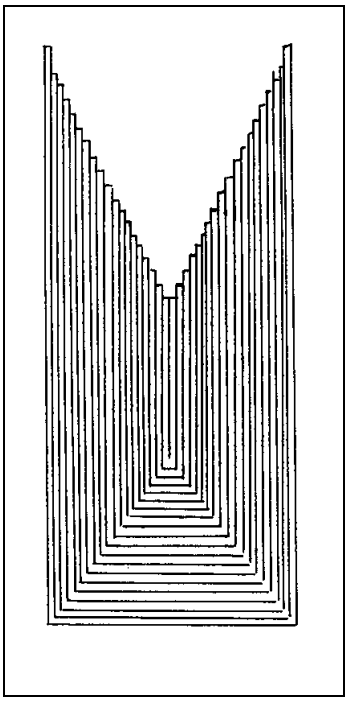

Figure 30.
The shell model of pipe formation.

Brearley´s simulation experiments with stearine melts initiated a theoretical model of pipe formation.

The solidification front moves from the outer parts of the ingot towards the centre of the melt. For each layer, which solidifies, the upper surface is lowered a distance, which corresponds to the solidification shrinkage of the solidified layer. This model forms the basis of the theoretical calculation of the shape of the pipe.

We start with a chill-mould with the data given below and make the following assumptions:

Internal width of the chill-mould $= x_o$
Internal length of the chill-mould $= y_o$
Internal height of the chill-mould $= z_o$

We neglect the cooling shrinkage and assume further that

- the chill-mould is filled with melt when the solidification starts
- the chill-mould cools the melt uniformly
- the melt has a very narrow solidification interval.

We will try to describe the shape of the pipe mathematically. A good method is to regard the solidification as a discontinuous process, where thin layers gradually solidify and by their solidification shrinkage causes stepwise lowering of the free surface of the melt.

We look at the chill-mould from above in figure 32. When the solidification has proceeded for some time, a layer of solid metal with the thickness $\Delta x$ respectively $\Delta y$ has been formed in the chill-mould. The region between the outer rectangle $x_o\, y_o$ and the inner rectangle $xy$ is filled with solid metal. Inside the rectangle $xy$ there is melt. The thin layer with thickness d$x$ respectively d$y$, which will solidify in next step, has been drawn in the figure.

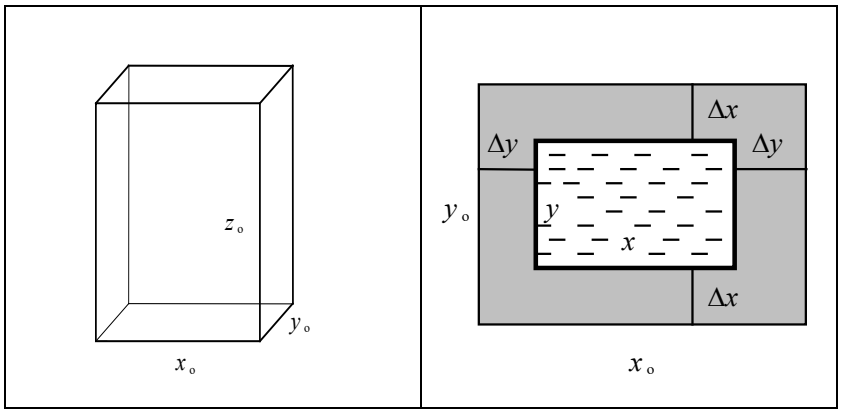


Figure 31. Left figure. Chill-mould with the sides $x_o$, $y_o$ and $z_o$.

Figure 32. Right figure. Horizontal cross-section of the chill-mould seen from above.

Figure 33 shows a vertical cross-section of the chill-mould. The solidification shrinkage of the layers of solidified metal around the inner walls of the mould with the thickness $\Delta x$, $\Delta y$ respectively $\Delta z$ at the bottom has resulted in a lowering of the upper surface with the amount d$Z$.

By aid of a material balance we can get a relation between the quantities given above and the density of the solid metal $\rho_s$ and the density $\rho_L$ of the melt.

Figure 33a. Left figure.
Vertical cross-section of the chill-mould. Consider the melt in the volume *xyz* before the thin layer in figure 33 b has solidified.

Figure 33 b. Right figure.
The thin layer has the thickness d*x* respectively d*y* on the side walls and d*z* at the bottom surface.
The solidification shrinkage of the layer has caused a lowering of the upper surface of the melt with the amount d*Z*.

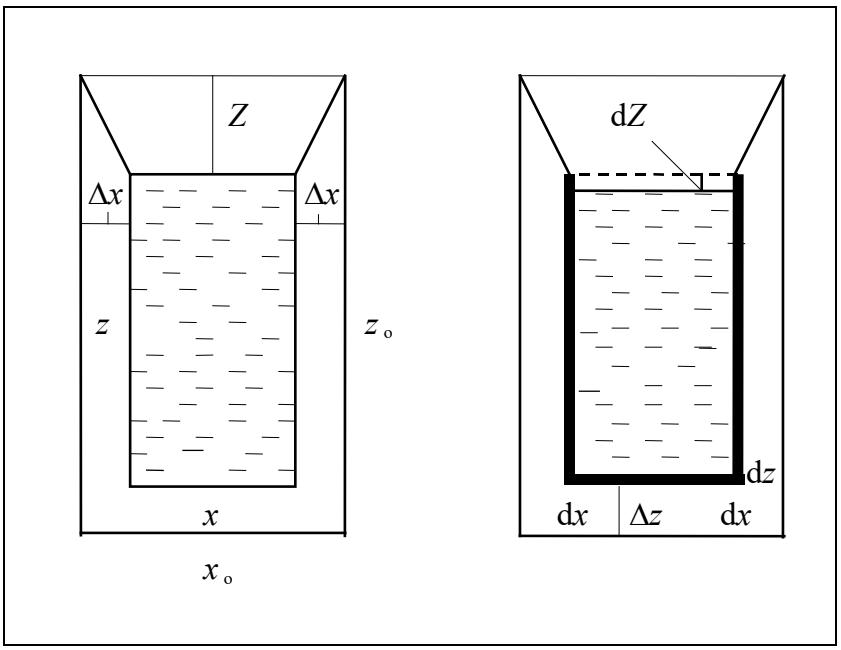


The volume of the melt before the thin layer has solidified is *xyz*. When the thin layer has solidified the remaining melt has the volume $(x-2\mathrm{d}x)\cdot(y-2\mathrm{d}y)\,)\cdot(z-\mathrm{d}z-\mathrm{d}Z)$. The figure 2 in the first two factors originates from *two* layers with the thickness d*x* respectively d*y* on the four vertical sides, which enclose the melt.

The thin layer consists of five planar plates with the total volume $2yz\mathrm{d}x + 2xz\mathrm{d}y + xy\mathrm{d}z$.

The mass is not changed by the fact that part of the melt solidifies:

$$\rho_{\mathrm{L}} xyz = \rho_{\mathrm{L}}(x-2\mathrm{d}x)\cdot(y-2\mathrm{d}y)\cdot(x-\mathrm{d}x-\mathrm{d}Z)+\rho_{\mathrm{S}}\,(2yz\mathrm{d}x+2xz\mathrm{d}y+xy\mathrm{d}z)$$

All terms of second order (of the type d*x*d*y*) can be neglected. After reduction the relation can be written

$$\rho_{\mathrm{L}} xy\mathrm{d}Z = (\rho_{\mathrm{s}}-\rho_{\mathrm{L}})\cdot 2yz\mathrm{d}x + (\rho_{\mathrm{s}}-\rho_{\mathrm{L}})\cdot 2xz\mathrm{d}y + (\rho_{\mathrm{s}}-\rho_{\mathrm{L}})\cdot xy\mathrm{d}z$$

or

$$\frac{\mathrm{d}Z}{\mathrm{d}x}\rho_{\mathrm{L}} xy = \frac{\rho_{\mathrm{s}}-\rho_{\mathrm{L}}}{\rho_{\mathrm{L}}}\cdot\left[\left(2yz+2xz\cdot\frac{\mathrm{d}y}{\mathrm{d}x}\right)+xy\cdot\frac{\mathrm{d}z}{\mathrm{d}x}\right]\cdot\mathrm{d}z \qquad (23)$$

Equation (23) is combined with the definition of solidification shrinkage:

$$\beta = \frac{\rho_s - \rho_L}{\rho_s} \tag{24}$$

which can be written

$$\beta = 1 - \frac{\rho_L}{\rho_s} \qquad \Rightarrow \qquad \frac{\rho_s}{\rho_L} = \frac{1}{1-\beta} \tag{25}$$

The last expression can be used to calculate

$$\frac{\rho_s - \rho_L}{\rho_L} = \frac{\rho_s}{\rho_L} - 1 = \frac{1}{1-\beta} - 1 = \frac{\beta}{1-\beta} \tag{26}$$

The relation (26) is inserted into equation (23) and we get:

$$\frac{1-\beta}{\beta} \cdot \frac{dZ}{dx} = \frac{2yz + 2xz \cdot \frac{dy}{dx}}{xy} + \frac{dz}{dx} \tag{27}$$

This is the differential equation which has to be solved to get $Z$ as a function of $x$, $y$ and $z$. It is rather complicated and has in most cases to be solved numerically.

If the solidification rates are equal along the vertical sides we have $dx = dy$. In most cases we also have $dz/dx = C$ where C is a constant. The differential equation (27) is then simplified to

$$\frac{1-\beta}{\beta} \cdot \frac{dZ}{dx} = \frac{2(x+y)z}{xy} + C \tag{28}$$

Nor can this equation be solved exactly, other than in some special cases. To proceed further we replace $x$, $y$ and $z$ with

$$x = x_o - 2\Delta x$$
$$y = y_o - 2\Delta y = y_o - 2\Delta x$$
$$z = z_o - C\Delta x - Z$$

Inserting these expressions into equation (28) we get

$$\frac{1-\beta}{\beta} \cdot \frac{dZ}{dx} = \frac{2(x_o + y_o - 4\Delta x)(z_o - C\Delta x - Z)}{(x_o - 2\Delta x)(y_o - 2\Delta x)} + C \tag{29}$$

In this version the differential equation can be solved numerically. The result is shown in figure 34. It can be seen that the pipe is very deep in the ingot. To get a better yield it is obviously advisable to use a hot top.

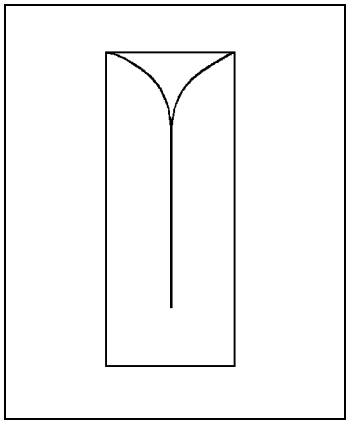

Figure 34.

Analytical solutions of equation (29) exist in some simple special cases, for example when the chill-mould has a square or circular cross-section and if the solidification rates from the sides and the bottom are equal. In these cases equation (29) is transformed into a linear differential equation, which can be solved by standard methods.

If the cross-section of the chill-mould is a square and the solidification rates at the sides and at the bottom are equal the following relations are valid:

$x_o = y_o$ $\qquad C = 1$

$x = y$ $\qquad$ and

$dx = dy = dz$ $\qquad \Delta x = \Delta y = \Delta z$

If these expressions are introduced into equation (29) and we solve the differential equation. In this case the solution will be:

$$Z = z_o - \frac{x_o}{2} - \frac{3\beta}{1-5\beta}\left(x_o - 2\Delta x\right) + \left(\frac{3\beta x_o}{1-5\beta} - z_o + \frac{x_o}{2}\right)\cdot\left(\frac{x_o - 2\Delta x}{x_o}\right)^{\frac{4\beta}{1-\beta}} \qquad (30)$$

---

**Example 5.**

A 2.6 ton ingot is to be cast in a chill-mould with the dimensions which are found in the left figure below. The chill-mould has a square cross-section. The solidification shrinkage is 0.050.

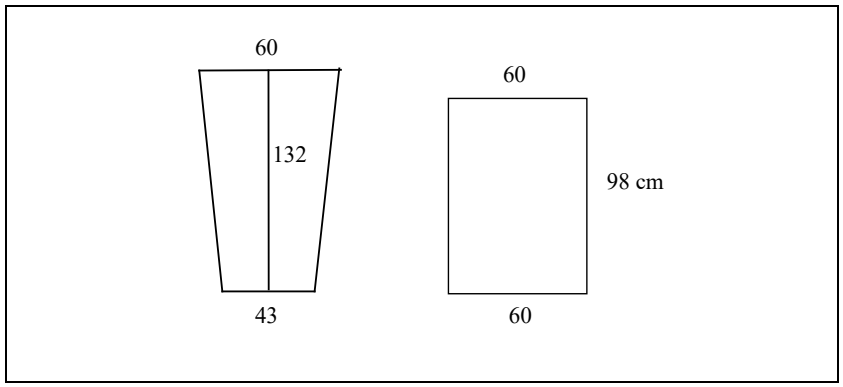


Left figure:
Chill-mould. The dimensions are given in cm.

Right figure:
Approximation to a square chill-mould.

a) Calculate the concave profile of the pipe as a function of the distance to the chill-mould wall and plot the result in a figure.

b) Calculate the maximum depth of the pipe.

**Solution:**

a) Since the chill-mould has a square cross-section it is reasonable to approximate the real chill-mould with a straight chill-mould with a constant cross-section area. We choose its side to 60 cm and adapt the height in such a way that the volume is equal in the two cases.

$x_o = 0.60$ m
$z_o = 0.98$ m
$\beta = 0.050$

These values are inserted into equation (29), which is valid in this case:

$$Z = 0.98 - \frac{0.60}{2} - \frac{3 \cdot 0.050}{1 - 5 \cdot 0.050}(0.60 - 2\Delta x) + \left(\frac{3 \cdot 0.050}{1 - 5 \cdot 0.050} - 0.98 + \frac{0.60}{2}\right) \cdot \left(\frac{0.60 - 2\Delta x}{0.60}\right)^{\frac{4 \cdot 0.050}{1 - 0.050}}$$

which can be reduced to

$$Z = 0.68 - 0.200 \cdot (0.60 - 2\Delta x) - 0.48 \cdot \left(\frac{0.60 - 2\Delta x}{0.60}\right)^{0.210} \qquad (1')$$

where $0 < \Delta x < x_o/2 = 0.30$

Equation (1′) is the desired function. In order to plot it we choose some suitable values of $\Delta x$ and calculate the corresponding values of $Z$.

| Δx | Z |
|---|---|
| 0.00 | 0.00 |
| 0.05 | 0.04 |
| 0.10 | 0.09 |
| 0.15 | 0.14 |
| 0.20 | 0.20 |
| 0.25 | 0.28 |
| 0.27 | 0.32 |
| 0.29 | 0.40 |
| 0.295 | 0.44 |
| 0.30 | 0.68 |

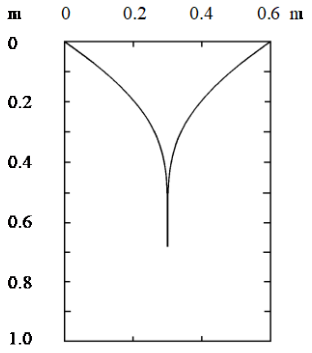

b) the maximum depth of the pipe corresponds to $\Delta x = x_o/2$. The value equals $z_o - x_o/2 = 0.98 - 0.60/2 = 0.68$ m since we have assumed that the solidification rate is the same from all sides in the whole ingot.

**Answer:** a) Se equation (1´) and the figure above.
b) The depth of the pipe is approximately 70 cm.

---

### 10.5.3 Theory of Pipe Formation in Ingots with Hot Top

In ingots, which will be warm-rolled later, insulated pores will be sealed. Provided that air has no admission to the walls of the pores and oxidize them, the pores have no destructive effect on the quality of the ingot.

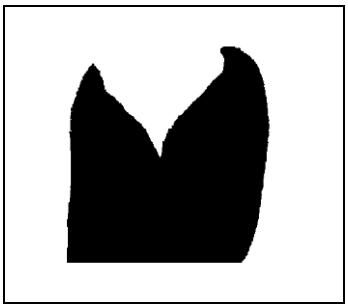

Figure 35.
”Fish-tail”.

On the other hand, a pipe is always exposed to contact with air and oxidation cannot be avoided. When an ingot with a pipe is warm-rolled a so-called ”fish-tail” appears. Remaining oxide on the surface of the pipe causes this defect. The oxide prevents the pipe from sealing. The damage will be more pronounced the bigger the pipe is and may have the consequence that a large fraction of the rolled ingot has to be discarded.

To avoid this, efforts are made to insulate or heat the upper surface of the ingot to make it solidify last of all. The best method is to place a so-called hot top on the upper surface of the ingot.

A hot top can be described as an insulated container. The insulation causes the ingot to solidify more slowly than the ingot as a whole. This is just the effect, which is attained. The slow solidification in the centre prevents the appearance of a deep pipe and the yield becomes essentially much better with than without a hot top.

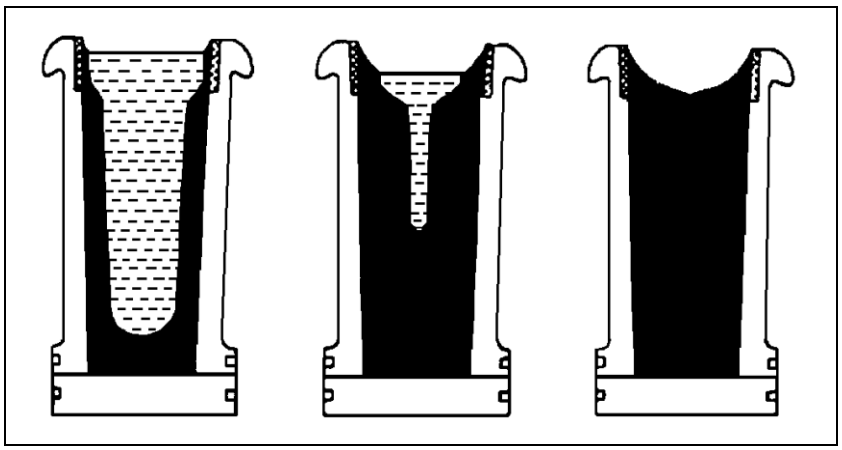

Figure 36.
Solidification process in ingots with a hot top.

The volume of a hot top equals 10-15 % of the total volume of the ingot. The better hot top is, the smaller will its volume be. A good hot top is made of a material with low heat capacitivity and low heat conduction. Unfortunately highly insulating and porous materials often have low mechanical strength and can not be used. The top must not be deformed by the melt.

An incorrect dimensioning of the top, i. e. too small height, may get the consequence that the pipe creeps into the ingot below the hot top, which has to be avoided. If this would occur before the centre of the ingot has solidified, the pipe might force its way very far down into the ingot.

**Theoretical Model**

By using a theoretical model of a hot top it is possible to make a rough estimation and calculate a suitable size of the top.

Figure 37 shows calculated solidus isotherms close to the hot top in an ingot. It can be seen that the isotherms are perturbed only within a relatively narrow region close to the boundary between the ingot and the hot top. The conclusion of this is that the ingot and the top can be treated as two separate bodies at a simple analysis and that the solidification time of each of them can be calculated separately.

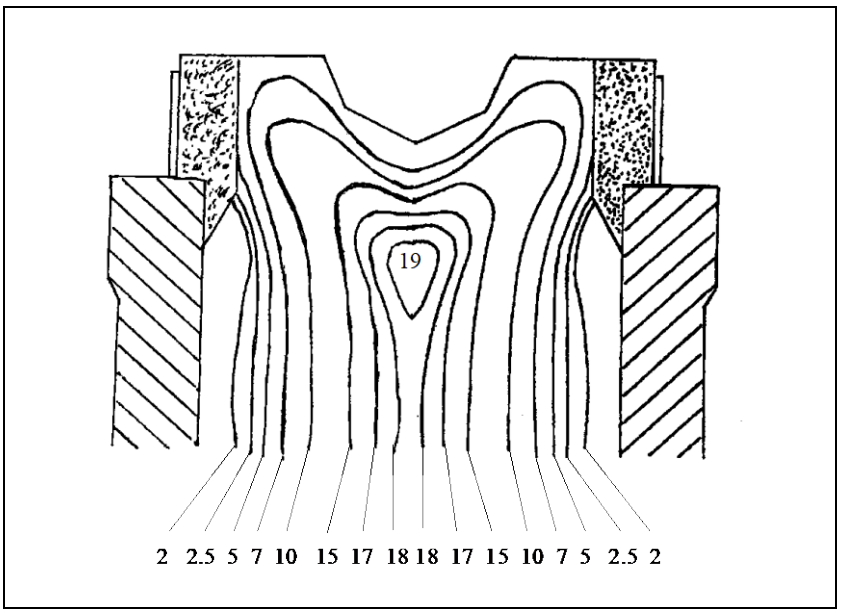


Figure 37.
The positions of the solidification front in an ingot with hot top at various times.
The time is given in hours after the start of the solidification.

By aid of mathematical models for the heat flow in a solidifying melt it is possible to calculate the temperature field and the position of the solidification front in the melt by aid of computers. These methods do not consider the shrinkage in a hot top during the solidification process. For such calculations it is convenient to use the same simple method as above for the solidification of the ingot and concentrate on the solidification shrinkage.

If we assume that the upper surface of the top does not solidify we can set up a simple material balance which gives the shrinkage in the top as a function of the amount solidified metal in top and ingot. When a thin layer solidifies in the top and the ingot the solidification shrinkage is compensated by melt, which fills this volume difference. The upper surface of the remaining melt sinks in proportion to the withdrawn melt.

The mass of the soaked melt is equal to the contribution of mass to the ingot:

$$\rho_{\mathrm{L}} A_{\mathrm{top}} \mathrm{d}Z_{\mathrm{top}} = \left(\rho_{\mathrm{s}} - \rho_{\mathrm{L}}\right)\left(\mathrm{d}V_{\mathrm{top}} + \mathrm{d}V_{\mathrm{ingot}}\right) \tag{31}$$

where

$A_{top}$ = cross-section area of the hot top
$dZ_{top}$ = shrinkage of the upper surface of the melt due to the solidification shrinkage of the thin layer
$dV_{top}$ = volume of the thin layer in the top which has solidified
$dV_{ingot}$ = volume of the thin layer in the ingot which has solidified
$\rho_S$ = density of the solid metal
$\rho_L$ = density of the melt.

To derive an expression of the solidified volumes we need to know the relative solidification rates in top, ingot and ingot bottom. Thus we introduce special designations for the relative solidification rates in the top respectively ingot bottom with the solidification rate in the *x*-direction as basis.

$$n = \frac{dx_{top}}{dx_{ingot}} \tag{32}$$

$$m = \frac{dz_{ingot}}{dx_{ingot}} \tag{33}$$

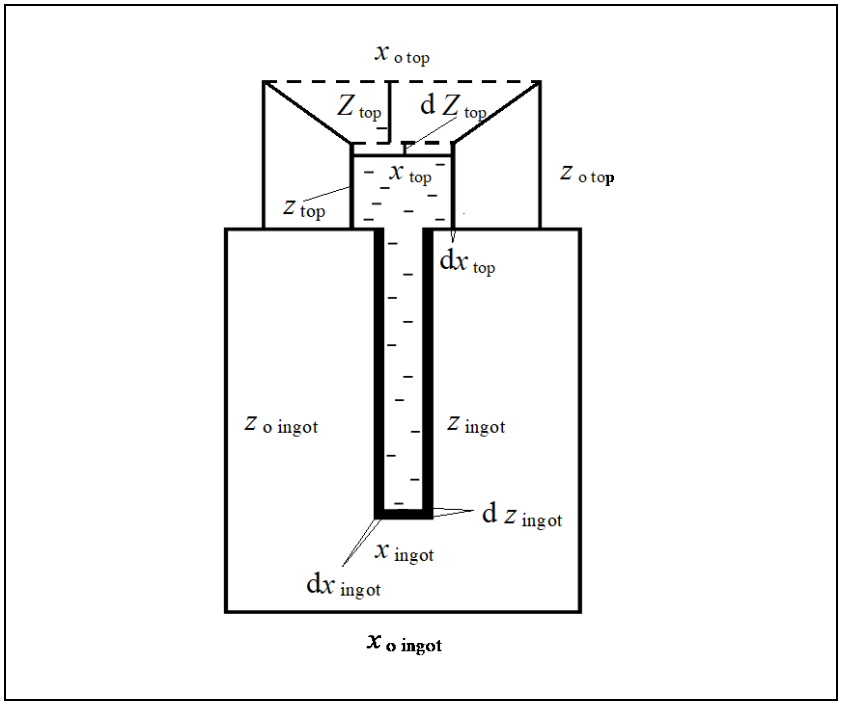


Figure 38.
Ingot with a hot top.
Definition of designations.

We disregard the fact that the chill-mould and the top are conical. It means that $A_{\text{top}}$ is independent of the height at a given time. The solidified volumes are also simple to calculate. For a rectangular ingot we have

$$A_{\text{top}} = x_{\text{top}} y_{\text{top}} \tag{34}$$

The solidified layer in the top has four vertical sides. If the solidification rates in the *x*- and *y*-directions are equal we get

$$\mathrm{d}V_{\text{top}} = 2\left(x_{\text{top}} + y_{\text{top}}\right) \cdot z_{\text{top}}\, \mathrm{d}x_{\text{top}} \tag{35}$$

The solidified layer in the ingot consists of four vertical sides plus bottom:

$$\mathrm{d}V_{\text{ingot}} = 2\left(x_{\text{ingot}} + y_{\text{ingot}}\right) \cdot z_{\text{ingot}}\, \mathrm{d}x_{\text{ingot}} + x_{\text{ingot}} y_{\text{ingot}} \mathrm{d}z_{\text{ingot}} \tag{36}$$

The relations (32), (33), (34), (35) and (36) are inserted into equation (31):

$$\begin{aligned}\rho_{\mathrm{L}} x_{\text{top}} y_{\text{top}} \mathrm{d}Z_{\text{top}} = \left(\rho_{\mathrm{s}} - \rho_{\mathrm{L}}\right) \cdot [\, & 2\left(x_{\text{top}} + y_{\text{top}}\right) \cdot z_{\text{top}}\, \mathrm{d}x_{\text{top}} + \\ & + 2\left(x_{\text{ingot}} + y_{\text{ingot}}\right) \cdot z_{\text{ingot}}\, \mathrm{d}x_{\text{ingot}} + x_{\text{ingot}} y_{\text{ingot}} \mathrm{d}z_{\text{ingot}}\,]\end{aligned} \tag{37}$$

By aid of the definition of solidification shrinkage $\beta = \dfrac{\rho_{\mathrm{s}} - \rho_{\mathrm{L}}}{\rho_{\mathrm{s}}}$ we can express the ratio below as a function of β (page 41):

$$\frac{\rho_{\mathrm{s}} - \rho_{\mathrm{L}}}{\rho_{\mathrm{L}}} = \frac{\beta}{1-\beta} \tag{26}$$

Equation (37) can be transformed into

$$\mathrm{d}Z_{\text{top}} = \frac{2\beta}{1-\beta} \cdot \frac{\mathrm{d}x_{\text{ingot}}}{x_{\text{top}} y_{\text{top}}} \cdot \left[ \mathrm{n} z_{\text{top}} \left(x_{\text{top}} + y_{\text{top}}\right) + z_{\text{ingot}} \left(x_{\text{ingot}} + y_{\text{ingot}}\right) + \frac{\mathrm{m} x_{\text{ingot}} y_{\text{ingot}}}{2} \right] \tag{38}$$

To facilitate a numerical solution of equation (38) we also introduce

$$x_{\text{ingot}} = x_{\text{o ingot}} - 2\Delta x \tag{39}$$

$$y_{\text{ingot}} = y_{\text{o ingot}} - 2\Delta x \tag{40}$$

$$z_{\text{ingot}} = z_{\text{o ingot}} - \text{m}\Delta x \qquad (41)$$

We may replace $x_{\text{ingot}}$, $y_{\text{ingot}}$ and $z_{\text{ingot}}$ with expressions (39), (40) and (41) in equation (38) to facilitate a numerical solution of this differential equation. The equation we get is combined with a description of the solidification rate of the ingot, often in the shape of a computer program.

The method will be illustrated in a simplified form in example 6.

---

**Example 6.**

A square ingot of steel with the dimensions 30x30x150 $cm^3$ is to be cast. The ingot will be equipped with a hot top by covering its surface with a 28 mm thick layer of quartz sand. The choise of height of the top for proper use is questioned.

Assume a value of the height of the top, which might be more suitable and

a) determine the total solidification time of the ingot

b) calculate the shape of the pipe and draw a figure which shows the ingot and the top when the last melt in the mould just has solidified and determine the depth of the pipe.

c) perform a calculation of the amount of melt which remain in the box when the whole ingot has solidified.

d) What practical measures are to be recommanded on basis of the calculations above with the casting immediately at hand?

Reasonable values of the constants required for the calculations are taken from tables. The solidification shrinkage of the steel is 0.050.

***Preparatory Discussion.***
***Choise of a Suitable Value of the Height of the Top***

In chapters 4 and 5 we have earlier discussed various models for calculation of solidification rates and temperature distribution at solidification. The shell thickness in a solidifying melt can with good approximation be described by a relation of the type

$$x\,(t) = S \cdot \sqrt{t} \qquad (1')$$

where
$x$ = thickness of the metal shell
$t$ = time
$S$ = a constant.

Experimental data show that the constant can be given the value $S = 3.2 \cdot 10^{-3}$ m/s. The growth rate of the shell is obtained by derivation of equation (1′) with respect to time:

$$\frac{\mathrm{d}x\,(t)}{\mathrm{d}t} = \frac{S}{2\sqrt{t}} \qquad (2')$$

Equation (2′) is valid only with the assumption that the width of the ingot is larger than its thickness (one-dimensional solidification). In spite of this condition we will use this simple relation and disregard the fact that the solidification rate increases at the end of the solidification at square cross-sections.

The hot top is most often made of sand or other insulating material. Sand has a lower density and lower melting point than the metal melt and has the advantage of not being changed chemically during the solidification process. The shell thickness in the top during the solidification can also be described by Chvorinov′s rule (page 8). Even in this case we get a parabolic growth law but with a different constant:

$$x\,(t) = C \cdot \sqrt{t} \qquad (3')$$

For casting of iron in quartz sand the value of the constant is $C = 8 \cdot 10^{-4}$ m/s.

We make a rough calculation in order to find a suitable value of the height of the hot top. Its cross-section can suitably be chosen equal to the cross-section of the ingot.

The volume of the ingot before solidification =
$= 0.30 \cdot 0.30 \cdot 1.50 = 1.35\ \mathrm{m}^3$

$\beta = 0.050$ which gives $1 - \beta = = 0.95$

The volume of the ingot after solidification ≈
$\approx 0.95 \cdot 0.135 = 0.128\ \mathrm{m}^3$

The volume of the ingot after solidification = $z_{\text{ingot}} \cdot 0.30 \cdot 0.30$

With the designations in the figure below we get

$$z_{\text{ingot}} = \frac{0.128}{0.30 \cdot 0.30} = 1.425 \text{ m}$$

Thus the hot top must at least have this height,

which gives $z_{\text{o top}} = 1.50 - 1.42 = 0.08 \text{ m} = 8 \text{ cm}$

In order to eliminate the risk that the pipe penetrates the hot top we choose $z_{\text{o top}} = 15$ cm for safety, i. e. nearly the double calculated value.

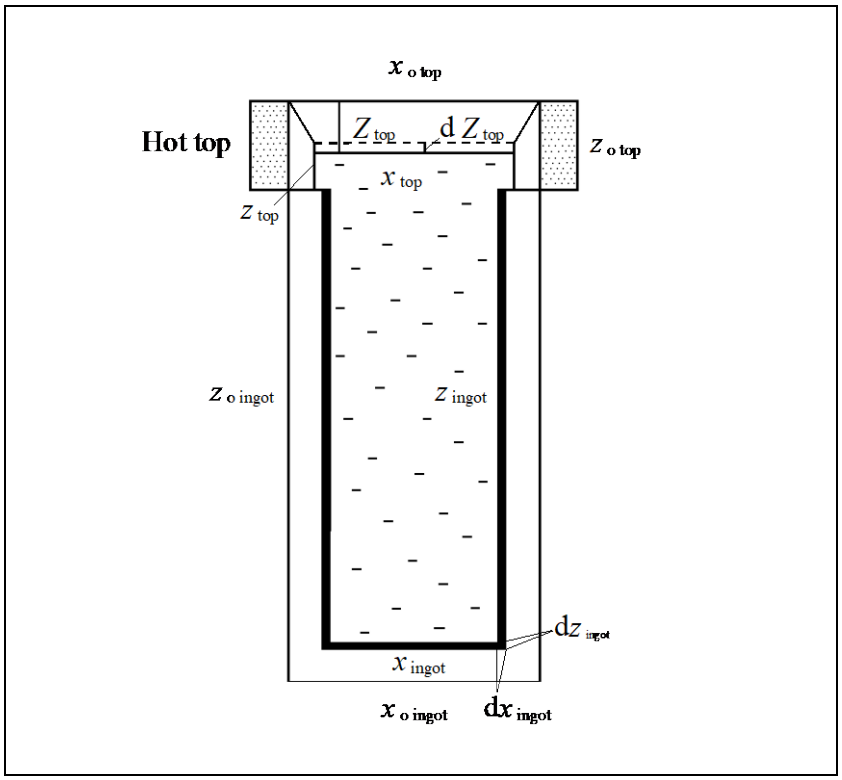


Vertical cross-section of a solidifying ingot with a hot top.

**Solution:**

We apply equation (31) which gives the sinking in the top at time $t$ as a function of solidified amount melt in top and ingot:

$$\rho_{\text{L}} A_{\text{top}} \text{d}Z_{\text{top}} = \left(\rho_{\text{s}} - \rho_{\text{L}}\right)\left(\text{d}V_{\text{top}} + \text{d}V_{\text{ingot}}\right) \qquad (4')$$

The volume of the top is small, compared to the volume of the ingot, and can thus be neglected.

$\frac{\rho_s - \rho_L}{\rho_L}$ can be transformed to $\frac{\beta}{1-\beta}$ (equation (26) page 41)

$A_{top}$ is the area of the melt in the top and equal to the square of the whole side minus two solidified layers:

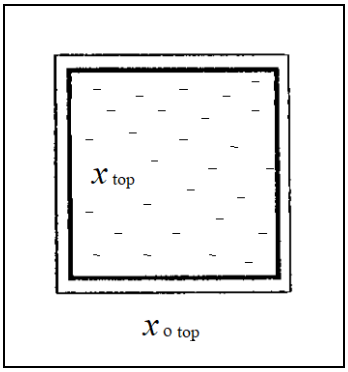


Solidification process in the hot top seen from above.

$$A_{top} = x_{top}^2 = \left(x_{o\,top} - 2C\sqrt{t}\right)^2 \qquad (5')$$

where the constant $C = 8 \cdot 10^{-4}$ m/s (see page 50).

We assume that the solidification in the ingot occur with the same rate in the *x*-, *y*- and *z*-directions.

The thickness of the solidified layer = $S \cdot \sqrt{t}$ where

$S = 3.2 \cdot 10^{-3}$ m/s and we get

$$x_{ingot} = \left(x_{o\,ingot} - 2S\sqrt{t}\right) \qquad (6')$$

$$y_{ingot} = \left(x_{o\,ingot} - 2S\sqrt{t}\right) \qquad (7')$$

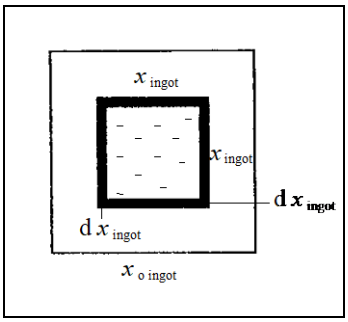


Solidification process in the ingot seen from above.

because the cross-section of the mould is square and

$$z_{ingot} = \left(z_{o\,ingot} - S\sqrt{t}\right) \qquad (8')$$

The number of surfaces is five, four vertical side surfaces and one bottom surface. The total area of the solidified layer has to be multiplied by $dx_{ingot}$ to give $dV_{ingot}$. We get $dx_{ingot}$ from equation (2′):

$$dx_{ingot} = \frac{S\,dt}{2\sqrt{t}} \qquad (9')$$

All these quantities are inserted into equation (31), which gives

$$\left(x_{o\,top} - 2C\sqrt{t}\right)^2 dZ_{top} = \frac{\beta}{1-\beta}\left[\left(4x_{o\,ingot} - 2S\sqrt{t}\right)\cdot\left(z_{o\,ingot} - S\sqrt{t}\right) + \left(x_{o\,ingot} - 2S\sqrt{t}\right)^2\right]\cdot\frac{S\,dt}{2\sqrt{t}} \qquad (10')$$

The volume of the top is approximately 10 % of the ingot volume. Thus it is reasonable to neglect the solidification shrinkage in the top, compared to the one in the ingot.

Initially we calculate the total solidification time of the ingot. The whole ingot has solidified when the thickness of the solidified metal equals half the square side of the mould.

$$S\sqrt{t_{\text{ingot}}} = \frac{x_{\text{o ingot}}}{2}$$

or

$$t_{\text{ingot}} = \left(\frac{x_{\text{o ingot}}}{2S}\right)^2 = \frac{0.30^2}{\left(2 \cdot 3.2 \cdot 10^{-3}\right)^2} = 2197 \text{ s} \approx 2200 \text{ s} = 37 \text{ min}$$

We divide the time into ten equal intervals and insert these values into equation (10′) and calculate successively $x_{\text{top}}$, $x_{\text{ingot}}$, $z_{\text{ingot}}$,, $\mathrm{d}Z_{\text{top}}$ and $Z_{\text{top}} = \Sigma\, \mathrm{d}Z_{\text{top}}$ by aid of known values of $S$ and $C$.

| $t$ | $\mathrm{d}t$ | $x_{\text{top}}$ | $x_{\text{ingot}}$ | $z_{\text{ingot}}$ | $\mathrm{d}Z_{\text{top}}$ | $Z_{\text{top}}$ |
|---|---|---|---|---|---|---|
| 0 | | 0.30 | 0.30 | 1.50 | 0.000 | 0.000 |
| 220 | 220 | 0.28 | 0.21 | 1.45 | 0.020 | 0.020 |
| 440 | 220 | 0.27 | 0.17 | 1.43 | 0.012 | 0.032 |
| 660 | 220 | 0.26 | 0.14 | 1.42 | 0.008 | 0.041 |
| 880 | 220 | 0.25 | 0.11 | 1.41 | 0.006 | 0.047 |
| 1100 | 220 | 0.25 | 0.09 | 1.39 | 0.005 | 0.052 |
| 1320 | 220 | 0.24 | 0.07 | 1.38 | 0.003 | 0.055 |
| 1540 | 220 | 0.24 | 0.05 | 1.37 | 0.002 | 0.057 |
| 1760 | 220 | 0.23 | 0.03 | 1.37 | 0.001 | 0.059 |
| 1980 | 220 | 0.23 | 0.02 | 1.36 | 0.001 | 0.059 |
| 2200 | 220 | 0.22 | 0.00 | 1.35 | 0.000 | 0.059 |

From the table it can be read that $x_{\text{top}} = 22$ cm and $Z_{\text{top}} = 6$ cm when the whole ingot just has solidified.

If we disregard the volume solidified metal in the top, the volume of the remaining melt in the hot top, when the whole ingot has solidified, is equal to

22 cm·22 cm·(15 – 6) cm = 22 cm·22 cm·9 cm

Since iron has the density $7.8 \cdot 10^3$ kg/m$^3$, the mass of the melt will be

$m = 0.22 \cdot 0.22 \cdot 0.09 \cdot 7.8 \cdot 10^3 = 34$ kg

**Answer:**

a) The whole ingot solidifies in approximately 37 min.

b)

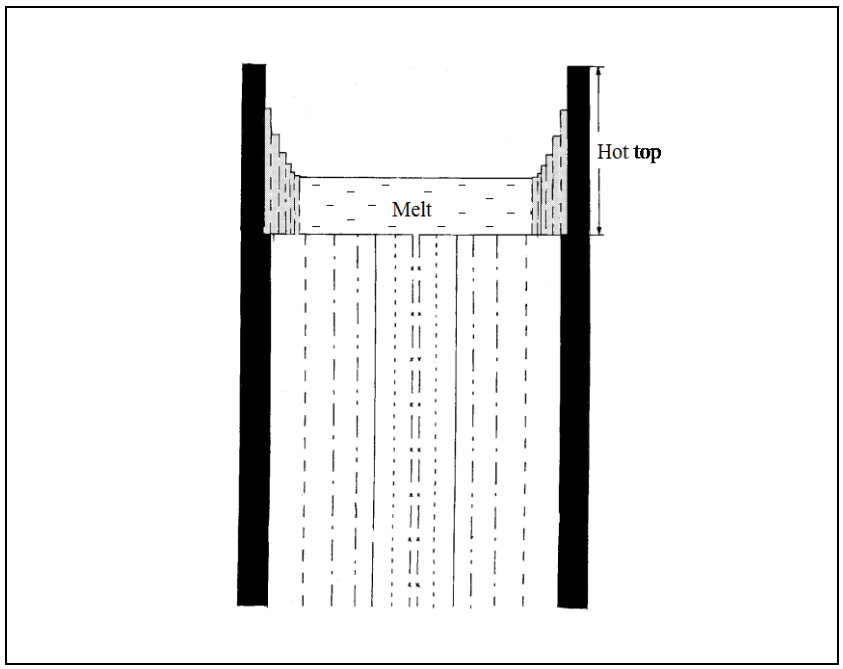


Melt +ingot, which has started to solidify.
A number of instant pictures of the position of the solidification front in the ingot respectively the top at various times during the solidification process have been drawn in the figure.

c) The remaining melt in the top when the ingot just has solidified weighs approximately 34 kg.

d) It is not enough with 28 mm quartz sand as a hot top. 15 cm is unnecessarily much. Since we have neglected the cooling shrinkage of the top we have to add approximately 10 % on the sinking 6 cm to take this into consideration. It ought to be enough with a layer of 80 mm quartz sand, which is in perfect agreement with our rough preparatory calculation.

---

A comparison between examples 5 and 6 shows convincingly the benefit of hot tops.

## 10.6 Solidification and Cooling Shrinkage at Continuous Casting

At continuous casting the melt must be strongly cooled since no metal melt shall be left inside the strand when it leaves the machine.

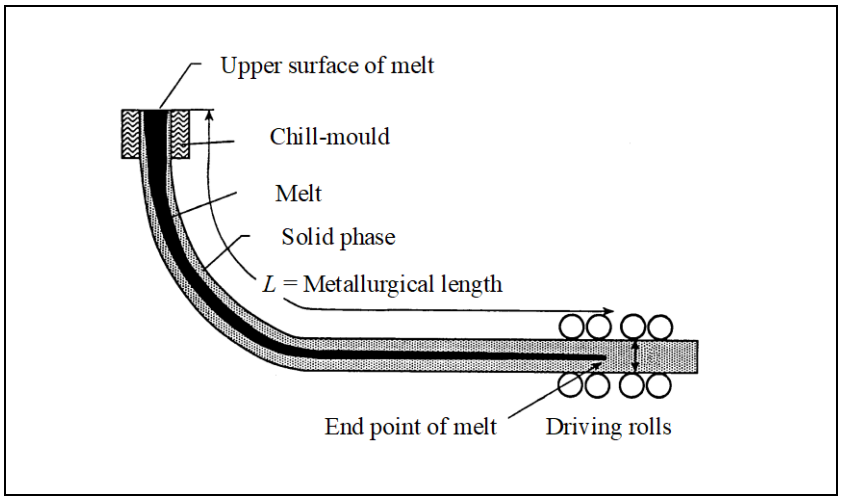


Figure 39.
Bent continuous casting machine with a curvature below the chill-mould.

Above the chill-mould there is a tundish, which is not drawn in the figure. The bending is a practical measure to achieve a lower building with reduced mechanical stress on the workshop floor.

If the walls and bottom of a chill-mould are strongly cooled a large temperature gradient is formed in the melt. The dendrites grow mainly in the direction of the temperature gradient and the shrinkage cavities appear in the shape of a narrow pipe in the centre (figure 40). This phenomenon has been treated for ingots in section 10.5.

Corresponding cooling conditions with strong temperature gradients are also valid at continuous casting, when the walls of the strand are cooled by water spraying in the chilled zone below the chill-mould. Pipe formation appears at the end of the solidification of the strand, when the supply of new melt from the tundish has ceased.

Pipe formation at continuous casting is discussed below and a theoretical model, developed by Fredriksson and Raihle, is introduced.

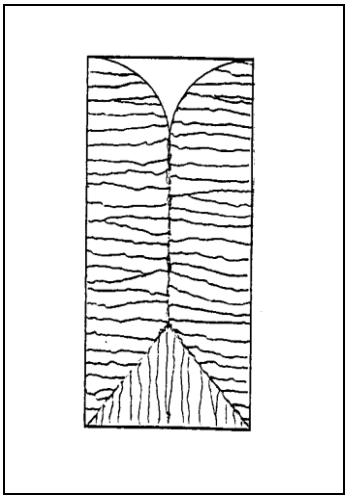

Figure 40.
Dendrite growth at ingot solidification with a great temperature gradient.

### 10.6.1 Pipe Formation at Continuous Casting

Pipe formation is normally connected with ingot casting. At ingot casting the pipe is mainly caused by solidification shrinkage.

At continuous casting melt is continuously added to the chill-mould and the volume decrease due to solidification and cooling shrinkage is thus compensated. The situation is changed at the end of the casting process when the supply of melt from the tundish above the chill-mould ceases. Then the conditions become comparable with the ones, which are valid at ingot casting and a pipe is formed at the end of the casting process.

The pipe volume can be reduced by different practical methods and is in most cases no major problem at continuous casting processes. However, the mechanism of pipe formation in a continuously cast strand is the same as the one of centreline segregation, which is a severe problem. It will be discussed in chapter 11.

The pipe is well developed in billets but less marked at casting of slabs. The reason for these differences is found in the design of the casting equipment and the casting conditions in the two cases. Here we will mainly discuss billet casting. However, in some cases calculations, valid for a one-dimensional model similar to a slab strand, are included, in order to illustrate the general calculation process.

Experimental examinations show that the pipe volume at continuous casting is so big that it can *not* be explained entirely by solidification shrinkage.

*The central cavities at continuous casting are caused by the combined solidification and cooling shrinkage.*

### 10.6.2 Theory of Pipe Formation at Continuous Casting

Solidification shrinkage in combination with cooling shrinkage is the origin of pipe formation in the strand at the final stage of the casting process. Figure 41 a gives a schematic sketch of the

strand during the solidification process. We assume that the cross-section area of the strand is a square with the side $x_o$.

We assume that the supply of melt is stopped at $t = 0$. At that time the upper surface of the melt had the initial position ABCD. At time $t$ it had the position A′B′C′D′ and at the time $t + dt$ the surface has sunk to the dotted position. During the time interval $dt$ the volume $dV_S$ has solidified. This causes a solidification shrinkage $dV_{sol} = dV_s \cdot \beta$, where $\beta$ is the solidification shrinkage (page 41), and a cooling shrinkage = $dV_{cool}$.

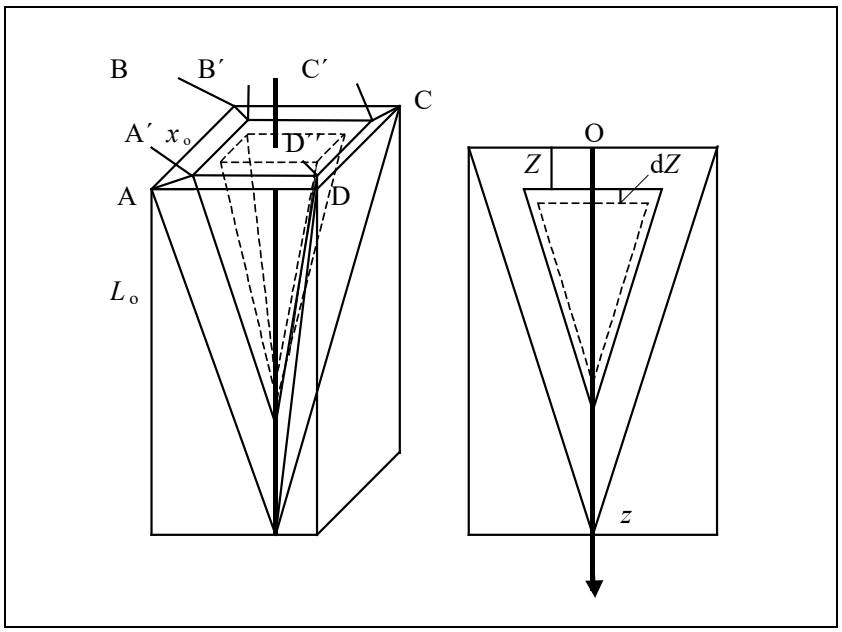


Figure 41a.
Schematic sketch of a solidifying strand.
The *left* picture shows the position of the solidification front at three different times – three pyramids inside of each other. The central one is dotted.
The *right* picture shows the cross-section of the strand in a vertical plane through the central axis and parallel with two of the vertical sides.
In reality the strand is much longer than the figure shows and, in addition, bent.

We introduce a coordinate system with the $z$-axis in the direction of the strand motion and the $xy$-plane perpendicular to the $z$-axis. The direction of the $z$-axis is initially vertical (figure 41 a) and horizontal when all the melt has solidified (figure 39).

The surface sinks with the amount $dz$ in the direction of the positive $z$-axis during the time $dt$, due to solidification and cooling shrinkage. We also assume that the densities of the solid respectively the melt are independent of $z$. Then a volume balance can replace the material balance. At distance $z$ from point O in figure 41 a the volume element $dV_{pipe}$ can be written:

$$dV_{pipe} = A \cdot dz = dV_{sol} + dV_{cool} = dV_s \cdot \beta + dV_{cool} \qquad (42)$$

where

$V_{pipe}$ = volume of the pipe
$dz$ = change of distance $z$ during the time interval $dt$
$A$ = cross-section area of the melt at distance $z$ from O along the strand
$dV_S$ = change in solidified volume during time interval $dt$
$dV_{sol}$ = change in solidified volume during time interval $dt$ due to solidification shrinkage
$\beta$ = solidification shrinkage = $(\rho_s - \rho_L)/\rho_L$
$dV_{cool}$ = change in solidified volume during time interval $dt$ due to cooling shrinkage.

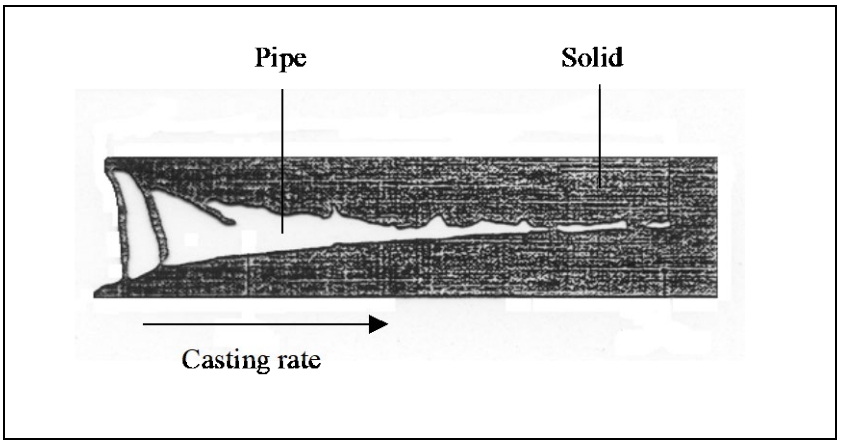


Figure 41 b.
Vertical cross-section of a pipe in the central region of a strand at continuous casting. The asymmetry of the pipe is due to the fact that the casting machine is bent and that the pipe is horisontal with the planar side downwards before the melt has solidified completely in the central region.

The left-hand side of equation (42) represents the change of the pipe volume during the time $dt$. The first term on the right-hand side corresponds to the solidification shrinkage during the time $dt$ and the second one to the cooling shrinkage during the time $dt$. The total pipe volume is obtained by integration of equation (42) with respect to time.

Figure 41 b shows the pipe in its horizontal position.

## Determination of the Solidification Shrinkage

### *Solidification Shrinkage Volume*

Calculation of the solidification shrinkage at continuous casting is performed mainly in the same way as was used for calculation of the pipe formed in an ingot without a hot top (page 38).

Consider the volume element in figure 42 with a square cross-section and height d$z$. The outer circumference is $4x_o$ and the thickness of the solidified layer is $x$. If the thickness increases by the amount d$x$ during the time d$t$ the volume increases by the amount d$V_s$ during the time d$t$ and we get

$$\frac{dV_s}{dt} = 4 \cdot (x_o - 2x) \cdot \frac{dx}{dt} \cdot dz \qquad (43)$$

where

$x_o$ = the side of the square strand
$x$ = thickness of the solidified shell
$z$ = coordinate along the strand ($z = 0$ at O in figure 41)
$V_s$ = solidified volume.

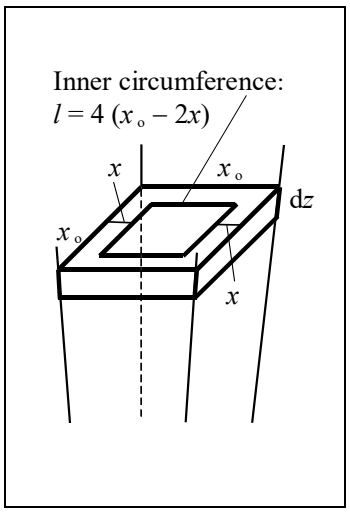

Figure 42.

Equation (43) is valid all the way along the strand. The thickness $x$ and its time derivative d$x$/d$t$ are not constant but vary with time and position. The total solidification volume can be calculated if the function d$x$/d$t$ is known. A reasonable example with a parabolic growth law is given below. The shape of the pipe will be discussed later.

---

**Example 7.**

Derive an expression for the volume of the solidification shrinkage of a square strand with the side $x_o$ at continuous casting. The metallurgical length is $L$. A parabolic growth law with the growth constant S is valid.

$$x = S \cdot \sqrt{t}$$

**Solution:**

Derivation of the growth law with respect to time gives

$$\frac{dx}{dt} = \frac{S}{2 \cdot \sqrt{t}} \qquad (1')$$

If the values of $x$ and d$x$/d$t$ are inserted into equation (43) we get by aid of figure 42

$$V_s = \int_0^{V_s} dV_s = \int_0^z dz \int_0^t 4 \cdot (x_o - 2S \cdot \sqrt{t}) \cdot \frac{S \cdot dt}{2 \cdot \sqrt{t}} \qquad (2')$$

where $z$ is distance of the volume element below the upper level of the chill-mould.

The time $t$ and the distance $z$ are related to each other by aid of the simple relation

$$t = \frac{z}{v_{\text{cast}}} \tag{3′}$$

if the casting rate $v_{\text{cast}}$ is assumed to be constant.

The expression (3′) of $t$ is introduced into equation (2′) and we get the total solidification shrinkage

$$V_{\text{s}} = \int_0^L \mathrm{d}z \int_0^{\frac{z}{v_{\text{cast}}}} 4\,(x_{\text{o}} - 2S \cdot \sqrt{t}) \cdot \frac{S \cdot \mathrm{d}t}{2 \cdot \sqrt{t}} \tag{4′}$$

where $L$ is the metallurgical length.

The double integral is solved in two steps. Integration with respect to $t$ gives

$$\int_0^{V_{\text{s}}} \mathrm{d}V_{\text{s}} = \int_0^L \mathrm{d}z \int_0^{\frac{z}{v_{\text{cast}}}} \left( 2x_{\text{o}} S \cdot \frac{\mathrm{d}t}{\sqrt{t}} - 4S^2 \cdot \mathrm{d}t \right) = \int_0^L \left( 4x_{\text{o}} S \cdot \sqrt{\frac{z}{v_{\text{cast}}}} - 4S^2 \cdot \frac{z}{v_{\text{cast}}} \right) \cdot \mathrm{d}z$$

Integration with respect to $z$ gives

$$V_{\text{S}} = \int_0^{V_{\text{s}}} \mathrm{d}V_{\text{S}} = \left[ \frac{8x_{\text{o}} S}{3 \cdot \sqrt{v_{\text{cast}}}} \cdot z^{\frac{3}{2}} - \frac{4S^2}{v_{\text{cast}}} \cdot \frac{z^2}{2} \right]_0^L$$

or

$$V_{\text{S}} = \frac{8x_{\text{o}} S}{3 \cdot \sqrt{v_{\text{cast}}}} \cdot L^{\frac{3}{2}} - \frac{2S^2}{v_{\text{cast}}} \cdot L^2 \tag{5′}$$

We now have an expression, which describes the solidified volume along the strand when the supply of melt has ceased and the parabolic growth law is valid. During the solidification the upper surface of the melt is successively lowered and a pipe is formed.

**Answer:** The total solidification shrinkage contributes to the pipe volume with the amount

$$\Delta V_{\text{sol}} = \beta \cdot V_{\text{s}} = \beta \cdot \left( \frac{8x_{\text{o}} S}{3 \cdot \sqrt{v_{\text{cast}}}} \cdot L^{\frac{3}{2}} - \frac{2S^2}{v_{\text{cast}}} \cdot L^2 \right)$$

---

## Determination of the Cooling Shrinkage

The cooling shrinkage can be described as the sum of two parts and depends on the temperature conditions at the centre and at the surface of the strand.

Alloys solidify over a temperature range equal to $T_L - T_S$. Within this temperature interval solidification heat is gradually released and the central temperature of the strand is constant or changes very little (figure 43) in contrast to the conditions, valid after the solidification fronts have met. When all the melt has solidified no further heat is released and the temperature at the centre then decreases rapidly (figure 43).

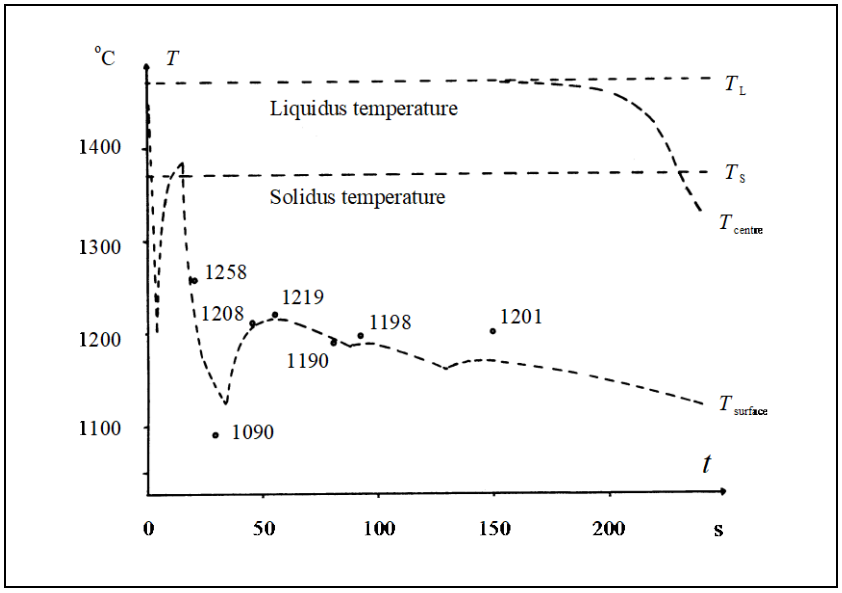


Figure 43.
Temperature at the centre respectively at the middle of a side of a square strand at continuous casting as a function of time.
Solidification interval = $T_L - T_S$.

The *first* part is the shrinkage of the solidified shell *before* the solidification fronts meet at the centre of the strand. This shrinkage consists of the shrinkage at the surface of the strand and the shrinkage of the interior of the shell.

Before the solidification fronts meet the temperature at the solidification fronts is approximately constant and equal to the liquidus temperature. Thus one may neglect the internal shrinkage caused by the temperature change at the solidification fronts. Its contribution to the pipe formation is negligible.

The external water-cooling lowers the surface temperature of the strand (figure 43). The whole strand shrinks and its surface moves inwards while the solidification front moves towards the centre. This surface shrinkage contributes to the pipe formation.

The *second* part is the shrinkage or dilatation *after* the union of the solidification fronts at the centre of the strand. The situation becomes completely different when the solidification fronts have met at the centre of the strand.

The cooling of the surface of the strand becomes low. The surface temperature decreases slowly and can be regarded as fairly constant (figure 43) and the contribution to the pipe formation is negligible.

The sudden and rapid temperature decrease at the centre when b the solidification fronts have met (figure 43) causes a central cooling shrinkage, which contributes to the pipe formation.

$$\Delta V_{\text{cool}} = \Delta V_{\text{surface}} + \Delta V_{\text{centre}} \tag{44}$$

It is hard to derive analytical expressions for these volume changes and we make some simplifications in our further treatment.

***Cooling Shrinkage Volume***

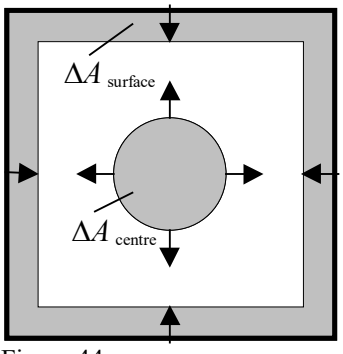

Figure 44.

The temperature change as a function of time is much smaller in the length direction (along the *z*-axis) than in the perpendicular directions. Consequently we can neglect the cooling shrinkage in the length direction and only take the changes of the cross-section *area* instead of the *volume* changes into consideration. The relation (44) can then be written

$$\Delta A_{\text{cool}} = \Delta A_{\text{surface}} + \Delta A_{\text{centre}} \tag{45}$$

or

$$\Delta A_{\text{centre}} = \Delta A_{\text{cool}} - \Delta A_{\text{surface}} \tag{46}$$

The formation of a pipe, which is a cavity in the centre, shows that the cooling shrinkage at the centre is directed *outwards*. $\Delta A_{\text{surface}}$ and $\Delta A_{\text{centre}}$ have opposite signs as is shown in figure 44.

Equation 46 can be interpreted in the following way:

1. If $\Delta A_{\text{centre}}$ is *larger* than $\Delta A_{\text{surface}}$ the central part of the strand shrinks more than the outer frame, i. e. the surface, allows. It means that *a cavity is formed* in the central region. This cavity becomes filled with melt from above and thus it contributes to the pipe at the top of the strand.
2. If $\Delta A_{\text{centre}}$ is *smaller* than $\Delta A_{\text{surface}}$ the central part shrinks less than the outer frame, i. e. the surface. It means that the central region becomes compressed and *no cavity is formed*. No contribution to the pipe at the top of the strand is obtained.

The first alternative will be treated below. The simplest way to find the total cooling shrinkage $\Delta A_{\text{cool}}$ is to calculate $\Delta A_{\text{surface}}$ and $\Delta A_{\text{centre}}$ separately and then add them.

### *Calculation of $\Delta A_{\text{surface}}$ when $T_{\text{surface}}$ Decreases and $T_{\text{centre}}$ is Constant*

The surface is cooled from outside, which results in a cooling rate $\mathrm{d}T_{\text{surface}}/\mathrm{dt}$ at the surface of the strand. The temperature in the centre of the strand is constant (figure 43 on page 60).

We assume that the temperature decreases *linearly* from the centre and outwards to the surface. If the temperature decreases with the amount $\mathrm{d}T_{\text{surface}}$ at the surface is sinks at the distance $x$ from the surface with the amount (see the right figure 45)

$$\mathrm{d}T_{\text{surface}}(x) = \frac{\frac{x_o}{2} - x}{\frac{x_o}{2}} \cdot \mathrm{d}T_{\text{surface}} \qquad (47)$$

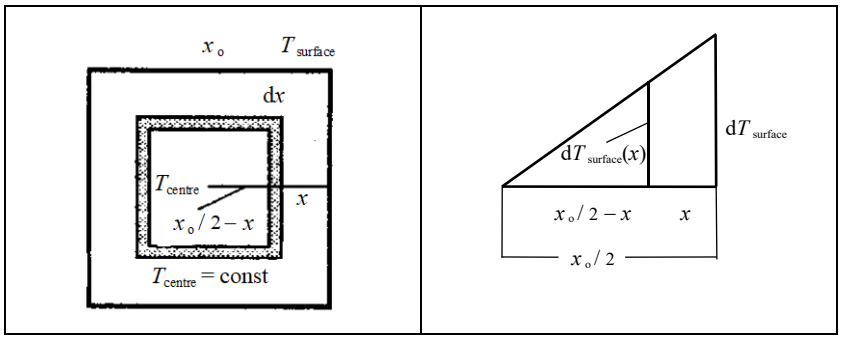


Figure 45.
Temperature distribution when $T_{\text{surface}}$ varies linearly in the cross-section area.

We will calculate the contribution of the surface shrinkage to the total cooling shrinkage of the square cross-section. The basic formula of surface dilatation is

$$\Delta A = \alpha_A \cdot A \cdot \Delta T \tag{48}$$

We apply it on the dark area element in the left figure above and integrate over the whole cross-section area

By aid of equation (47) and the relation $\alpha_A = 2\,\alpha_l$ we get the shrinkage of four area elements:

$$\mathrm{d}A_{\text{surface}} = 2\,\alpha_l \;\cdot\; 4\cdot(x_o - 2x)\cdot \mathrm{d}x \;\cdot\; \frac{\frac{x_o}{2} - x}{\frac{x_o}{2}} \cdot \mathrm{d}T_{\text{surface}}$$

$\alpha_A$ four area elements $T_{\text{surface}}(x)$

The cooling shinkage of the whole cross-section when $T_{\text{surface}}$ decreases by the amount $\Delta T_{\text{surface}}$ is then

$$\Delta A_{\text{surface}} = \int_0^{\frac{x_o}{2}} 2\,\alpha_l \cdot 4\cdot(x_o - 2x)\cdot \mathrm{d}x \cdot \frac{\frac{x_o}{2} - x}{\frac{x_o}{2}} \cdot \Delta T_{\text{surface}} = \frac{4}{3}\cdot \alpha_l \cdot x_o^2\, \Delta T_{\text{surface}} \tag{49}$$

***Calculation of $\Delta A_{\text{centre}}$ when $T_{\text{centre}}$ Decreases and $T_{\text{surface}}$ is Constant***

When the solidification is complete no more solidification heat is generated. The temperature $T_{\text{centre}}$ decreases rapidly while $T_{\text{surface}}$ can be regarded as approximately constant.

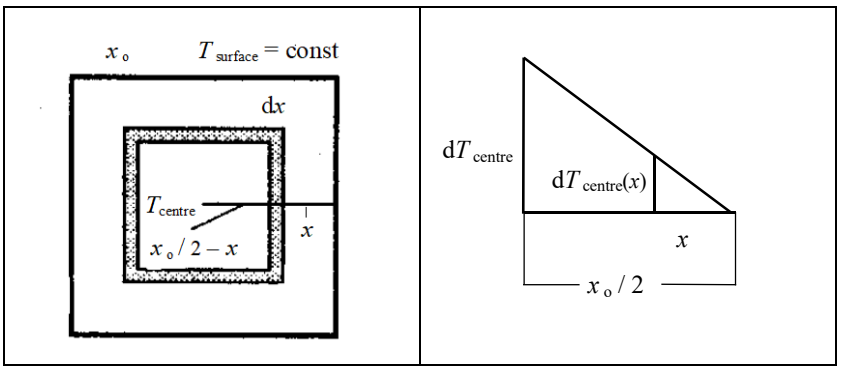


Figure 46.
Temperature distribution when $T_{\text{centre}}$ varies linearly in the cross-section area.

As above we assume that the temperature decreases linearly, in this case from the centre outwards to the surface of the strand.

If the temperature decrease in the centre is $\mathrm{d}T_{\text{centre}}$ then the temperature fall at the dark area element (left figure 46) is

$$\mathrm{d}T_{\text{centre}}(x) = \frac{x}{\frac{x_o}{2}} \cdot \mathrm{d}T_{\text{centre}} \tag{50}$$

In the same way as above we get (right figure 46) the shrinkage of the area element

$$\mathrm{d}A_{\text{centre}} = 2\,\alpha_l \;\cdot\; 4 \cdot (x_o - 2x) \cdot \mathrm{d}x \;\cdot\; \frac{x}{\frac{x_o}{2}} \cdot \mathrm{d}T_{\text{centre}}$$

$\alpha_A$ four area elements $\mathrm{d}T_{\text{centre}}(x)$

The central cooling shrinkage of the whole cross-section area when $T_{\text{centre}}$ decreases by the amount $\Delta T_{\text{centre}}$ equals

$$\Delta A_{\text{centre}} = \int_0^{\frac{x_o}{2}} 2\,\alpha_l \cdot 4 \cdot (x_o - 2x) \cdot \mathrm{d}x \cdot \frac{x}{\frac{x_o}{2}} \cdot \Delta T_{\text{centre}} = \frac{2}{3} \cdot \alpha_l \, x_o^2 \, \Delta T_{\text{centre}} \tag{51}$$

***Calculation of the Total Cooling Shrinkage Area $\Delta A_{\text{cool}}$***

Equation (45) on page 62 gives the net cooling shrinkage area when a pipe is formed:

$$\Delta A_{\text{cool}} = \Delta A_{\text{centre}} + \Delta A_{\text{surface}} = \frac{2}{3} \cdot \alpha_l \, x_o^2 \, \Delta T_{\text{centre}} - \frac{4}{3} \cdot \alpha_l \, x_o^2 \, \Delta T_{\text{surface}} \tag{52}$$

where

$\Delta A_{\text{cool}}$ = total shrinkage of the cross-section area = average area of the pipe, formed in the strand.

$\Delta A_{\text{surface}}$ = fraction of $\Delta A_{\text{cool}}$, which emanates from the surface shrinkage

$\Delta A_{\text{centre}}$ = fraction of $\Delta A_{\text{cool}}$, which emanates from the centre shrinkage.

As mentioned on page 62 $\Delta A_{\text{cool}}$ has a physical significance only if it is positive. The minus sign appears in equation (52) because the movement of the outer surface is opposite to the movement of the central region (see text and figure on page 62).

***Condition for Pipe Formation in Terms of Cooling Rates***

From the derivations on pages 63-65 we can conclude that

$$G = \frac{\Delta T_{surface}}{\Delta T_{centre}} = \frac{dT_{surface}}{dT_{centre}} = \frac{\frac{dT_{surface}}{dt}}{\frac{dT_{centre}}{dt}} \tag{53}$$

The G-factor, defined by equation (53), can be used to express $\Delta A_{cool}$ in terms of $\Delta T_{centre}$ and the ratio of the cooling rates at the centre respectively at the strand surface. As $\Delta T_{surface} = G \cdot \Delta T_{centre}$ equation (52) can be written

$$\Delta A_{cool} = \frac{2}{3} \cdot \alpha_l \cdot x_o^2 \left(1 - 2G\right) \cdot \Delta T_{centre} \tag{54}$$

where

| | | |
|---|---|---|
| $\alpha_l$ | = | length dilatation coefficient |
| $x_o$ | = | cross-section side of the strand |
| $dT_{surface}/dt$ | = | cooling rate at the surface of the strand |
| $dT_{centre}/dt$ | = | cooling rate at the centre of the strand |
| G | = | G-factor, the ratio of the cooling rates $(dT_{surface}/dt)/(dT_{centre}/dt)$ |
| $\Delta T_{centre}$ | = | change of temperature at the centre. |

It can be concluded from equation (54) that it is the G-factor, the ratio of the cooling rate at the surface and the cooling rate at the centre, that decides whether a pore is formed or not.

- If $G < 0.5 \quad \Rightarrow \quad \Delta A_{cool} > 0 \quad \Rightarrow$ contribution to pipe

The cooling rate at the surface < half the cooling rate at the centre. A pore is formed and melt tries to soak downwards to fill it. If the melt cannot advance, due to narrow channels, a pipe is formed in the strand.

- If $G > 0.5 \quad \Rightarrow \quad \Delta A_{cool} < 0 \quad \Rightarrow$ no contribution to pipe

The cooling rate at the surface > half the cooling rate at the centre. No pore is formed. The centre is exposed to thermal stress, which may cause central cracks. This matter is treated in section 10.7.8.

## Determination of the Volume and Shape of the Pipe

### *Volume of the Pipe*

Equations (53) and (54) above show that the cooling rate at the surface of the strand has a great influence on the pore volume.

The cooling rate is affected by the casting rate and the efficiency of the water cooling in the cooling zone of the casting machine. The cooling rates can be calculated by solving the heat equations given in chapter 5.

$\Delta A_{\text{cool}}$ is calculated from equation (54). The lower integration limit of the time integral is the time when the solidification fronts meet. The upper limit is the time when the temperature in the centre has reached the solidus temperature.

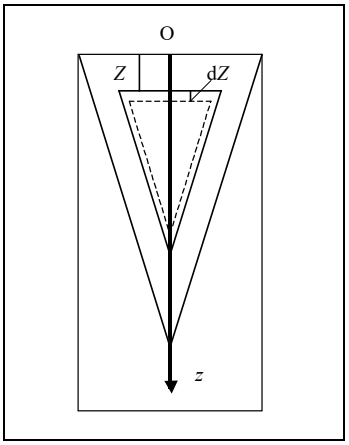

Figure 47. (Part of Figure 41 a) Two-phase region at the centre of the strand.

The area calculated in this way is the total area shrinkage due to the thermal contraction. In order to find the contribution to the volume of the pipe one has to multiply the area with the length of the strand where this shrinkage occurs. $\Delta A_{\text{cool}}$ can be regarded as an average cross-section of the pipe. In this case it is reasonable to use the total metallurgical length $L$.

The volume of the pipe is the sum of the solidification shrinkage and the cooling shrinkage. According to equation (42) on page 57 and equation (52) on page 65 the general expression for the pipe volume of a square strand can be written

$$V_{\text{pipe}} = \beta \cdot V_{\text{s}} + \left( \frac{2}{3} \cdot \alpha_{l}\, x_{\text{o}}^{2}\, \Delta T_{\text{centre}} - \frac{4}{3} \cdot \alpha_{l}\, x_{\text{o}}^{2}\, \Delta T_{\text{surface}} \right) \cdot L \quad (55)$$

or, by aid of equation (54),

$$V_{\text{pipe}} = \beta \cdot V_{\text{s}} + \frac{2}{3} \cdot \alpha_{l} \cdot x_{\text{o}}^{2} \left(1 - 2\text{G}\right) \cdot \Delta T_{\text{centre}} \cdot L \quad (56)$$

The method to calculate the pipe volume is illustrated below.

---

**Example 8.**

Set up an expression for the pipe volume for a square strand with the cross-section side $x_{\text{o}}$ at continuous casting when the temperature in the centre is equal to the solidus temperature of the alloy is $T_{\text{s}}$.

Assume that the thickness of the solidified layer of the strand follows the growth law

$x = S \cdot \sqrt{t}$ $x = S \cdot \sqrt{t}$

**Solution and Answer:**

The volume of the pipe is obtained by introducing the expressions in the answer in example 7 on page 60 and equation (54) on page 66 into equation (56).

$$V_{\text{pipe}} = \beta \cdot \left( \frac{8 x_{\text{o}} S}{3 \cdot \sqrt{v_{\text{cast}}}} \cdot L^{\frac{3}{2}} - \frac{2 S^{2}}{v_{\text{cast}}} \cdot L^{2} \right) + \frac{2}{3} \cdot \alpha_{l} \cdot x_{\text{o}}^{2} \left(1 - 2\text{G}\right) \cdot \left(T_{\text{L}} - T_{\text{S}}\right) \cdot L$$

where

| | | |
|---|---|---|
| $\beta$ | = | solidification shrinkage = $\left(\rho_{\text{s}} - \rho_{\text{L}}\right) / \rho_{\text{L}}$ |
| $S$ | = | growth constant |
| $L$ | = | metallurgical length (figure 39 on page 55) |
| $v_{\text{cast}}$ | = | casting rate |
| G | = | ratio of the cooling rates at the surface and at the centre of the strand |
| $\alpha_{l}$ | = | length dilatation coefficient |
| $x_{\text{o}}$ | = | length of the side of the square strand |
| $T_{\text{L, S}}$ | = | liquidus respectively solidustemperature of the alloy. |

---

***Shape of the Pipe***

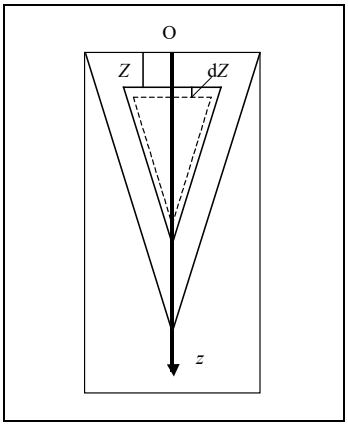

Figure 48.

The shape of the pipe is described if we calculate the depth $Z$ as a function the thickness $x$ of the solidified shell.

During the pipe formation the upper level of the melt sinks when the supply of melt from the tundish has ceased. The decrease $Z$ of the liquid surface can be calculated in a similar way as in the case of ingot solidification, which was presented in section 10.5.2 on page 38.

For a continuous square strand (see figure 42 on page 59) the following relation is valid

$$A \cdot \text{d}Z = (x_{\text{o}} - 2x)^{2} \cdot \text{d}Z = \beta \cdot \text{d}V_{\text{s}} + L \cdot \text{d}A_{\text{cool}} \qquad (57)$$

However, the calculations in the case of a pipe at continuous casting are much more complicated than in the case of an ingot pipe. In the latter case only the solidification shrinkage is involved as the temperature can be regarded as constant.

At continuous casting the temperature conditions and the cooling rates at the surface and at the centre of the strand as well as the growth of the solid shell as a function of the geometrical co-ordinates influences the shape of the pipe. When all functions and quantities are introduced into the differential equation (64) it can be solved but the solution will be omitted here. In most cases only numerical solutions are possible.

### *Comparison between Theory and Experiments*

At low casting rates the theoretical calculations of the solidification and cooling shrinkages fit very well with the observed values of the pipe depth. This can be seen in figure 49 below. The assumptions we have made are obviously realistic. The model of continuous casting given above is acceptable.

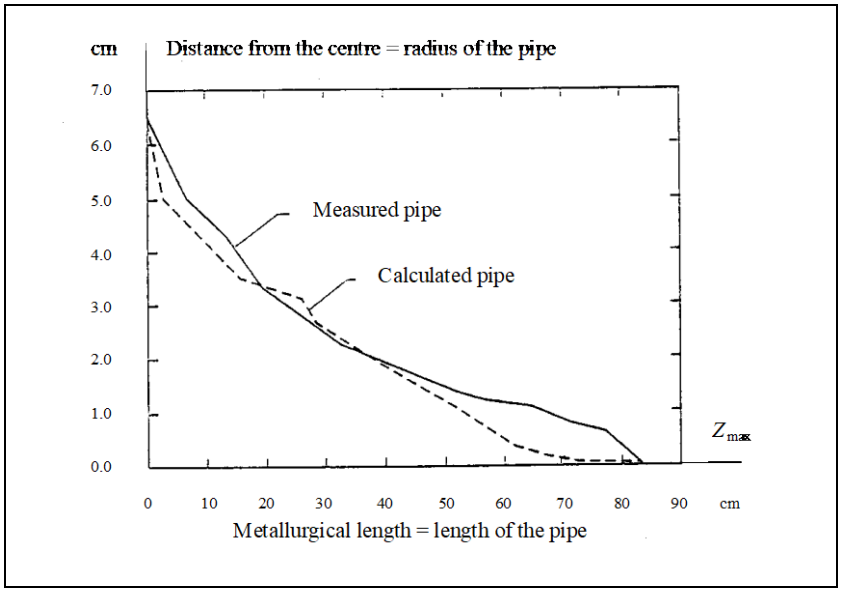


Figure 49.
Pipe at continuous casting.
Casting rate 1.9 m/min.

Figure 41 b on page 58 illustrates the appearance of a typical pipe at continuous casting.

## 10.7 Thermal Stress and Crack Formation at Solidification and Cooling Processes

### 10.7.1 Basic Concepts and Relations

A bimetallic thermometer consists of two ribs made of different metals and firmly attached to each other. The double rib is straight at a certain temperature. If its temperature is increased or decreased it bends in one direction or in the opposite one. Its motion can be transferred to a pointer and the thermometer can be calibrated and graded.

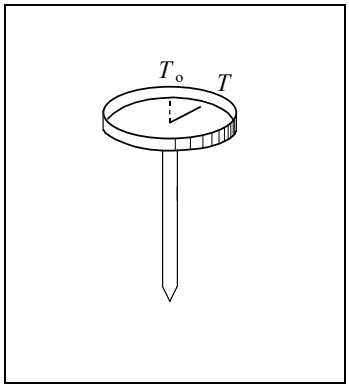


Figure 50 a.
Bimetallic thermometer.

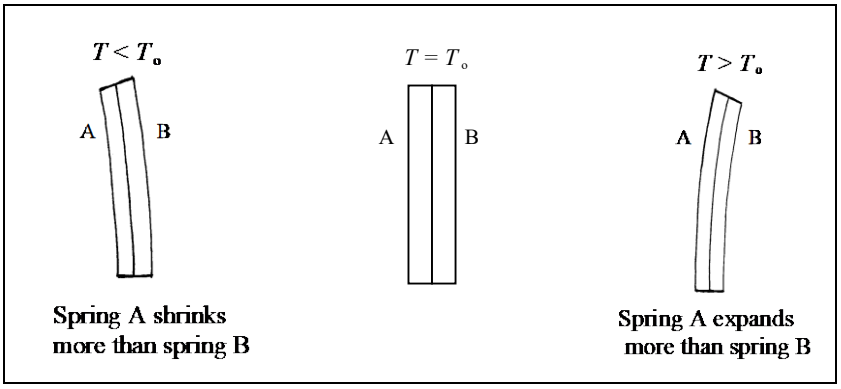


Figure 50 b.
Principle of a bimetallic thermometer.

**Some Concepts and Definitions**

In the example with the bimetallic thermometer both ribs have the same length at the initial temperature. When it is changed, the ribs increase of decrease their lengths with different amounts. This causes mechanical forces in the materials, which result in bending of the ribs, which take new equilibrium positions as a function of the temperature change.

At a temperature change the material ”tries” to change its state of extension due to the thermal dilatation. If the thermal dilatation is allowed to develop freely no stress will arise. If the thermal dilatation is prevented stress will appear in the material.

Forces in solid materials, caused by temperature changes, will be called *thermoforces*. In order to be able to treat them quantitatively we will repeat some concepts and laws of solid mechanics.

By *stress* we mean *force per unit area.* It the force $F$ is perpendicular to the surface with area $A$, the stress is called *normal stress* which is designated by $\sigma$

$$\sigma = \frac{F}{A} \tag{58}$$

If the force lies in the surface plane it is called *shear stress* and is designated by $\tau$

$$\tau = \frac{F}{A} \tag{59}$$

By *dilatation* we mean the *relative length change*, i. e. the *ratio of the length change and the length.*

$$\varepsilon = \frac{\Delta l}{l} \tag{60}$$

where ε is a dimensionless quantity.

## Hooke´s Laws of Tensile and Shear Stresses

Bodies, which are exposed to stresses, will be deformed. The deformations may have two alternative sources:

- mechanical forces
- temperature differences in the material.

### *Deformation at Tensile Stress*

If the relative length change or the dilatation ε, which arises in a rod due to the tensile stress σ, is small then the tensile stress is proportional to the dilatation

$$\sigma = E \cdot \varepsilon \qquad \text{Hooke´s law} \tag{61}$$

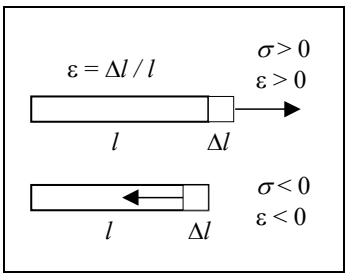

Figure 51.

where the constant $E$ is a material constant, which is called the *modulus of elasticity*.

σ is *positive* for a *tensile* force and *negative* for a *compressive* force. Both are normal stresses.

ε is *positive* in case of *elongation* and *negative* at *contraction*.

*Lateral Contraction*

When the rod in figure 51 is prolonged due to the tensile stress σ its cross-section will shrink. At small tensile stresses the relative transverse contraction $\varepsilon_{trans}$ is proportional to the dilatation in the length direction

$$\varepsilon_{trans} = -\nu \cdot \varepsilon \tag{62}$$

where the proportionally constant $\nu$ is called *Poisson´s number*. For metals this number usually has a value ≈ 0.3.

*Deformation at Shear Stress*

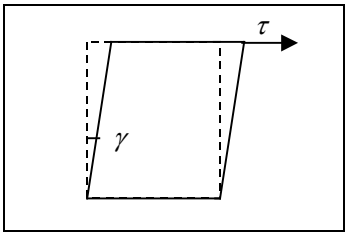

Figure 52.

A shear stress (the force in the surface plane) gives rise to a deformation of a body or an element. The deformation caused by a shear stress is called *shear* or *shearing.* The shearing γ is the change of an originally right angle (see figure 52). At low loads Hooke´s law of shear is valid:

$$\tau = G \cdot \gamma \tag{63}$$

where $G$ is the *modulus of shearing.*

***Relation between Modulus of Elasticity and Modulus of Shearing***

Many materials, especially metals, are isotropic, i. e. have the same properties in all directions. For such materials it is possible to derive a relation between $E$, $G$ and $\nu$. This relation is

$$G = \frac{E}{2\,(1+\nu)} \tag{64}$$

## Stresses and Dilatations in Materials Caused by Temperature Differences

A rod of length $l$ is exposed to a temperature change $\Delta T$ and no external forces act on it. Then we have

$$l + \Delta l = l\left(1 + \alpha \Delta T\right) \tag{65}$$

where

$l$ = length of rod at temperature $T$
$\Delta l$ = change of length at temperature change $\Delta T$
$\alpha$ = length dilatation coefficient.

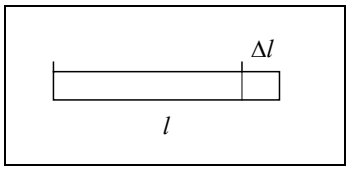

Figure 53.

The temperature change $\Delta T$ gives rise to the length change $\Delta l$

$$\Delta l = l\alpha\, \Delta T \tag{66}$$

$\Delta l/l$ is equal to the dilatation ε and we get

$$\varepsilon = \alpha \Delta T \tag{67}$$

If the rod is exposed to *both* a temperature change $\Delta T$ *and* a stress $\sigma$ simultaneously we can calculate the dilatations, which appear, independently of each other, and then add them (superposition principle). Thus the total dilatation can be written

$$\varepsilon = \frac{\sigma}{E} + \alpha \Delta T \tag{68}$$

Equation (68) can be used to calculate the thermal stress in a rod by the following reasoning. The rod has the initial position, which is illustrated in figure 54 a.

If the rod were free to expand in the $x$-direction (figure 54 b) the dilatation would be $\alpha\Delta T$. On the other hand if the rod were fixed between two rigid walls it would be prevented from extension (figure 54 c). The condition $\Delta l = 0$ is valid and consequently $\varepsilon = 0$ and thermal stress arises in the material.

The thermal stress $\sigma$ which acts on the cross-section of the fixed rod if the temperature increases by the amount $\Delta T$, can be calculated if we insert the condition $\varepsilon = 0$ into equation (68):

$$0 = \frac{\sigma}{E} + \alpha\, \Delta T \tag{69}$$

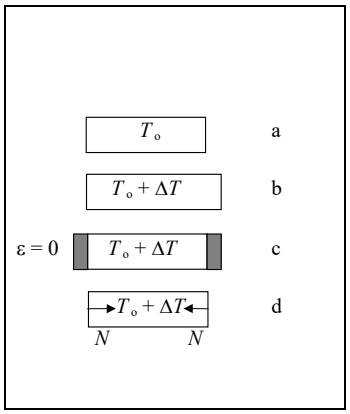

Figure 54.
a) Initial position.
b) Free dilatation.
c) Prevented dilatation.
d) Prevented dilatation. Normal forces replace the rigid walls.

i.e. the thermal stress can be written

$$\sigma = -E\alpha\Delta T \tag{70}$$

The negative sign in equation (70) indicated that the stress is directed inwards and the forces are compressive.

## Hooke´s Generalised Law

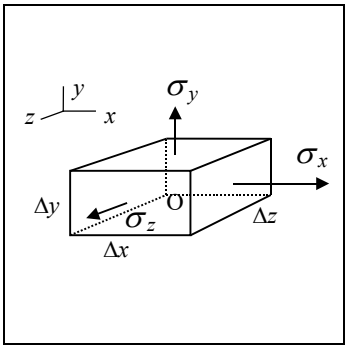


Figure 55.
The components of the tensile stress in the *x*-, *y*- and *z*-directions have only been drawn on three of the six surfaces for the sake of clearness. On the other surfaces there are normal stresses of corresponding sizes and opposite directions $-\sigma_x$, $-\sigma_y$, and $-\sigma_z$.

Consider a small volume element of an isotropic material, which is exposed to a tensile stress $\sigma$ and a temperature increase $\Delta T$ We want to calculate the dilatation, which they cause.

In the general case we start with equation (68) and calculate the components of the dilatation in the *x*-, *y*- and *z*-directions. At the calculation the lateral contraction has to be considered. By aid of equation (62) and equation (68) we get table 3 below, which gives Hooke´s generalised law in composants:

$$\varepsilon_x = \frac{1}{E}\left[\sigma_x - \nu\left(\sigma_y + \sigma_z\right)\right] + \alpha\,\Delta T \tag{71 a}$$

$$\varepsilon_y = \frac{1}{E}\left[\sigma_y - \nu\ \left(\sigma_x + \sigma_z\right)\right] + \alpha\,\Delta T \tag{71 b}$$

$$\varepsilon_z = \frac{1}{E}\left[\sigma_z - \nu\ \left(\sigma_x + \sigma_y\right)\right] + \alpha\,\Delta T \tag{71 c}$$

Table 3. Hooke´s generalised law in components.

| | $\sigma_x$ | $\sigma_y$ | $\sigma_z$ | $\alpha T$ |
|---|---|---|---|---|
| $\varepsilon_x$ | $\frac{\sigma_x}{E}$ | $-\nu\frac{\sigma_y}{E}$ | $-\nu\frac{\sigma_z}{E}$ | $\alpha\cdot\Delta T$ |
| $\varepsilon_y$ | $-\nu\frac{\sigma_x}{E}$ | $\frac{\sigma_y}{E}$ | $-\nu\frac{\sigma_z}{E}$ | $\alpha\cdot\Delta T$ |
| $\varepsilon_z$ | $-\nu\frac{\sigma x}{E}$ | $-\nu\frac{\sigma_y}{E}$ | $\frac{\sigma_z}{E}$ | $\alpha\cdot\Delta T$ |

Below we will restrict the treatment to one-dimensional calculations of thermal stress with known temperature distributions as a basis. Initially we will discuss some simple cases to show the principle of the calculations.

**Thermal Stresses in Materials**

Thermal stresses may exist in materials, which have been produced from melts, which solidify or get heated in connection with design or use. Panes of glass and art glass may for example contain enclosed thermal stresses, which may result in a breakdown without any obvious external reason. Other examples are turbines, jet motors and nuclear reactors where thermal stresses have to be considered at construction and use.

The following types of equations are set up to solve thermoelastic problems:

1. Equilibrium equations, which involve the forces and stresses, which act on the material.
2. Geometrical relations, which the dilatations have to fulfil for compatibility reasons.
3. Equations which describe the materials (for example Hooke´s law) and involve stresses, dilatations and temperature differences.

These equations occur in all problems where thermal stresses and thermal dilatations are to be calculated. In each special problem there are, in addition

4. Specific boundary conditions.

Many of the listed equations are linear partial differential equations. The solutions are *additive*, i. e. a combined problem can be parted into several separate subproblems, which can be solved separately and then be added to give the final solution (the superposition principle).

In cases, where one-dimensional dilatation is considered, the calculations will often be considerably simpler if a fictive so-called *fixed normal force* $\mathrm{d}N\,(\Delta T) = -E\alpha\Delta T$ is introduced. It

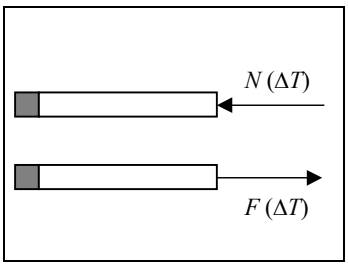

Figure 56.

acts on each little element to prevent dilatation, when the temperature increases by the amount $\Delta T$. Secondly $\Delta T$ is a function of one or several position-determining co-ordinates. The fixed normal forces do not exist in reality and it is thus necessary to introduce an additional force of equal size and opposite direction to the fixed normal force $N(\Delta T)$.

$$F(\Delta T) = \iint_A E\alpha\Delta T \cdot \mathrm{d}A \tag{72}$$

From equation (72) the stress, which acts on a cross-section $A$, can be calculated:

$$\sigma = \frac{F}{A} \tag{73}$$

The reason for using the average stress in the calculations is that it does not matter in what way all the subforces are distributed, at positions, which deviate slightly from the end surface. This statement is called Saint-Venant´s principle. It is thus possible to use $F$ in the calculations instead of all the small real subforces and the average stress instead of the real stresses, which act on the surface elements.

The thermal stress, which acts on an internal area element, is equal to the sum of the average stress, caused by the force $F(\Delta T)$ and the negative fixed normal stress.

$$\sigma^{\mathrm{T}} = \frac{\iint_A E\alpha\Delta T \cdot \mathrm{d}A}{A} - E\alpha\Delta T \tag{74}$$

An example will illustrate the principle of calculation.

---

**Example 9.**

The temperature in a rectangular metal plate with the constant thickness $2c$ is a linear function of $y$ and independent of $x$ and $z$ (see figure on next page). The plate can expand freely in the $y$-direction. Calculate the thermal stresses in the $x$- and $z$-directions if

$$\Delta T = \frac{y}{c} \cdot \Delta T_{\mathrm{o}}$$

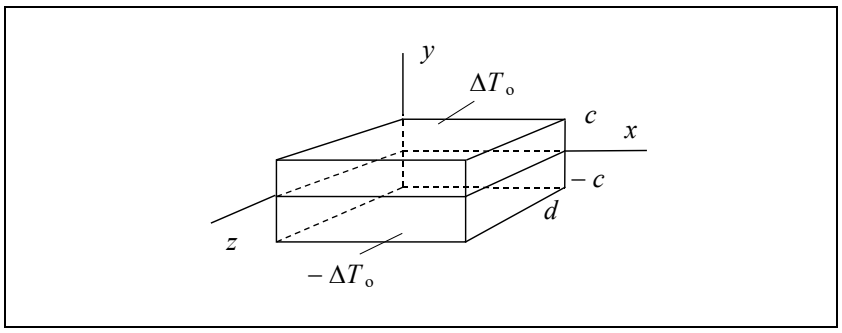


Temperature distribution in a thin rectangular metal plate with the sides 2*l* and 2*c*.

**Solution:**

Since the plate can expand freely in the *y*-direction no stress will appear in this direction, i. e.

$$\sigma_y = 0 \qquad (1')$$

We also know that no expansion can occur in the *x*- and *z*- directions,. i. e.

$$\varepsilon_x = \varepsilon_z = 0 \qquad (2')$$

Inserting (1′) and (2′) into equation (71 a) gives

$$0 = \varepsilon_x = \frac{1}{E}\left(\sigma_x - v\sigma_z\right) + \alpha\,\Delta T \qquad (3')$$

Inserting (1′), (2′) and (3′) into equation (71 c) gives

$$0 = \varepsilon_z = \frac{1}{E}\left(\sigma_z - v\sigma_x\right) + \alpha\,\Delta T \qquad (4')$$

By combining equations (3′) and (4′) we get the fixed stresses

$$\sigma_x = \sigma_z = \frac{-E\alpha\,\Delta T}{1-v} \qquad (5')$$

We insert the relation $\Delta T = \frac{y}{c}\cdot\Delta T_o$ into equation (5′) and get

$$\sigma_x = \sigma_z = \frac{-E\alpha\,\Delta T_o}{1-v}\cdot\frac{y}{c} \qquad (6')$$

or

$$\overline{\sigma_x} = \overline{\sigma_z} = \frac{F_x}{2cd} = \frac{1}{2cd}\int_{-c}^{+c} E\alpha\,\Delta T \cdot d \cdot \mathrm{d}y = \frac{E\alpha\,\Delta T_o d}{2cd}\int_{-c}^{+c}\frac{y}{c}\cdot \mathrm{d}y = 0 \qquad (7')$$

(6′) and (7′) are inserted into equation (74), which gives

$$\sigma_x = \sigma_z = 0 - \frac{E\alpha\,\Delta T_o}{1-\nu}\cdot\frac{y}{c}$$

The total thermal stress will thus be equal to the expressions in equation (6′).

**Answer:** The stresses are $\sigma_x = \sigma_z = \dfrac{-E\alpha\,\Delta T_o}{1-\nu}\cdot\dfrac{y}{c}$.

---

The maximum thermal stress in example 9 above will be ($y = c$)

$$\sigma_x = \sigma_z = \frac{-E\alpha\,\Delta T_o}{1-\nu} \qquad (75)$$

It is true that the thickness of the plate is not included in equation (7′) but a thicker plate has generally a greater temperature difference between its two parallel surfaces than a thin one. The risk that a plate of brittle material breaks due to thermal stresses is thus greater for a thick plate than for a thin one.

In many applications one side of the plate stays in contact with hot gases of varying temperatures. The result is a varying heat flow through the plate, caused by the temperature variations, and alternating positive and negative dilatations of the material. This gives a risk of cracks in the material after long use.

### 10.7.2 Thermal Stress and Dilatation at Solidification and Casting Processes

At ingot castings and continuous casting a solidifying shell is formed as soon as the melt gets into contact with the chill-mould. During the solidification and cooling process the temperature is strongly changed as a function of position and time. Strong thermal stresses appear as a consequence of the temperature gradients in the solidifying shell.

If the thermal stresses are so large that the elasticity limit is exceeded surface cracks, intermediate cracks or centre cracks appear in the material, which strongly deteriorate the final product.

The sizes of the thermal stresses also depend on the rate of the temperature variations in the material. If they are very rapid, the effect will be larger than at slower temperature variations and is described as *thermal chock.*

If a material is exposed to repeated cyclic temperature variations the effect can be described as *thermal fatigue* of the material. The phenomenon must be taken into consideration at construction and production. Besides, it is necessary to watch thermal fatigue carefully because it causes risk of crack formation, which under special circumstances may give disastrous consequences, for example for jet motors in air-crafts or tubes in nuclear power plants.

Below we will discuss different types of thermal stresses, mathematical models for calculation of thermal stresses and the corresponding dilatations and also thermal stress and dilatation at continuous casting.

### 10.7.3 Mathematical Models of Thermal Stress at Unidirectional Solidification

The condition for calculation of thermal stresses is complete knowledge of the temperature in the material as a function of position and time.

*Two* mathematical models are required for thermal stress calculations, one for calculation of the temperature variations and another one for calculation of the mechanical stress dilatation process on the basis of the known temperature distribution in position and time.

This is a difficult and time-consuming task. In the general case there are seldom exact, analytical solutions. Many different calculation methods have been developed, which give more or less accurate solutions. The most common numerical method is based on the *finite element method,* the FEM-method. Another method is based on bar theory.

In some cases the calculations can be simplified by calculations in one or two instead of three dimensions. One may for example assume that a stress or a dilatation is planar.

One example of a planar stress is a thin plate with a temperature $T(x,y)$, which only varies in the plane of the plate and is constant in the $z$-direction, i. e. in the direction of thickness. The stresses in the $z$-direction can be neglected, i. e. stresses occur only in the $xy$-plane.

It is reasonable to assume a planar dilatation when one dimension is dominating and the temperature is a function of this dimension. As an example a long cylinder with fixed ends can be mentioned. There is no axial motion, which means that $\varepsilon_z = 0$.

The simplest analysis of thermal stresses involves only elastic stresses (normal stresses and shear stresses). If the material is very ductile and the thermal stresses strong enough, the dilatation will no longer depend linearly on the stress but a non-linear plastic term (plastic stress) has to be added, which complicates the solution considerably.

**Thermal Stress at Unidirectional Solidification**

At ingot casting, and especially at continuous casting, different types of cracks and other defects appear in the solidified material. These cracks arise during the cooling process when the steel has a temperature slightly below the solidus temperature. Thus it is more urgent to study the dilatations than the stresses themselves.

Calculations of thermal stresses and dilatations at unidirectional solidification are much more complicated than the ones in example 9 on page 76. In this case we had a stationary temperature fields, while the temperature at unidirectional solidification is a function of both position and time.

At a careful calculation of the temperature distribution at unidirectional solidification it is necessary to consider the temperature field both in the solidifying shell and in the two-phase region.

### *Calculation of the Temperature Distribution in the Solid Phase*

The temperature distribution at unidirectional solidification is in principle the one shown in figure 57.

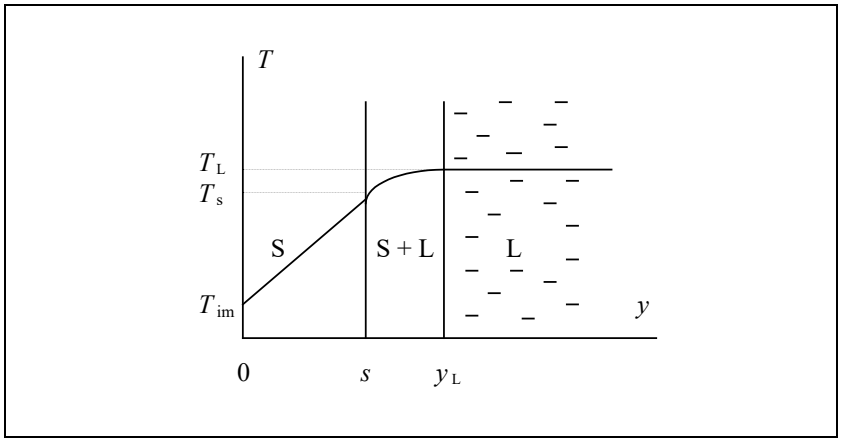


Figure 57.
Unidirectional solidification with no excess temperature.

The heat flow occurs in the $y$-direction and the problem can thus be treated as one-dimensional. $T_L$ is constant while the surface temperature $T_{im}$ of the metallic shell and the thickness $s$ and the position of the solidification front $y_L$ are functions of time.

The calculation of the temperature distribution and the thermal stresses during the solidification and cooling process can be performed by three different methods.

1. We can assume $T(y,t)$ to be a square function of $y$ and determine the constants by aid of known boundary conditions.
2. We assume $T(y,t)$ to be a function of the third degree of $y$ and determine the constants by aid of known boundary conditions.
3. We use FEM (Finite Element Method).

FEM is the most accurate method and can be regarded as the true answer. A comparison between FEM-calculations and calculations, based on method 2, is given in figure 58 on page 83.

### *Calculation of Thermal Stresses and Dilatations*

On the basis of the alternative temperature fields, derived by aid of FEM respectively the third-degree function of *y,* the dilatations and thermal stresses can be calculated as functions of *y* and *t*.

This task is much more difficult than the calculations we performed in example 9. In that case we had a stationary temperature field, i. e. *T* is a function of position but not of time.

At calculation of thermal stresses and dilatations at unidirectional solidification the temperature *T* is a function of *both* the position *y* and the time *t* as indicated above.

It can be shown that the total dilatation $\varepsilon^{u}$ as a function of *y* and *t* at unidirectional solidification can be written

$$\varepsilon^{u}(y,t) = \int_{t^*}^{t} \left[ \frac{1}{s} \int_{0}^{s} \frac{\partial \varepsilon^{T}}{\partial t} \mathrm{d}y \right] \cdot \mathrm{d}t + \varepsilon^{T}(T_{\text{rigid}}) - \varepsilon^{T}(T) \qquad (76)$$

where

$\varepsilon^{u}$ = total dilatation at unidirectional solidification

$\varepsilon^{T}$ = thermal dilatation caused by the sum of the average thermal stress and the negative fixed normal stress (page 74)

$s$ = position of the solidification front at time $t$

$t^*$ = the time when the solidification front reaches position $y$

$T$ = temperature at position $y$ and time $t$

$T_{\text{rigid}}$ = temperature at which the material is rigid enough to resist compressive and tensile stresses. The temperature is chosen between $T_{\text{L}}$ and $T_{\text{s}}$, often at the temperature when the fraction of solid is 0.60.

The co-ordinate system has been chosen perpendicular to the solidification front with $y = 0$ at the surface of the shell. $s$ is the position of the solidification front at time $t$. $y$ is situated within the solid phase, i. e. within the limits $0 \le y \le s$ .

At the first sight it is difficult to see that the right hand side of equation (76) is a function of *y*. However, the lower limit $t^*$ is a

function of $y$ as $t^*$ is the time when the solidification front reaches position $y$. The relation can be written

$$s(t^*) = y \tag{77}$$

The result of the calculations (equation (76) in combination with the known temperature distribution), which are performed by a computer, is shown in figure 58.

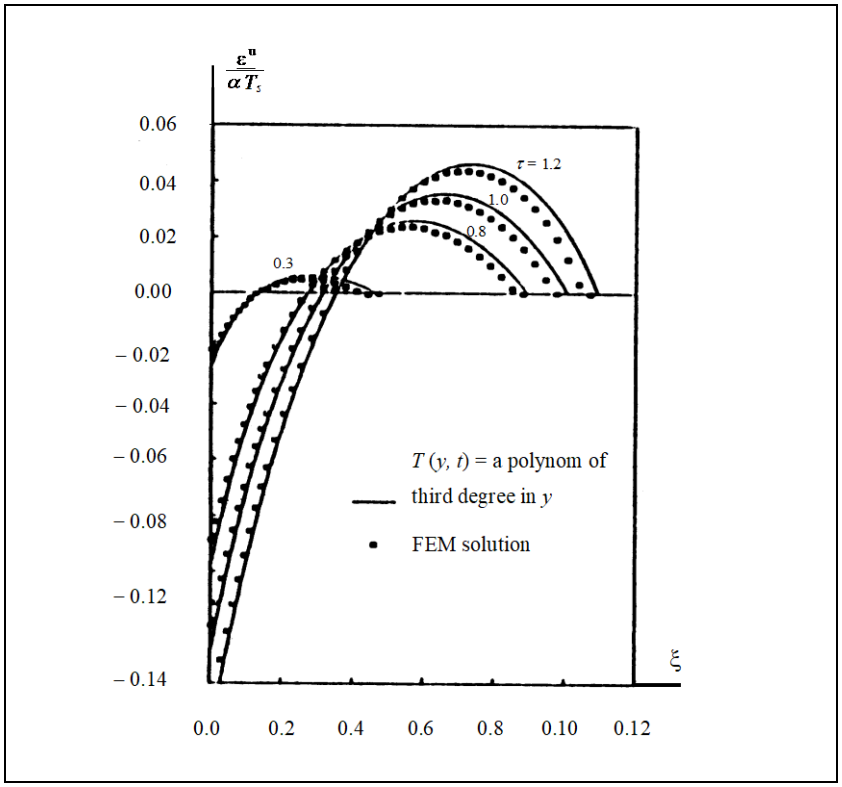


Figure 58.
Calculated dilatations $\varepsilon^u$ at unidirectional solidification as a function of the distance $y$ from the surface of the solidified shell at various times.

In the figure dimensionless quantities are used:

$$\xi = \frac{Q_o^*}{kT_s} \cdot y$$

where $Q_o^*$ = thermal flow at $t = 0$ and $y = 0$.

$$\tau = \left(\frac{Q^*}{T_s}\right)^2 \cdot \frac{t}{\rho ck}$$

where $Q^*$ = thermal flow at $t = 0$ and position $y$.

It can be seen from the figure that a temperature field of the third degree gives a good agreement with ”the true answer” FEM, especially for low $y$-values.

## Simplified Method for Calculation of the Dilatation at Unidirectional Solidification

The calculations behind the curves in figure 58 above are extensive and time-consuming even if computers are used. It may be worth while to try to find simplified methods for the

calculations even if simplified assumptions are necessary. Obviously these simplifications leads to a worse result, compared to reality, than the methods described above. The advantage is that a comparatively rapid and rather good information is obtained, which immediately can be applied and tested in industry. Besides, a better understanding of the course of the calculations, is achieved.

We make the following assumptions:

1 No consideration is taken to the solidification interval of the alloy. We start with a known temperature distribution, which is valid for a pure metal. The assumption implies that $T_S = T_L$.

2 Temperature distribution and functions for the surface temperature and thickness of the solidifying shell are taken from chapter 4 and 5 in this book.

The calculation method is illustrated concretely as a solved example. In analogy with the more accurate calculations we will use equation (71) for calculation of the dilatations.

---

**Example 10.**

In a foundry one worries about crack formation at continuous casting and wants to design the casting process in such a way that the risk of cracks and other defects, caused by thermal stresses, becomes a minimum. A first step is to map the risks of crack formation. The task to do this is entrusted to you.

Derive approximate expressions of

a) the surface temperature $T_{im}$ of the solidifying shell as a function of the shell thickness $s$ the thickness $s$ of the solidifying shell as a function of time $t$

b) the dilatation $\varepsilon^u$ as a function of $y$.

c) Perform the calculations a) - c) and give the dilatation as a function of $y$ in the shape of a table and a diagram at two alternative shell thicknesses, $s = 0.01$ m and $s = 0.02$ m.

For the planned casting process the data in the margin are valid. The temperature of the cooling water $T_o \leq 100$ °C.

| Material constants | |
|---|---|
| $k$ | = 30 W/mK |
| $h$ | = 750 W/m$^2$K |
| $-\Delta H$ | = 2.17·10$^{10}$ J/m$^3$ |
| $T_S$ | = 1500 °C |
| $\alpha$ | = 10$^{-5}$ K$^{-1}$ |

At the calculations the temperature distribution given below and known functions for surface temperature $T_{im}$ can be used. The required time to achieve a given shell thickness of the strand, can be taken from figure 17 on page 31 in chapter 4, equation (45) and equation (48) on page 34 in chapter 4.

$$T_{im} = \frac{T_L - T_o}{1 + \frac{h}{k} y_L(t)} + T_o \qquad (1')$$

and

$$t = \frac{\rho(-\Delta H)}{T_L - T_o} \cdot \frac{y_L}{h} \cdot \left(1 + \frac{h}{2\,k} \cdot y_L\right) \qquad (2')$$

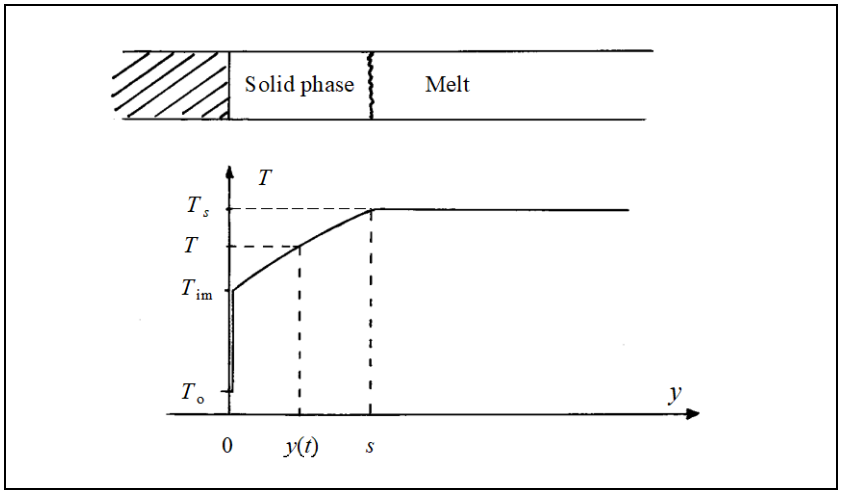


**Solution:**

a)

In order to get the thickness of the solidifying shell as a function of time we start with equation (2′) with the new designations:

$$t = \frac{\rho(-\Delta H)}{h\left(T_s - T_o\right)} \cdot s \cdot \left(1 + \frac{h}{2k} \cdot s\right) \qquad (3')$$

and solve $s$ as a function of $t$ from this second order equation

$$s^2 + \frac{2k}{h} \cdot s = \frac{2k\left(T_s - T_o\right)}{\rho\left(-\Delta H\right)} \cdot t \qquad (4')$$

which has the positive solution

$$s = -\frac{k}{h} + \sqrt{\left(\frac{k}{h}\right)^2 + \frac{2k\left(T_s - T_o\right)}{\rho\left(-\Delta H\right)} \cdot t} \qquad (5')$$

which is the desired solution.

b)

Equations (1′) and (2′) have to be adapted to the designations used in equation (76) on page 82. The designation $y_L$ ís replaced by $s$ and $T_L$ by $T_s$.

$T_{im}$ is the temperature of the solidifying shell, close to the mould. Thus we get directly

$$T_{im} = \frac{T_s - T_o}{1 + \frac{h}{k} \cdot s} + T_o \qquad (6')$$

c)

To find the desired function we start with equation (76). It is valid for unidirectional solidification.

$$\varepsilon^u(y,t) = \int_{t^*}^{t} \left[ \frac{1}{s} \int_0^s \frac{\partial \varepsilon^T}{\partial t} \mathrm{d}y \right] \cdot \mathrm{d}t + \varepsilon^T(T_s) - \varepsilon^T(T) \qquad (7')$$

where $t^*$ is the time when the solidification front passes position $y$:

$$s(t^*) = y \qquad (8')$$

We know from example 9 on page 76 that $\varepsilon^T = \alpha \Delta T$ and assume that $\alpha$ is a constant, independent of time and temperature. We have

$$\alpha = \frac{\mathrm{d}\varepsilon^T}{\mathrm{d}t} = \text{constant}$$

and we get

$$\varepsilon^{T}(T_S) - \varepsilon^{T}(T) = \alpha(T_S - T) \qquad (9')$$

We will also need the function $\frac{\partial \varepsilon^{T}}{\partial t}$, which is obtained by partial derivation of equation (9′) with respect to time:

$$\frac{\partial \varepsilon^{T}}{\partial t} = \alpha \cdot \frac{\partial T}{\partial t} \qquad (10')$$

In order to get at useful expression of $\frac{\partial T}{\partial t}$ we will set up the equation of the inclined line in the figure on page 85:

$$T(y,t) = \frac{T_S - T_{im}}{s} \cdot y + T_{im} \qquad (11')$$

Partial derivation of equation (11′) with respect to time gives

$$\frac{\partial T}{\partial t} = \frac{s \cdot \left( -\frac{\partial T_{im}}{\partial t} \right) - \frac{\partial s}{\partial t}(T_S - T_{im})}{s^2} \cdot y + \frac{\partial T_{im}}{\partial t} \qquad (12')$$

Equation (12′) introduced another unknown derivative, $\frac{\partial T_{im}}{\partial t}$. It can be obtained by aid of equation (6′), which can be transformed into

$$T_{im} = \frac{T_S - T_o}{1 + \frac{h}{k} \cdot s} + T_o = \frac{T_S + T_o \frac{h}{k} \cdot s}{1 + \frac{h}{k} \cdot s} \qquad (13')$$

Equation (13′) is partially derived with respect to time and we get

$$\frac{\partial T_{im}}{\partial t} = \frac{T_o \frac{h}{k} \cdot \frac{\partial s}{\partial t}\left(1 + \frac{h}{k} \cdot s\right) - \frac{h}{k} \cdot \frac{\partial s}{\partial t}\left(T_S + T_o \frac{h}{k} \cdot s\right)}{\left(1 + \frac{h}{k} \cdot s\right)^2} \qquad (14')$$

We must also find an expression of $\frac{\partial s}{\partial t}$. It is obtained by partial derivation of equation (5′) with respect to time:

$$\frac{\partial s}{\partial t} = \frac{\frac{k\left(T_S - T_o\right)}{\rho\left(-\Delta H\right)}}{\sqrt{\left(\frac{k}{h}\right)^2 + \frac{2k\left(T_S - T_o\right)}{\rho\left(-\Delta H\right)} \cdot t}} \qquad (15')$$

Inserting (9′), (10′), (12′) and (14′) into equation (7′) and integration gives

$$\varepsilon^u(y,t) = \alpha\left[\int_{t^*}^{t}\left(\frac{1}{s}\int_0^s \frac{s\cdot\left(-\frac{\partial T_{im}}{\partial t}\right) - \frac{\partial s}{\partial t}\cdot\left(T_S - T_{im}\right)}{s^2}\cdot y + \frac{\partial T_{im}}{\partial t}\right)\cdot \mathrm{d}y\,\mathrm{d}t + T_S - T\right] =$$

$$= \alpha\left[\int_{t^*}^{t}\left(\frac{1}{s}\int_0^s \frac{s\cdot\left(-\frac{\partial T_{im}}{\partial t}\right) - \frac{\partial s}{\partial t}\cdot\left(T_S - T_{im}\right)}{s^2}\cdot\frac{s^2}{2} + \frac{\partial T_{im}}{\partial t}\cdot s\right)\cdot \mathrm{d}t + T_S - T\right]$$

or

$$\varepsilon^u(y,t) = \alpha\left[\int_{t^*}^{t}\left(\int_0^s \frac{\frac{\partial T_{im}}{\partial t}}{2} - \frac{\frac{\partial s}{\partial t}\cdot\left(T_S - T_{im}\right)}{2s}\right)\cdot \mathrm{d}t + T_S - T\right] \qquad (16')$$

which is a function of $y$ as $t^*$ is a function of $y$.

d)

The expressions for $\frac{\partial T_{im}}{\partial t}$, $\frac{\partial s}{\partial t}$, $T_{im}$, $s$ and $T$ are taken from equations (14′), (15′), (5′), (6′) and (11′) for calculation of $\varepsilon^u$. $t^*$ is calculated from equation (8′).

The calculations are made by aid of a computer. The result is given in the table.

| $y$ m | $t^*$ s | $\varepsilon^u(y,t)$ for $s$ = 0.010 m | | $y$ m | $t^*$ s | $\varepsilon^u(y,t)$ for $s$ = 0.020 m |
|---|---|---|---|---|---|---|
| 0.0001 | 0.18 | – 0.156 | | 0.0001 | 0.18 | – 0.49 |
| 0.0010 | 1.85 | – 0.099 | | 0.0020 | 3.74 | – 0.30 |
| 0.0019 | 3.55 | – 0.052 | | 0.0039 | 7.45 | – 0.14 |
| 0.0028 | 5.24 | – 0.015 | | 0.0058 | 11.36 | – 0.02 |
| 0.0037 | 7.07 | 0.013 | | 0.0077 | 15.41 | 0.06 |
| 0.0046 | 8.88 | 0.033 | | 0.0096 | 19.63 | 0.11 |
| 0.0055 | 10.73 | 0.045 | | 0.0115 | 24.01 | 0.14 |
| 0.0064 | 12.61 | 0.050 | | 0.0134 | 28.56 | 0.15 |
| 0.0073 | 14.54 | 0.047 | | 0.0153 | 33.27 | ..0.13 |
| 0.0082 | 16.51 | 0.038 | | 0.0172 | 38.15 | 0.09 |
| 0.0091 | 18.50 | 0.022 | | 0.0191 | 43.20 | 0.03 |
| 0.0100 | 20.54 | 0.000 | | 0.0200 | 45.64 | 0.00 |

**Answer:**

a) $$s = -\frac{k}{h} + \sqrt{\left(\frac{k}{h}\right)^2 + \frac{2k\left(T_s - T_o\right)}{\rho\left(-\Delta H\right)} \cdot t}$$

b) $$T_{im} = \frac{T_s - T_o}{1 + \frac{h}{k} \cdot s} + T_o$$

c) $$\varepsilon^u(y,t) = \alpha \left[ \int_{t^*}^{t} \left( \int_0^s \frac{\frac{\partial T_{im}}{\partial t}}{2} - \frac{\frac{\partial s}{\partial t} \cdot \left(T_S - T_{im}\right)}{2s} \right) \cdot \mathrm{d}t + T_S - T \right]$$

d) See table above.

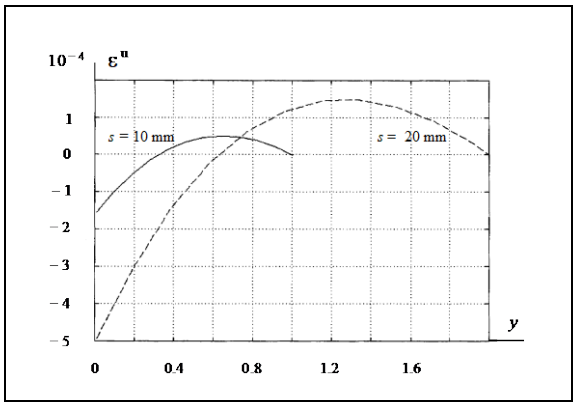


---

### 10.7.4 Air Gap Formation due to Thermal Contraction

In chapter 5, section 5.5.1 and 5.5.2 on pages 28-37 we discussed the formation of an air gap between a mould and a solidifying shell. The basis for the discussion was the heat transport through the shell across the air gap. The formation of an air gap was shortly described as a contraction of the solidified shell.

Here we will complete the discussion on air gaps, analyse the phenomenon from the aspect of thermal stress and report some general experimental results.

#### Principal Description of Air Gap Formation

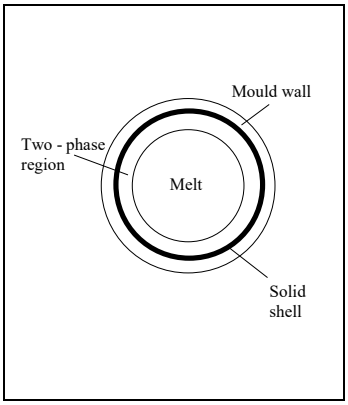


Figure 59.

Consider a cylindrical chill-mould wall (figure 59) under a constant hydrostatic pressure. Immediately after the casting, which is assumed to occur instantly, a thin shell is formed close to the chill-mould wall. The thickness of the shell grows, its average temperature decreases and the temperature gradient becomes steeper. When the cooling shell gradually grows the hydrostatic pressure from the melt will press the shell towards the mould but the temperature decrease dominates over this effect after a certain time and the cooling shell contracts in all directions.

If the cast metal is an alloy with a broad solidification interval the whole shell is not compact at the beginning but contains melt between the crystals and between the dendrites of each crystal with a higher concentration of alloying elements than the solid phase. This is also the situation for the inner part of the casting during the continued solidification process.

The surface wall of the chill-mould warms up due to the heat transport from the solid shell. Its temperature increases gradually and the surface wall *expands* slightly and moves inwards at the beginning. However, the contraction of the shell is larger than the expansion of the mould wall. At a certain thickness the shell looses the contact with the chill-mould and an air gap, which grows continuously, is formed.

## Correlation between Air Gap Width and Heat Transfer Coefficient

Intense efforts have been made to determine the overall heat transfer coefficient and its time dependence. All such experiments show uniformly the same result. A typical example is given in figure 60, which shows the heat transfer coefficient at permanent mould casting as a function of time.

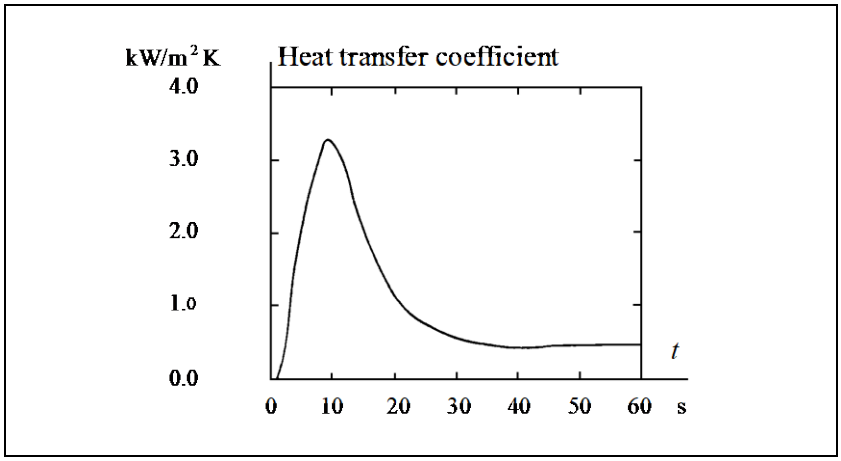


Figure 60.
Heat transfer coefficient of an AlSi-alloy at permanent mould casting as a function of time.

The heat transfer coefficient reaches a maximum after a rapid increase, followed by a gradual decrease to a constant value. The rapid increase during the first seconds can be explained as a gradual build-up of the metallostatic pressure during mould filling.

A large number of parameters, among them the metallostatic pressure from the melt and the roughness of the mould surface influence the maximum value of $h$.

After passage of the maximum value, $h$ starts to decrease, due to air gap formation. Measurements on the air gap formation process offer a quite complicated problem. Nevertheless a large number of successful results have been reported. In most cases transducers have been used. An example of such measurements will be presented here.

The relative displacements of the mould and the metal, due to expansion and contraction due to temperature variations, are measured. The result is illustrated in figure 61. Movements

towards the centre of the cylinder are considered as positive. Negative values correspond to movements towards the periphery.

The upper curve in figure 61 shows the contraction of the metal. The lower curve represents the expansion of the mould when the solidified shell is strong enough to withstand the metallographic pressure.

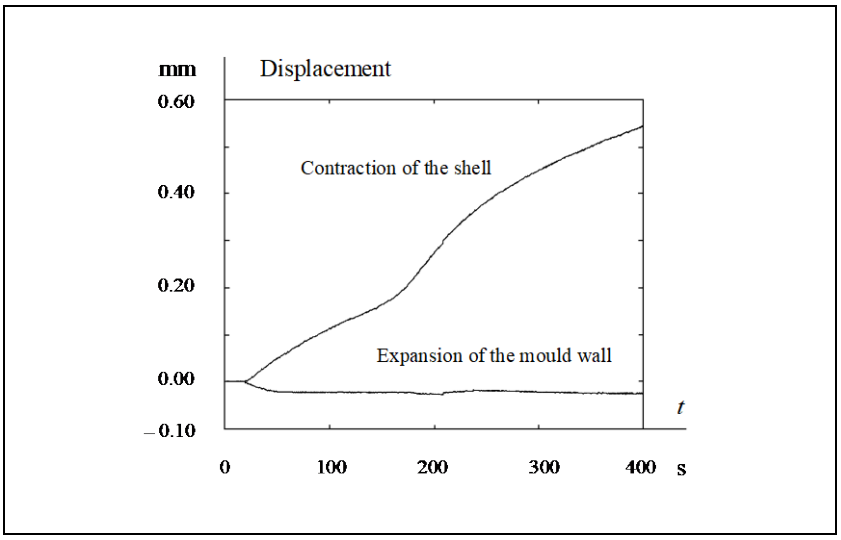


Figure 61.
Average displacement of the metal (upper curve) respectively the mould (lower line) as a function of time.

The measurements have been analysed theoretically. The air gap was calculated by use of thermal contraction due to temperature gradients. During the solidification process a certain fraction of lattice defects is formed. The defects get annealed and the material shrinks during this process.

The calculated air gap and the heat transfer coefficient, derived from the air gap, vary with time as shown in figures 62 and 63. Time is chosen as zero at the start of the solidification. In figure 62 the calculated thermal air gap and the air gap due to vacancy condensation are shown together with the sum of the two effects.

The calculations show that it is not possible to fit the calculated thermal air gap, due to thermal shrinkage only, with the measured air gap. Addition of the effect from vacancy condensation to the thermal shrinkage gives results, which fit with the measured data for the contraction of the casting during the solidification.

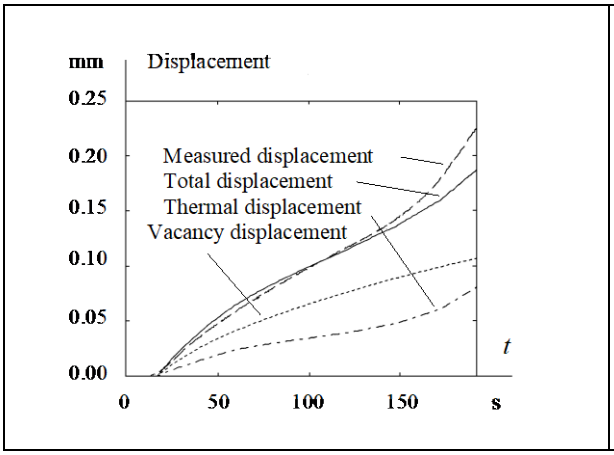


Figure 62.
Displacement of solidifying shell due to thermal shrinkage, vacancy condensation and the sum of the two effects. The calculated total displacement is compared with experimental values.

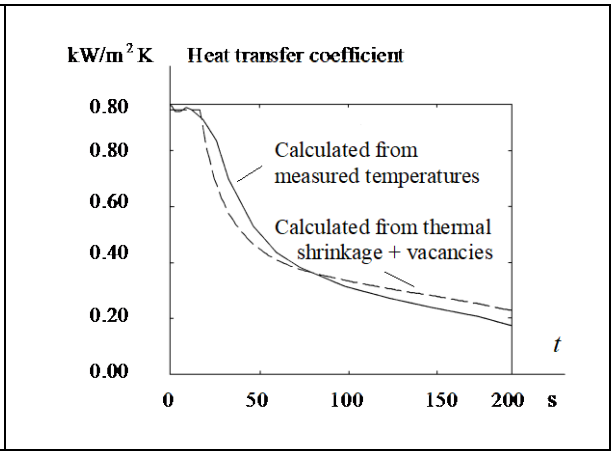


Figure 63.
Heat transfer coefficient from temperature measurements, respectively calculated from air gap due to thermal shrinkage and vacancy condensation.

Even the small quantities of entrapped vacancies, found in these experiments, have a large influence on the gap formation.

The effect of the air gap is expressed macroscopically as an heat transfer coefficient of the gap by aid of the well-known relation

$$h = \frac{k}{\delta} \tag{78}$$

where

$h$ = heat transfer coefficient of air
$k$ = thermal conductivity of air
$\delta$ = width of the air gap.

The heat transfer coefficients, which correspond to the calculated air gaps, can be derived by aid of equation (78). If these $h$-values are plotted as a function of time, the dotted curve in figure 63 is obtained.

The heat transfer coefficients were also determined from experimental temperature measurements. If these values are plotted as a function of time the continuous curve in figure 63 is obtained. The two curves show a satisfactory agreement.

### 10.7.5 Air Gap Formation in Ingots

When a melt is teemed into a chill-mould it starts to solidify because heat is transported away from the melt and outwards through the chill-mould. The solid phase nucleates on the cold mould surface and form a layer, which grows inwards, perpendicular to the surface.

At the beginning of the solidification process the solidification rate is mainly controlled by the heat transport from the solidifying shell and the chill-mould. A thin film of solidified steel is formed at the bottom and walls of the cold chill-mould, which fixes the external shape of the ingot. The thin shell cannot resist the pressure from the internal liquid steel mass but is pressed towards the chill-mould wall and becomes deformed in such a way that the outer dimensions of the shell initially keeps constant.

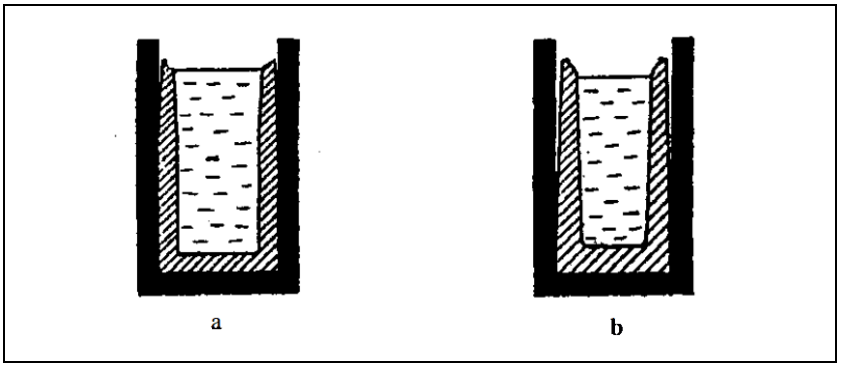


Figure 64.
a) The steel shell starts to loose the contact with the upper part of the chill-mould.
b) The steel shell has lost the contact with the chill-mould almost completely.

When the thickness of the steel shell grows its mechanical strength becomes large enough to resist the pressure from the liquid steel. The shell cools, shrinks and the ingot looses the contact with the chill-mould wall, at first in the upper part of the chill-mould where the pressure of the steel melt is lowest (figures 64 a).

At the moment when the shell looses the contact with the mould wall the heat transport conditions becomes radically changed. The heat transfer is strongly reduced due to the air insulation between the ingot and the chill-mould. The temperature becomes lower in the lower part of the ingot because the heat transport is more efficient there. This results in an ingot shell

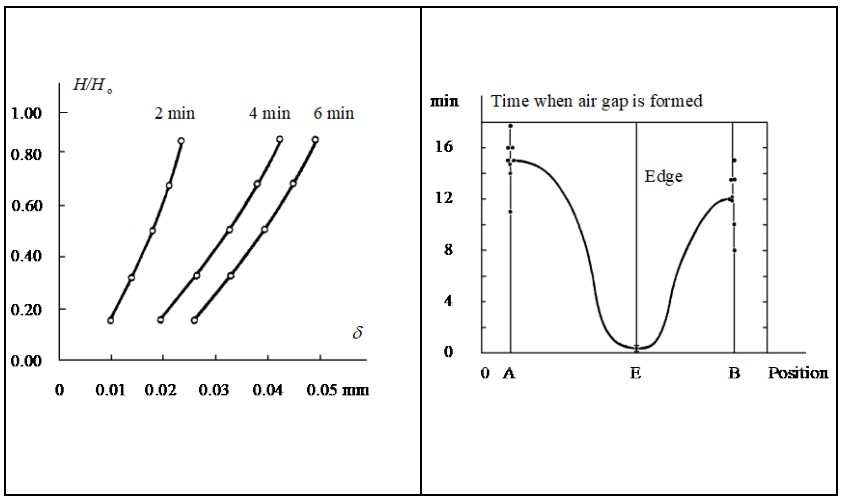


Figure 65. Left figure.
Air gap thickness $\delta$ as a function of the relative height $H/H_o$ of the ingot and the solidification time.

Figure 66. Right figure.
Time of air gap formation as a function of position.
$t = 0$ corresponds to the start of the casting process. Points A and B are explained in figure 67.

with increasing thickness downwards. Later the ingot looses the contact with the chill-mould wall entirely (figure 64 b). The continued heat transport through the steel shell controls the lateral solidification rate.

Figure 65 shows the thickness of the air gap as a function of the height of the ingot. The contact with the walls is not lost uniformly. This is evident from figure 66, which shows the time for air gap formation as a function of position. The air gap is initially formed at the corners and later on at the sides of the chill-mould.

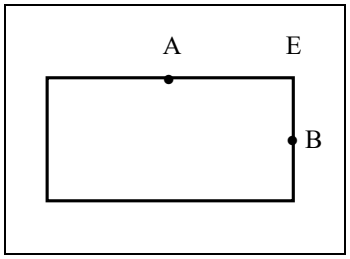


Figure 67.
Cross-section of an ingot, seen from above.

In most cases the shrinkage of the ingot shell causes a deformation of the ingot section because the shrinkage stress is inhomogeneously distributed in the corners and at the sides of the ingot, due to cooling of various strength.

### 10.7.6 Elastic Properties of Steel at High Temperatures. Hot Cracks

During solidification and/or hot working of metallic materials so-called hot cracks will appear in the material at temperatures immediately below the solidus temperature. Bishop, Ackerlind and Pellini have shown that thin films of melt occur in the interdendritic region and at the crystal boundaries. Such films deteriorate the plastic properties and reduce the ductility of the

material considerably. Hot cracks are caused by thermal strain in the material and propagate via the streaks of melt along the grain boundaries.

External forces and/or inconvenient design of the mould contribute to the hot cracks. By elimination of these sources of cracks as much as possible, the risk of hot cracks will be reduced. It is also urgent to know the plastic properties of the materials as function of temperature for judgement of the size and extension of the thermal strain and thus the risk of hot cracks.

## Experimental Method

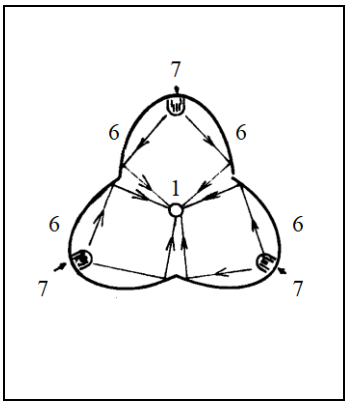


Figure 68.
1. Sample material.
2. Ellipsoid-shaped mirrors.
7. Heat sources.

Experimental determination of the ductility of steel as a function of temperature offers several difficulties. One reason is that the technique of measurement is difficult at the high temperatures in question. Another reason is that the microstructure of the material influences the result. The same ductility and thermal strain is *not* obtained at a certain temperature of measurement if the measurements are performed on directly solidified material (melt which has solidified and cooled down to the temperature of measurement) or on reheated material (from room temperature to the temperature of measurement).

Fredriksson and Rogberg have developed a simple equipment for measurement of ductile stresses at high temperatures (figures 68 and (69).

The heat source of consists of three ellipsoid-shaped reflectors and three 800 W halogen lamps. The heating filament of each lamp is situated in one of the foci of the ellipsoid and the sample in the other common focus of all three ellipsoids. In this way a sample can be heated to the liquidus temperature in 3-4 minutes. The molten zone adopts the shape of a pear and is kept in position by the surface tension. The temperature is measured by thermocouples.

By aid of thermocontrol equipment the molten zone can be cooled at a predetermined cooling rate and in such a way a

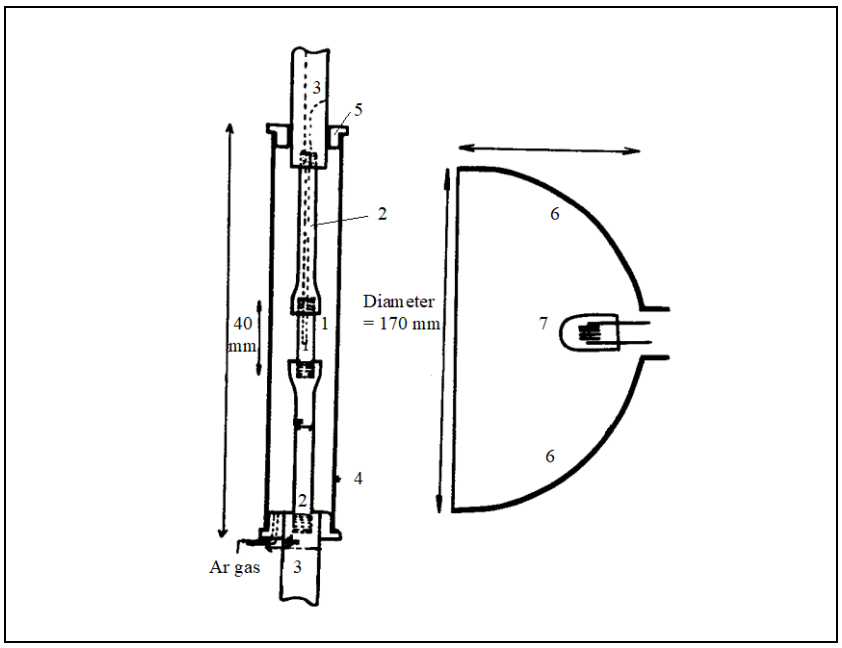


Figure 69.
Sketch of a ductile test equipment.
1. Sample.
2. Holder.
3. Tensile rods.
4. Silicia tube.
5. Sealing joints.
6. Ellipsoid-shaped mirrors
7. Heat source.

casting process can be simulated. When the temperature has reached the desired value, the sample is exposed to ductile stress. Ductile force and dilatation are measured simultaneously and are registered directly by a recorder.

**Ductility of Steel at High Temperatures**

As a measure of ductility, the area reduction ψ in per cent is used.

$$\psi = \frac{A_{\text{before}} - A_{\text{after}}}{A_{\text{before}}} \cdot 100 \qquad (79)$$

where $A_{\text{index}}$ is the cross-section area before respectively after the ductile test.

Alloying elements or impurities with low solubility and low diffusion rate in the solid phase normally reduces the ductility and increases the tendency of crack formation strikingly. One example is phosphorus, which increases the crack formation in 25%Cr10%Ni austenite steel. On the other hand phosphorus does not change the tendency of crack formation in steel, which solidifies as ferrite, because its solubility and diffusion rate in ferrite is much higher than in austenite.

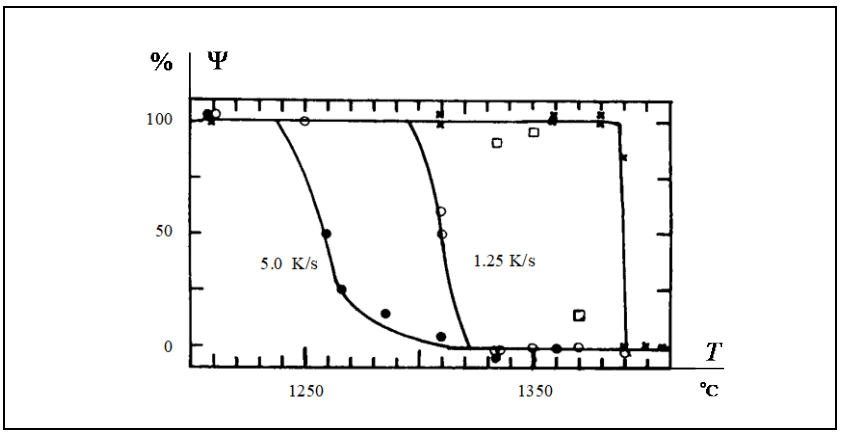


Figure 70.
Ductility of steel as a function of temperature.

Designations:
x reheated material
o direcly solidified material, cooling rate 1.25 K/s
• direcly solidified material, cooling rate 5.0 K/s
□ heat-treated material.

Figure 70 shows the area reduction ψ as a function of temperature for three different types of carbon steel, one directly solidified, one reheated (page 96) and one heat-treated.

It can be seen from figure 70 that

- the transition from ductile to brittle material (low ductility) occurs in a reheated material within a narrow temperature interval, which is called *transition temperature* $T_{tr}$. In the other cases the transition interval is broader.
- Reheated material has a considerably higher transition temperature than directly solidified material, 70-100 °C higher depending on the degree of homogenisation.
- The higher the cooling rate is, the lower the transition temperature will be.

The transition from brittle to ductile material can also be observed in other ways. One can measure the mechanical rupture limit $\sigma_{rl}$, which is required to pull apart the sample, as a function of temperature.

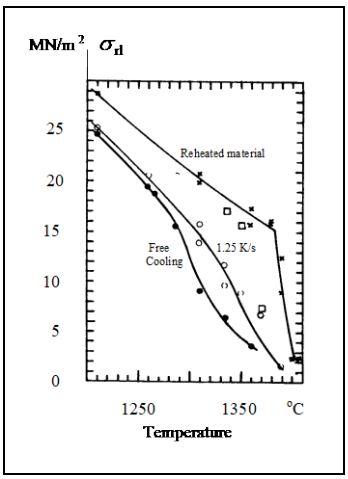


Figure 71.
Ductile stress curves of carbon steel as a function of temperature. The designations are the same as in figure 70.

In figure 71 $\sigma_{rl}$ as a function of temperature within the temperature interval 1210-1410 °C is illustrated for the same carbon steel as in figure 70. For reheated material the transition from brittle to ductile material is as abrupt as in figure 70. The transition temperature is 1390 °C.

For the directly solidified materials the transition is not equally evident. At 1350 ºC the samples with free cooling (5 K/s) still have a relatively high rupture limit (ductile strength) in spite of low ductility.

**Ductility of Stainless Steel at High Temperatures**

Stainless steel generally contain relatively high percentages of Cr and Ni, for example 18-8 steel, but also small amounts of other elements, for example C, Si, Mn, P and N.

Fredriksson and Rogberg have performed ductile tests on about 20 different stainless steel alloys, among them some with low Ni-concentration, which solidify as ferrite (δ-solidification), and some with high Ni-concentration, which solidify primarily as austenite (γ-solidification). This enabled a comparison between alloys with different structures.

Figures 72 a and 72 b show the area reduction at δ- respectively γ-solidification as a function of temperature.

From the figures 72 it is obvious that the transition temperatures of the γ-alloy are *lower* than the ones of the δ-alloy. Another discrepancy between the γ- and δ-alloys is the influence of the cooling rate on the transition temperatures. These matters are further discussed on pages 100-101.

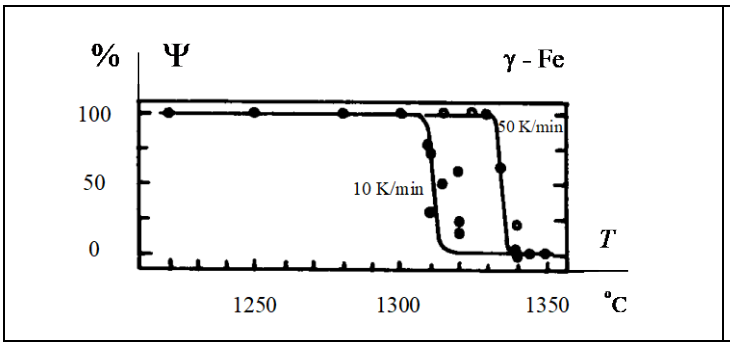


Figure 72 a.
Area reduction as a function of temperature for an Fe(γ)-Cr-Ni alloy at two different cooling rates. The transition temperature increases with increasing cooling rate for the γ-alloy.

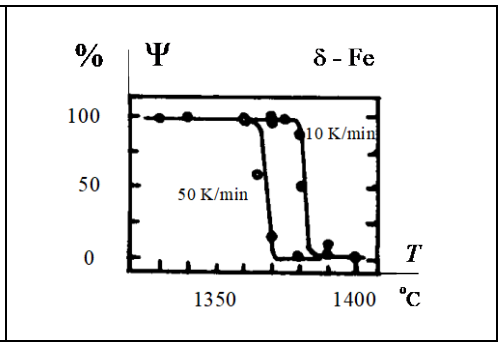


Figure 72 b.
Area reduction as a function of temperature for an Fe(δ)-Cr-Ni alloy at two different cooling rates. $T_{tr}$ decreases with increasing cooling rate for the δ-alloy.

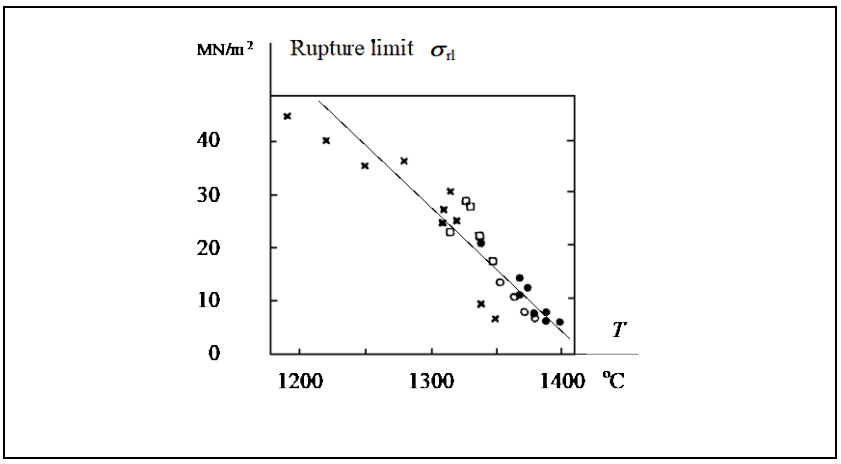


Figure 73.
Maximum ductile stress, i. e. rupture limit, as a function of temperature at two different cooling rates for γ-alloy respectively δ-alloy.

Cooling rates:

| The γ-alloy: | The δ-alloy: |
|---|---|
| x 10 K/min | • 10 K/min |
| □ 50 K/min | o 50 K/min. |

The mechanical rupture limit $\sigma_{rl}$ as a function of temperature for the δ- respectively γ-alloys are illustrated in figure 73. Both alloys show similarities with the directly solidified steel alloy (figure 71). No sharp transition temperature of the rupture limit, like the one measured for the ductility, can be distiguished.

The stainless steels also have a considerable strength at temperatures above the transition temperature $T_{tr}$. Their values of $\sigma_{rl}$ are of the same magnitude as the one of carbon steel.

## Theory of Hot Crack Formation

All alloys show a transition from brittle to ductile structure at a temperature close to the solidus temperature or just below this temperature. The brittle region causes crack formation during many casting and solidification processes. These cracks are called *hot cracks* or *solidification cracks.*

Solidification cracking is often described to occur in the presence of liquid films when ductile stresses are applied, for example thermal stresses. These liquid films, which are found in the interdendritic areas or at grain boundaries, reduce the risk of hot cracks.

However, this is not always in agreement with the observations. The figures 72 a and b show that the transition temperature occurs far below the solidus temperature in the Fe-Cr-Ni based alloys when they solidify as austenite.

If the liquid film theory were right the transition temperature should decrease with increasing cooling rate, since the micro-segregation increases with increasing cooling rate and thus the solidification temperature should decrease. This is true for Fe-Cr-Ni alloys, which solidify with δ-structure. However, the experiments do not verify this prediction for Fe-Cr-Ni alloys, which solidify with γ-structure. For the γ-alloys the transition temperature increases with increasing cooling rate (page 99).

In the 1990$^{th}$ Fredriksson presented a new solidification model, which includes the effects of vacancies, formed during the solidification. The vacancies formed during the solidification process will then condense at dislocations or grain boundaries. The condensation causes strain and stresses during this process and results in contraction of the solidified material. If the vacancies condense, for instance at grain boundaries, the result will be formation of hot cracks. A ductile stress will also generate new vacancies and the condensation of these contributes to the formation of hot cracks.

The theory claims that supersaturation of vacancies will nucleate cracks and favour the growth of cracks. The nucleation of a crack is assumed to occur by heterogeneous nucleation, which depends on the supersaturation of vacancies in the solid. Figure 74 shows the relation between the thermal stress, which has to be exceeded in order to form a crack, and the supersaturation of vacancies, required to nucleate a crack. The supersaturation is described as a factor times the equilibrium fraction of vacancies.

This thermal stress can easily be achieved in iron base alloys, especially during addition of sulphur, phosphorous and oxygen. This may be the explanation why sulphur and phosphorous are notorious elements for causing hot cracks during solidification, even if the alloy has such low concentrations of these elements that liquid films cannot possibly form. The dotted curve shows the case when the crack is nucleated in a strain field.

According to the model, the diffusion of vacancies from the bulk solid to the crack tip controls the crack growth. The driving force for crack propagation is the difference between the vacancy concentration at the supersaturated solid and the crack tip. It will thus be proportional to the diffusion rate of vacancies from the supersaturated solid to the crack tip or simply a function of the supersaturation of vacancies.

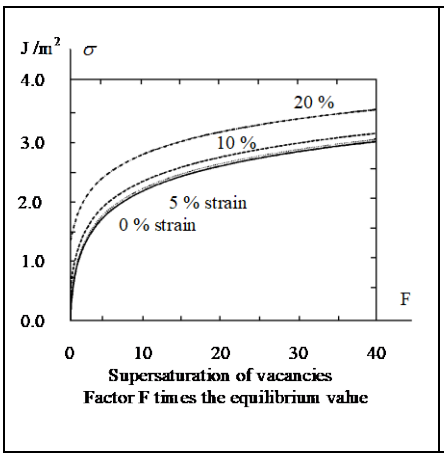


Figure 74.
Thermal stress as a function of the supersaturation of vacancies for nucleation of a crack, for different strain values on the sample of γ-Fe at $T = 1500\ ^{o}C$.

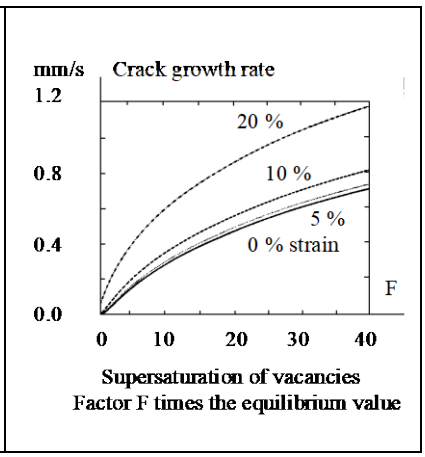


Figure 75.
Growth rate of a crack as a function of the supersaturation of vacancies at three different strain values and at $\Delta\sigma = 1\ J/m^2$. Sample of γ-Fe at $T = 1500\ ^{o}C$.

The crack growth rate as a function of the supersaturation of vacancies is shown in figure 75. With no strain at all the growth rate will be of the order 100 μm/s. The dotted curve in figure 75 shows that a strain ≤ 5 % has little effect on the growth rate of the crack.

The growth rate of cracks is rather fast and the model thus implies that the transition temperature of ductility is related to the nucleation of a crack. It is important for the nucleation of a crack that the supersaturation of vacancies, formed in the solid during the solidification process, can be maintained. This is not desirable and it is urgent to find an annealing process, which reduces the supersaturation of vacancies, for example temperature decrease.

The transition temperature from brittle to ductile structure are influenced by the

- supersaturation of vacancies
- diffusion rate of vacancies
- distance between the vacancy sinks, i. e. the structure coarseness
- time of diffusion of vacancies, which is related to the cooling rate.

### 10.7.7 Hot Crack Formation at Component Casting

Plastic and elastic deformation of castings was discussed in chapter 8 on page 34. Residual stresses often remain in cast components, which results in a risk of distorsion of the component. The stresses can be released by heat treatment (chapter 8).

In the case of component casting the heat treatment temperature to release residual stresses is close to room temperature The thermal contraction will also become critical at high temperatures when the alloy is in the brittle region. Hot cracking will thus occur.

A cast component never contracts completely freely during the casting process. The mould restrains the contraction as is illustrated in figure 76.

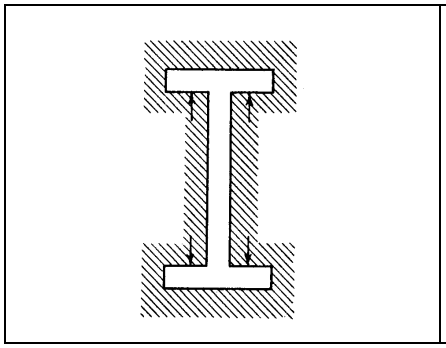

Figure 76 a.
Mould restraint, a typical design feature, which causes contraction stress.

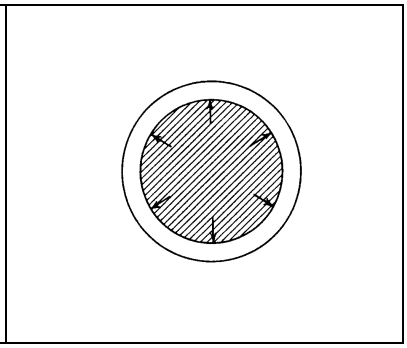

Figure 76 b.
Core restraint, a typical design feature, which causes contraction stress.

As soon as the casting has reached a temperature below the transition temperature from brittle to ductile structure there is very little risk of crack formation.

The risk of crack formation is thus concentrated to the temperature interval between the transition temperature and the temperature in the two-phase region solid/liquid where the fraction of solid is large enough for the material to resist stress. The larger this temperature interval is the larger is the risk of cracks in the material.

---

**Example 11.**

A casting of the shape illustrated in figure 76 a is to be cast in a steel alloy with the properties described below. It is urgent to analyse the risk of crack formation. Experimental values of the stress as a function of temperature for the steel are known and given in the margin figure.

The thermal expansion coefficient of the steel is $2.0 \cdot 10^{-5}\ \mathrm{K}^{-1}$. The elasticity modulus of the steel can be written as a function of temperature:

$$E = \left[1.1 + 0.10 \cdot (T_{cr} - T)\right] \cdot 10^3 \quad \mathrm{N/mm^2}$$

where $T_{cr}$ is the critical temperature for elastic deformation.

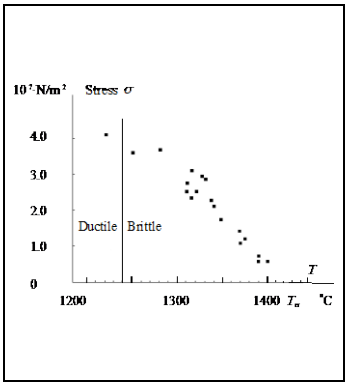


a) Calculate the thermal stress in the cast material as a function of temperature if the material cannot contract freely. Hooke´s law is assumed to be valid. Plot the function in the figure in the margin. The function represents the rupture limit of the material as a function of the test temperature. The transition temperature between brittle and ductile structure is shown in the figure.

b) Discuss the risk of hot crack formation in the material on the basis of the experimental values in the margin figure.

**Solution:**

a) Hooke´s law (equation (61) on page 71) can be written

$$\sigma = \varepsilon \cdot E \qquad (1')$$

According to (equation (67) on page 73) the dilatation ε can be written

$$\varepsilon = \alpha \cdot \Delta T = \alpha \cdot (T_{cr} - T) \qquad (2')$$

Equations (1´) and (2´) are combined with the expression of $E$, given in the text, transformed into SI units.

$$\sigma = \alpha \cdot (T_{cr} - T) \cdot E = 2.0 \cdot 10^{-5} \cdot (T_{cr} - T) \cdot \left[1.1 + 0.10 \cdot (T_{cr} - T)\right] \cdot 10^3 \cdot 10^6 \qquad (3')$$

The function is plotted in the figure in the answer.

An average straight line is drawn in the figure in the text. It represents the thermal stress as a function of the temperature and is plotted in both figures in the answer.

The temperature, at which the material breaks, is obtained when the thermal stress is equal to or larger than the rupture limit, i. e. at the intersection point between the rupture limit curve and the straight line. If the intersection point is located in the brittle zone the material breaks. If the point is situated in the ductile zone, the material expands and the rupture limit is never reached.

**Answer:**

a) The desired function, which represents the rupture limit versus temperature, is

$$\sigma = 2.0 \cdot 10^{4} \cdot (T_{cr} - T) \cdot \left[1.1 + 0.10 \cdot (T_{cr} - T)\right]$$

It is plotted in the right figure below.

b) The straight line in the left figure corresponds to the stress in the material as a function of temperature. It is also drawn in the right figure by aid of the two points (1240 $^{o}$C, $4.5 \cdot 10^{7}$ N/m$^{2}$) and [(1430 $^{o}$C, 0). The intersection point corresponds to $T$ = 1320 $^{o}$C.

Thus there is a large risk of hot crack formation at temperatures ≥ 1320 $^{o}$C where the thermal stress exceeds the rupture limit.

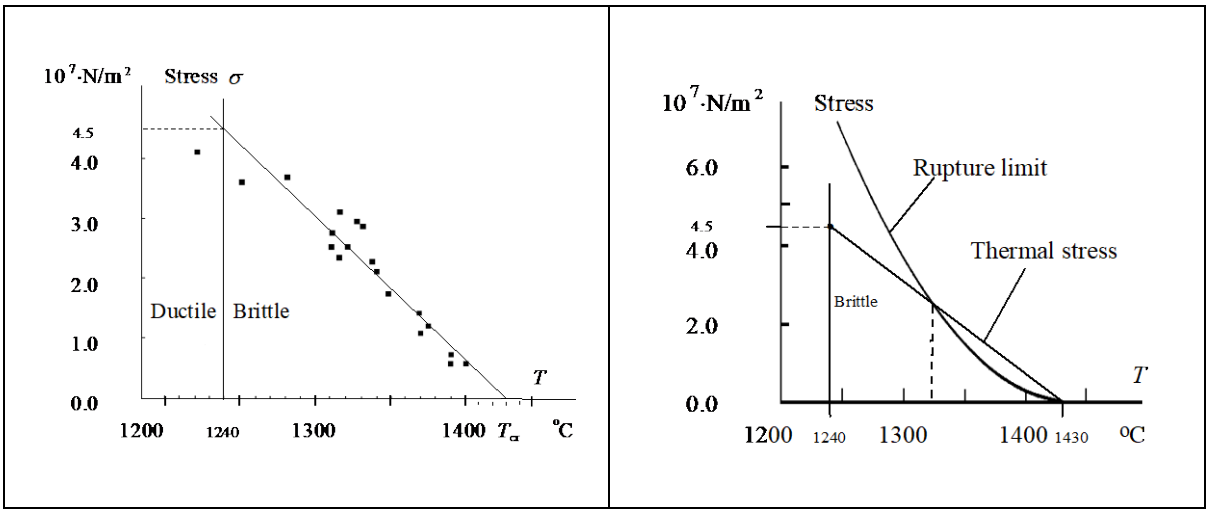


---

### 10.7.8 Thermal Stress and Crack Formation at Continuous Casting

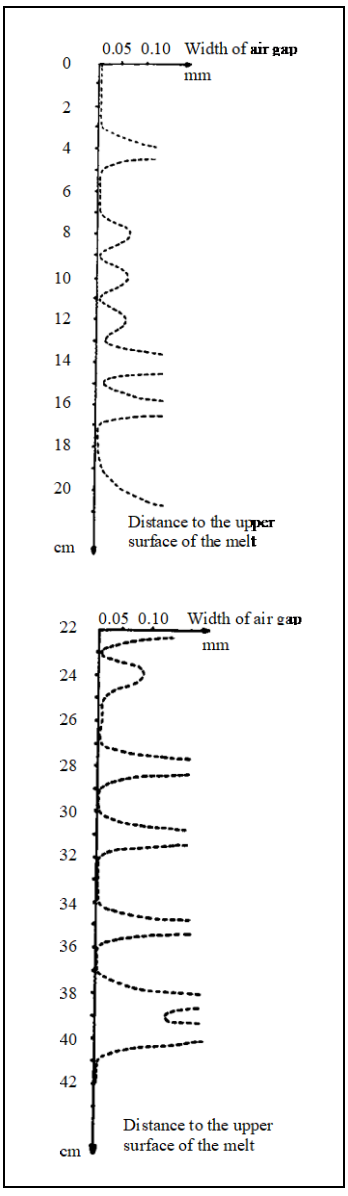


Figure 77.
Width of air gap between shell and chill-mould as a function of the depth under the upper surface of the melt for a steel billet (14 cm x 14 cm).

At continuous casting both the primary and the secondary cooling are strong and the cooling rate is high. When the melt is poured into the chill-mould and meets its cold walls a shell is formed very rapidly. The solidifying shell cools initially rapidly because the contact between shell and chill-mould is good. When the shell cools it shrinks and an air gap is formed between the chill-mould and the shell as soon as the latter has been stable enough to resist the ferrostatic pressure. The thermal conduction is decreases with increasing air gap and the surface temperature of the shell increases.

A complex interaction between the thickness and the temperature of the solidifying shell results in a varying growth rate along the shell, both in its length direction and along its peri-phery. Every tiny variation of the growth rate of the shell automatically changes its surface temperature. These temperature variations cause thermal stresses and result in risk of surface cracks.
Knowledge of the growth rate of the solidifying shell is thus of utmost importance for calculation of the sizes of the thermal stresses and for the possibility of designing the chill-mould and the secondary cooling in an optimal way.

When the shell has reached the centre of the cross-section of the strand at the end of the metallurgical length the temperature in the centre, which initially has been rather constant, will fall rapidly. This process causes thermal stresses within the interior of the strand and results in risk of centre cracks.

The risk of crack formation is a severe problem at continuous casting. Below we will discuss the air gap more in detail and then return to thermal stresses and crack formation.

#### Air Gap between Shell and Chill-Mould

Experimental investigations show that the thickness of the shell inside the chill-mould varies (figure 77). These variations cause changes of the surface temperature and growth rate of the shell during the solidification process.

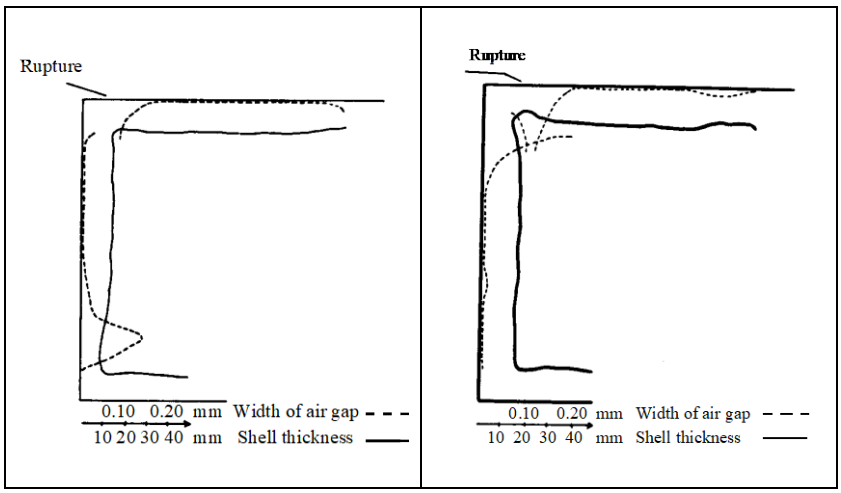


Figure 78. Left figure. Shell thickness (continuous line) and air gap width (dotted line) in a steel billet 27 cm below the upper surface of the melt.
Figure 79. Right figure. Shell thickness (continuous line) and air gap width (dotted line) in a steel billet 37 cm below the upper surface of the melt.

Figures 78 and 79 above illustrate the variation of the air gap around the periphery of a strand. This type of variations also causes variations of the surface temperature of the shell around the periphery and in the length direction.

The air gap is primarily formed at the corners. Figure 80 a shows how the air gap is formed only a few seconds after the casting start and how it increases with time.

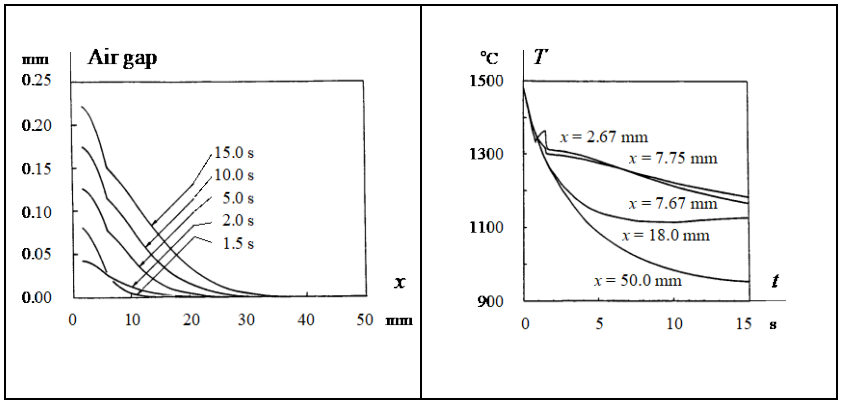


Figure 80 a. Left figure. Calculated air gap of a billet 10 cm x 10 cm at the casting rate 2.8 m/s and chill-mould height = 70 cm.
Figure 80 b. Right figure. Calculated surface temperature at various distances from the corner for the same billet as in figure 80 a.

Figure 80 b shows that the temperature near the corner, where the air gap is very large, is much higher than at the middle of the side. In order to counteract the reduced heat conduction the chill-mould is made conical to decrease the air gap. The best result is obtained if the conicity of the chill-mould is larger at the upper part than in the lower part.

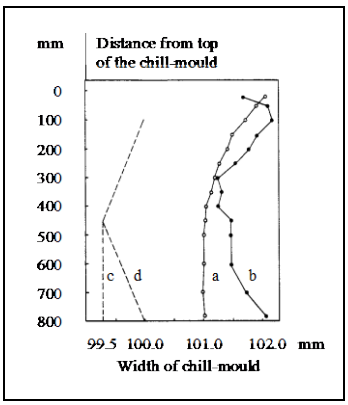


Figure 81.
Shapes of billet profiles.
a) new industry chill-mould
b) industry chill-mould,
used 350 times
c) simulated new chill-mould
d) simulated used chill-mould.

There is a relation between the risk of surface cracks and the degree of use of the chill-mould. In order to examine this relation a casting process has been simulated both for a chill-mould, which has been used many times, and for a new one.

The curves a and b in figure 81 show the model chill-moulds and their real prototypes (figure 22 on page 36 in chapter 5). For the sake of simplicity the diameter of the model chill-mould has been chosen to 100 mm.

The results of the simulation calculations are shown in the figures 82 and 83 below.

The results of the simulation calculations are summarised in figure 84, which shows the calculated surface temperature as a function of time for four different distances from the corner in the two cases.

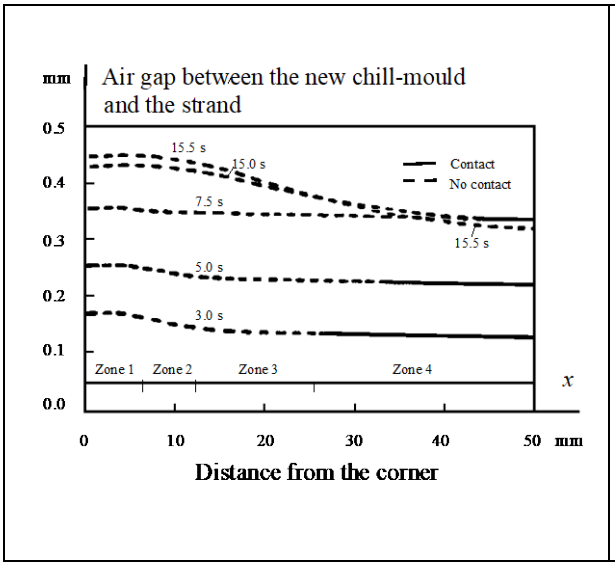


Figure 82.
Calculated distance between the new chill-mould and the surface of the strand as a function of the distance from the corner at 5 different times. Continuous lines indicate contact between shell and chill-mould. Dotted lines indicate that the strand surface is surrounded by air.

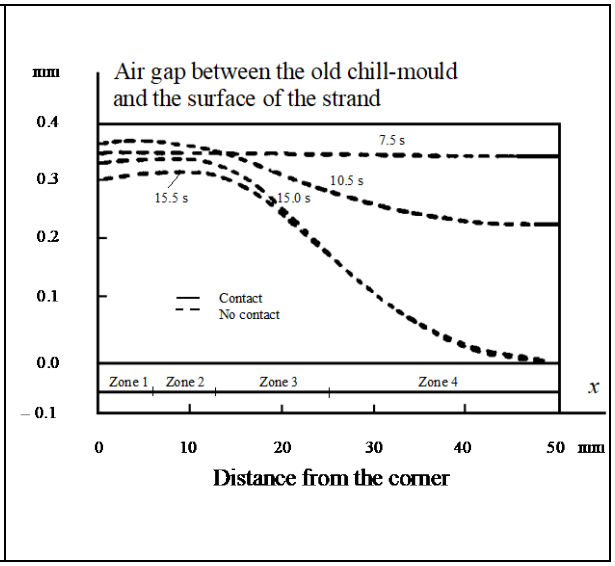


Figure 83.
Calculated distance between the old chill-mould and the surface of the strand as a function of the distance from the corner at 5 different times. Continuous lines indicate contact between shell and chill-mould. Dotted lines indicate that the strand surface is surrounded by air.

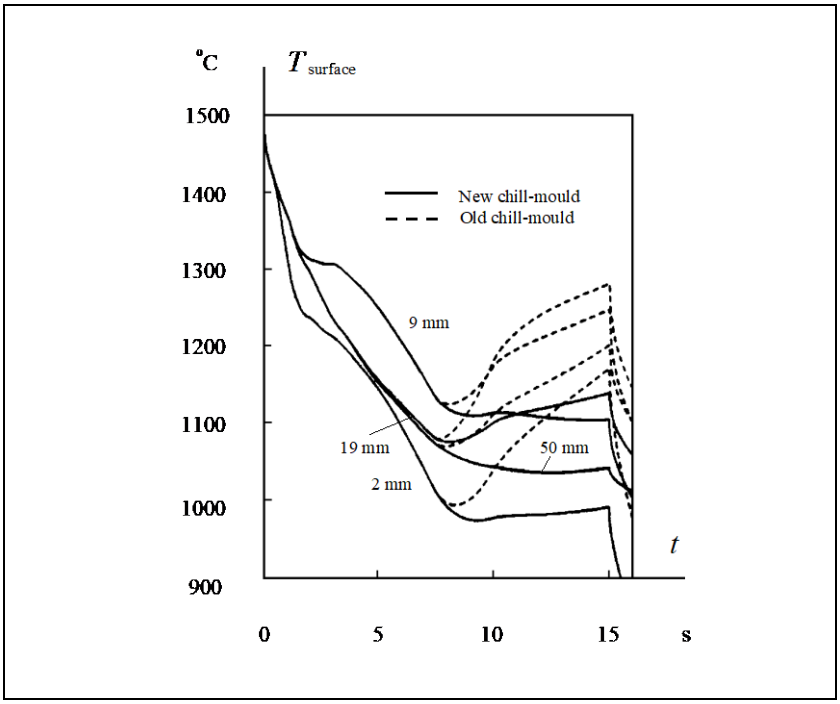


Figure 84.
Calculated surface temperatures as a function of time for four different distances from the corner for the new respectively the old chill-mould.

The two cases are identical during the first 7.5 seconds but differ strongly later.

An uneven distribution of the thermal stresses in the chill-moulds cause an irre-gular order of the curves corresponding to different parameter distances.

Figure 84 shows that the larger air gap in the old chill-mould causes a considerable temperature increase in its lower part. It can also be seen that the temperatures at the corners in both the old and the new chill-moulds are lower than elsewhere. This is an effect of a more effective heat transport at the corners than at other places. This was discussed on page 48 in chapter 4.

## Types of Hot Cracks at Continuous Casting

The risk of formation of hot cracks during continuous casting is very large. Figure 85 and table 4 on next page give a survey of the many different kinds of cracks, which have been observed in continuously cast strands.

The cracks can be divided into two main groups:

- Internal cracks
- Surface cracks

A review of the most important types is given on next page.

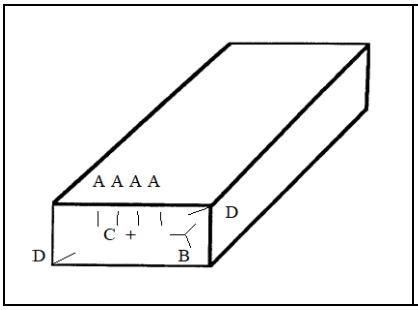


Figure 85 a.
Strand section with some different types of internal cracks.

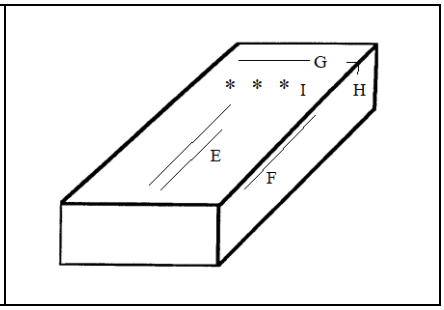


Figure 85 b.
Strand section with some different types of surface cracks.

Table 4. Survey of observed cracks in continuously cast steel strands.

| Internal cracks | Surface cracks |
|---|---|
| A: Midway cracks<br>B: Triple point cracks<br>C: Centreline cracks<br>D: Diagonal cracks | E: Longitudinal midface cracks<br>F: Longitudinal corner cracks<br>G: Transverse midface cracks<br>H: Transverse corner cracks<br>I: Star cracks |

## Surface Cracks

### *Cracks Inside the Chill-Mould*

Thermal stresses are caused by differences in cooling rate between different parts of the solidifying shell. As long as the strand is situated inside the chill-mould the cooling rate in the interior parts of the shell will be larger than the one at the surface. The result is thermal stresses near the solidification front and compression of the surface.

In order to give a concrete picture of the thermal stresses at continuous casting we will continue the simulation calculations for the case with the old chill-mould (figure 81 d). The thermal stresses have been calculated at different points in the *xy*-plane (the length direction of the strand is *z*-axis) at time $t$ = 15 s and are plotted in a diagram as vectors. It takes 15.0 s for the strand

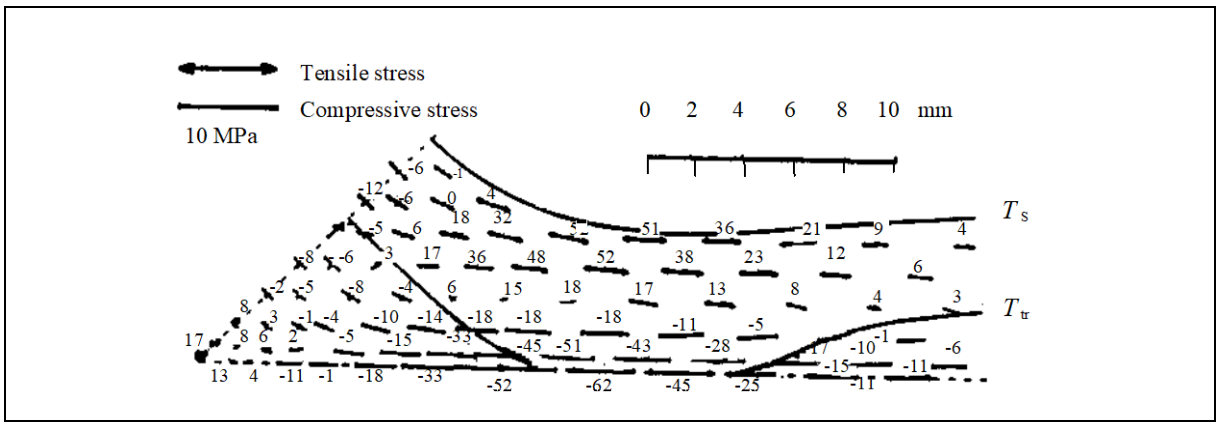


Figure 86.
Calculated directions and sizes of the thermal stresses in the *xy*-plane (arrows) and calculated dilatations (figures times $10^{-4}$) at the exit out of the chill-mould ($t$ = 15.0 s).

to pass the chill-mould and figure 86 thus shows the stress pattern just before the exit out of the chill-mould.

In figure 86 the solidus curve $T_s$ and the calculated transition temperature curve $T_{tr} = T_s - 100$ °C have been inserted. The material is assumed to be brittle within the region between these two curves.

In addition the mechanical dilatations $\varepsilon_x^m$ in the *x*-direction are plotted in the shape of figures. It can be seen that this dilatation has its maximum within the zone where the material is brittle. The maximum value exceeds many times the criterion of 0.2 % which is normally used for crack formation. Thus there is a great risk of internal longitudinal cracks, perpendicular to the surface.

### *Outside the Chill-Mould*

At the exit out of the chill-mould and at the entrance into the secondary cooling zone the sudden thermal conduction away from the whole surface, is caused by water cooling. The distribution of the thermal stresses and the mechanical stresses is totally changed and the dilatations appear in the surface region instead of the region inside the interior of the strand. Figure 87 illustrates the new stress conditions.

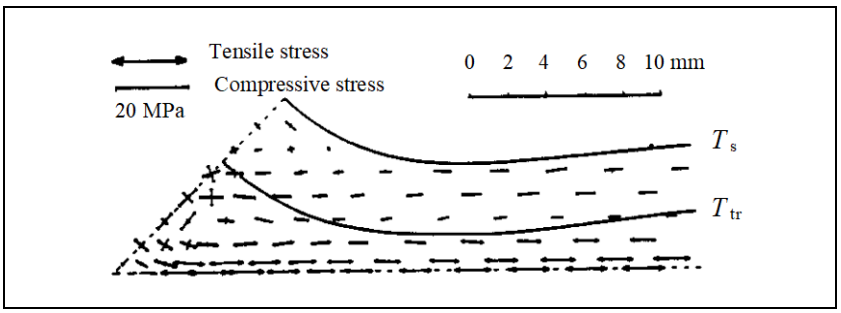


Figure 87.
Stresses in the *xy*-plane after the exit out of the chill-mould ($t$ = 15.5 s). The length direction of the strand is *z*-axis.

The stresses have been calculated after casting in the old chill-mould at $t$ = 15.5 s, i. e. just below the chill-mould and have been plotted into figure 87 together with the isotherms $T_S$ and $T_{tr}$. These thermal stresses decline rather rapidly. The simulation calculations show that they are replaced by torsion stresses, caused by the ferrostatic pressure, after some seconds.

Simulation calculations for the new chill-mould show that the process in principle is the same as the one described above, but there are also important differences, which we will come back to on page 113 (figures 88 and 89).

**Risk Regions of Crack Formation**

In order to give a concrete example of mapping risk regions of crack formation we will return to the simulation calculations and the comparison we made on pages 108-109 between an old and frequently used chill-mould and a new one. These calculations have been used as basis of figures 88 and 89.

Figures 88 and 89 give a comparison between the new and the old chill-mould with respect to risk regions of crack formation. They show calculated distances from the strand surface as a function of time for various lines/regions in a plane, perpendicular to the surface at a certain distance ($x$ = 19 mm) from the corner. This distance corresponds to the distance from the corner to the centre of the hot surface region in both cases (see figure 84 on page 109).

The difference in width of the risk zones of internal crack formation ($\varepsilon_x^m > 0.2$ %) and brittleness illustrates the influence of a new versus an old chill-mould on the cooling process and on the risk of internal cracks.

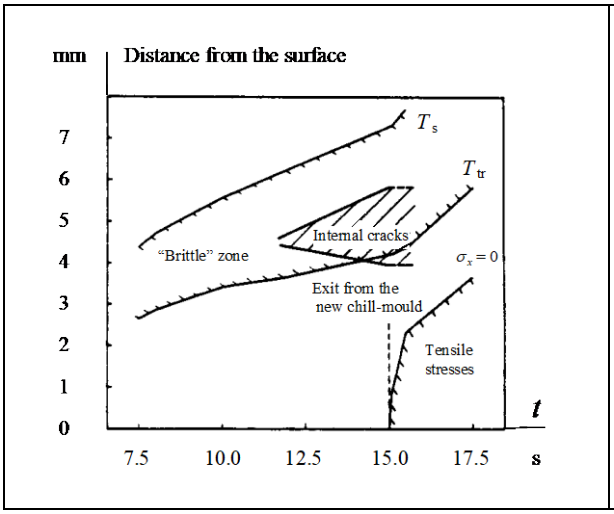


Figure 88.
Distance $y$ from the surface as a function of time for the new chill-mould.

Position and extension of some regions of special interest at $x$ = 19 mm have been drawn in the figure.

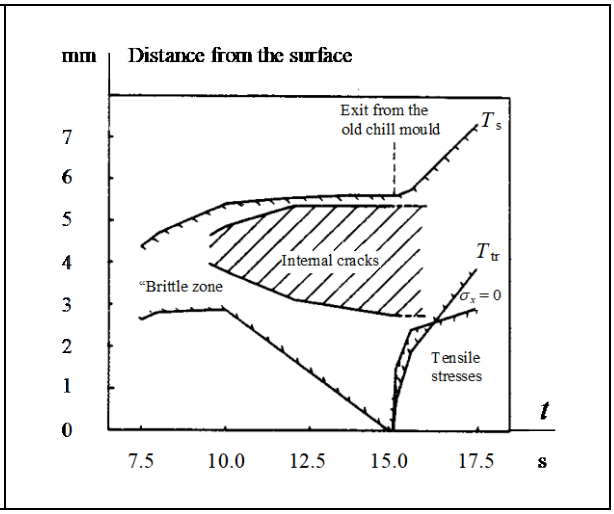


Figure 89.
Distance $y$ from the surface as a function of time for the old chill-mould.

Position and extension of some regions of special interest at $x$ = 19 mm have been drawn in the figure.

After passage of the chill-mould ($t$ > 15 s) the region of thermal stresses increases and advances, i. e. the distance from the surface increases. In the case of the old chill-mould (figure 89) the tensile stresses even reach the brittle zone in less than one second, immediately after the exit out of the chill-mould. This results of course in a severe risk of crack formation.

## Internal Cracks

The major reason for centre and ”halfway” cracks in strands is the thermal contraction of the solidified shell. They are caused by differences in cooling rates between the surface and the centre at the end of the metallurgical length. When the centre starts to solidify there is a rapid drop of temperature along the central axis as we found in section 10.6.2. If there is no corresponding temperature drop at the surface of the strand, thermal contraction will occur. In case of a slab the strand bulges and a longitudinal crack is formed. In case of billets star-like cracks are formed in the central parts of the strand.

Halfway cracks are one of the most common types of internal cracks found in continuously cast billets and slabs. The mechanism of formation can be postulated. The forecast is based on the results of both industrial measurements and thermo-mechanical strain analysis under different boundary conditions.

Halfway cracks form between the dendrites in the columnar zone, which runs perpendicularly to the high-ductile strains, which develop in the material. The dominant source of stresses, which causes crack formation, is reheating of the slab surface. The stresses, which cause halfway cracks, depend mainly on

- the magnitude of the reheating of the surface
- the thickness of the solid shell
- the width of the mushy zone.

The magnitude of the surface reheating is related to the design of the secondary cooling cycles and the level of the surface temperature.

### 10.7.9 Methods of Reduction of the Negative Effects of Thermal Stresses

**General Measures**

It is impossible to avoid strong temperature changes in the material at casting and cooling. On the other hand the production of castings may be designed in such a way that the risk of crack formation is minimised. Theoretical and practical knowledge of the kind discussed earlier in this section on thermal stresses constitute the basis of judgement of the best method.

The following general principles are valid:

- Moulds and chill-moulds should be designed as free from sharp edges and corners as possible.
- The compositions of the alloys to be used ought to be chosen in such a way, that the materials get maximum ductility within the limits of other demands upon the products.

- The cooling should be designed in such a way that the temperature differences between different parts of the casting become as small as possible during the solidification and cooling process.
- The mechanical action on the casting during the sensitive temperature interval between the solidus temperature and the transition temperature should be kept as small as possible, because then the risk of hot cracks is considerable.
- Strong cooling often results in more thermal stress than soft cooling.

**Measures at Continuous Casting**

In section 10.7.8 we found that the risk of crack formation is often large at continuous casting, due to the large temperature gradients and rapid changes of the surface temperature.

- The risk of *surface cracks* can be reduced by keeping the surface temperature as constant as possible during cooling.

  It is thus important that the chill-mould is made conical, in order to keep the air gap as constant as possible during the solidification process. The best result is achieved if the conicity of the chill-mould is made larger in the upper part than in the lower one. In this way it is possible to avoid that the heat transport is strongly reduced, which would cause changes of the temperature conditions (see figure 86 on page 111).

- The risk of *centre cracks* can be reduced by increasing the cooling of the surface strongly at the end of the metallurgical length (thermal reduction). This reduces the large difference in cooling rates at the surface and in the centre, which normally appears when the centre has solidified. The same effect can be achieved by mechanical reduction, i. e. when the strand is exposed to a strong mechanical pressure at the end of the metallurgical length.